



## ATLAS Note

ATL-COM-PHYS-2019-962

26th May 2021



1

# 2 WZ + Heavy Flavor Production in pp collisions 3 at $\sqrt{s} = 13$ TeV

4

The ATLAS Collaboration<sup>1</sup>, Aaron Webb<sup>a</sup>, Peter Onyisi<sup>a</sup>

5

<sup>a</sup>*Univ. of Texas at Austin*

6

A measurement of the cross-section for production of WZ with an associated heavy flavor jet  
7 is performed using  $140 \text{ fb}^{-1}$  of proton-proton collision data at  $\sqrt{s} = 13$  TeV from the ATLAS  
8 experiment at the LHC. A measurement of the fully leptonic decay mode,  $WZ \rightarrow l\nu ll$ , is  
9 performed. The cross-section of  $WZ + b$  and  $WZ + \text{charm}$  in various fiducial regions is  
10 measured.

11

© 2021 CERN for the benefit of the ATLAS Collaboration.

Reproduction of this article or parts of it is allowed as specified in the CC-BY-4.0 license.

## 12 **Contents**

13	<b>1 Changes and outstanding items</b>	<b>3</b>
14	1.1 Changelog	3
15	1.1.1 Changes relative to v8	3
16	1.1.2 Changes relative to v7	3
17	1.1.3 Changes relative to v5	4
18	1.1.4 Changes relative to v4	4
19	1.1.5 Changes relative to v3	4
20	1.1.6 Changes relative to v2	5
21	1.1.7 Changes relative to v1	5
22	1.2 Outstanding Items	5
23	<b>2 Executive Summary</b>	<b>6</b>
24	<b>3 Data and Monte Carlo Samples</b>	<b>6</b>
25	3.1 Data Samples	7
26	3.2 Monte Carlo Samples	7
27	<b>4 Object Reconstruction</b>	<b>9</b>
28	4.1 Trigger	9
29	4.2 Light leptons	10
30	4.3 Jets	11
31	4.4 B-tagged Jets	11
32	4.5 Missing transverse energy	12
33	4.6 Overlap removal	12
34	<b>5 Event Selection and Signal Region Definitions</b>	<b>13</b>
35	5.1 Event Preselection	13
36	5.2 Fit Regions	17
37	5.3 Non-Prompt Lepton Estimation	33
38	5.3.1 $t\bar{t}$ Validation	33
39	5.3.2 Z+jets Validation	36
40	<b>6 tZ Separation Multivariate Analysis</b>	<b>40</b>
41	6.1 Top Mass Reconstruction	41
42	6.2 tZ BDT	41
43	6.3 tZ Interference Studies	45
44	<b>7 Systematic Uncertainties</b>	<b>47</b>
45	<b>8 Results</b>	<b>54</b>
46	8.1 Fit Procedure	54
47	8.2 Results of the Simultaneous Fit	55
48	8.3 Inclusive 1+2 Jet Fit	66

49	8.4 Alternate tZ Inclusive Fit	70
50	8.4.1 tZ Inclusive Fit	70
51	8.4.2 Floating tZ	70
52	<b>9 Conclusion</b>	<b>71</b>
53	<b>A Appendices</b>	<b>74</b>
54	<b>Appendices</b>	<b>74</b>
55	A.1 Non-prompt lepton MVA	74
56	A.2 Non-prompt CR Modelling	76
57	A.3 DSID list	80

---

## 58 List of contributions

---

Aaron Webb	Main analyser. Responsible for ntuple production, fits, and note writing.
Peter Onyisi	Advisor to Aaron Webb. Analysis design and implementation strategy.

---

61 **1 Changes and outstanding items**

62 **1.1 Changelog**

63 This is version 9

64 **1.1.1 Changes relative to v8**

- 65     • Included more references to appendices in the text
- 66     • Expanded explanation of fiducial region definition
- 67     • Previous draft claimed that both standard and custom PLVs were used. Text is fixed to  
68       state that a custom PLV is used for lepton iso, but standard lepton id is used
- 69     • Included plots of PLV output, included WPs used
- 70     • specified that non-prompt CR plots are post correction
- 71     • changed title of results section

72 **1.1.2 Changes relative to v7**

- 73     • Moved from LO to NLO tZ sample
- 74     • Add additional plots of Z+jets and ttbar CRs in Section [A.2](#)
- 75     • Clarified CDI file used, MC ptag, PFlow jet algorithm
- 76     • Included overlap removal procedure
- 77     • Included details on PLV
- 78     • Added plots of missing tZ BDT input features for each fit region
- 79     • Changed reference on PLV to recent ttH/ttW note
- 80     • Included alternate fits with WZ+1-2 jet inclusive, tZ floating

81 **1.1.3 Changes relative to v5**

- 82     • added list of DSIDs to an appendix  
 83     • included systematics on jet migrations  
 84     • Updated results section to include simultaneous fit over 1-jet and 2-jet bins, describe  
 85        unfolding procedure  
 86     • Updated other sections to account for this change  
 87     • Included info about migrations in Section 5.2

88 **1.1.4 Changes relative to v4**

- 89     • Fixed various typos, clarified wording  
 90     • Expanded info about JER uncertainties, electron systematics, theory uncertainties  
 91     • removed a table on lepton selection, included information in the text instead  
 92     • Plotted lepton Pt Z and W for Zjet CR, rather than lep 1 and 2  
 93     • fixed binning in kinematic plots  
 94     • Included prefit and postfit yield tables  
 95     • added signal modelling systematics  
 96     • included alternate fit studies with tZ included in signal

97 **1.1.5 Changes relative to v3**

- 98     • Merged introduction into executive summary, including unblinding details and list of  
 99        SRs/CRs used  
 100     • listed ptag used (p4133), and release (AB 21.2.127)  
 101     • Included table reftab:xsecUnc listing x-sec uncertainties used  
 102     • Removed selection criteria listed in table ?? (QMisID, AmbiguityType) that were removed  
 103        from the analysis  
 104     • specified variable used to make truth jet flavor determination (HadronConeExclTruthLa-  
 105        belIID)  
 106     • fixed bug in MtLepMet calculation, updated selection/fits to account for this  
 107     • Included plots of MtLepMet and PtZ, swapped lep 1 and 2  $p_T$  plots for lep W and lep Z  
 108        plots

- 109     • updated tZ BDT training to reduce overfitting, updated plots to include error bars, feature  
110     importance
- 111     • updated table 8 to clarify selection, fix the tZ\_BDT cut used
- 112     • replace a few broken ntuples which included large weight events
- 113     • include DL1r distribution for Z+jets and  $t\bar{t}$  VRs
- 114     • Expanded section on fakes, included information on derived scale factors from VRs.
- 115     • Changed the kinematic plots to include  $p_T(Z)$  and  $m_T(W)$ , list lepton  $p_T$  based on W and  
116     Z candidates.

### 117     **1.1.6 Changes relative to v2**

- 118     • Added alternate VBS samples to include missing b-jet diagrams
- 119     • Included a section on tZ interference effects, ??.
- 120     • Updated to reflect changes for 2018, including the move to PFlow jets, DL1r, updated  
121     trigger, and updated AnalysisBase version (now 21.2.127)
- 122     • Revised fit regions, using separate 1-jet and 2-jet fits, with all 2-j regions included
- 123     • updated plots for tZ BDT, added details about the model
- 124     • Included truth jet information

### 125     **1.1.7 Changes relative to v1**

- 126     • Added GRL list
- 127     • Fixed latex issue in line 92, typo in line 172
- 128     • Added tables 6 and ??, summarizing the event and object selection
- 129     • Added table 2, which includes the DSID of samples used
- 130     • Included reference to WZ inclusive paper in introduction

## 131     **1.2 Outstanding Items**

- 132     • Unblind, update plots and fits to include data
- 133     • Add cross-section, significance once unblinded

## 134 2 Executive Summary

135 The production of  $WZ$  in association with a heavy flavor jet represents an important background  
 136 for many major analyses. This includes any process with leptons and b-jets in the final state,  
 137 such as  $t\bar{t}H$ ,  $t\bar{t}W$ , and  $t\bar{t}Z$ . While precise measurements have been made of  $WZ$  production  
 138 [1],  $WZ +$  heavy flavor remains poorly understood. This is largely because the QCD processes  
 139 involved in the production of the b-jet make it difficult to simulate accurately. This introduces a  
 140 large uncertainty for analyses that include this process as a background.

141 Motivated by its relevance to the  $t\bar{t}H$  multilepton analysis, we perform a study of the fully  
 142 leptonic decay mode of this channel; that is, events where both the W and Z decay leptonically.  
 143 Because  $WZ$  has no associated jets at leading order, while the major backgrounds for this channel  
 144 tend to have high jet multiplicity, events with more than two jets are rejected. This gives a final  
 145 state signature of three leptons and one or two jets.

146 Events that meet this selection criteria are sorted into pseudo-continuous b-tagging regions based  
 147 on the DL1r b-tag score of their associated jets. This is done to separate  $WZ +$  b-jet events from  
 148  $WZ +$  charm and  $WZ +$  light jets. These regions are fit to data in order make a more accurate  
 149 estimate of the contribution of  $WZ +$  heavy-flavor, where heavy-flavor jets include b-jets and  
 150 charm jets. The full Run-2 dataset collected by the ATLAS detector, representing  $139 \text{ fb}^{-1}$  of  
 151 data from pp collisions at  $\sqrt{s} = 13 \text{ TeV}$ , is used for this study.

152 Section 3 details the data and Monte Carlo (MC) samples used in the analysis. The reconstruction  
 153 of various physics objects is described in Section 4. Section 5 describes the event selection applied  
 154 to these samples, along with the definitions of the various regions used in the fit. The multivariate  
 155 analysis techniques used to separate the  $tZ$  background from  $WZ +$  heavy flavor are described in  
 156 Section 6. Section 7 describes the various sources of systematic uncertainties considered in the  
 157 fit. Finally, the results of the analysis are summarized in Section 8, followed by a brief conclusion  
 158 in Section 9.

159 **The current state of the analysis shows blinded results for the full Run-2 dataset. Regions  
 160 containing >5%  $WZ+b$  events are blinded, and results are from Asimov, MC only fits.**

## 161 3 Data and Monte Carlo Samples

162 Both data and Monte Carlo samples used in this analysis were prepared in the xAOD format,  
 163 which was used to produce a Dx AOD sample in the HIGG8D1 derivation framework. The HIGG8D1  
 164 framework is designed for the  $t\bar{t}H$  multi-lepton analysis, which targets events with multiple  
 165 leptons as well as tau hadrons. This framework skims the dataset to remove unneeded variables  
 166 as well as entire events. Events are removed from the derivations that do not meet one of the  
 167 following selections:

- 168     • at least two light leptons within a range  $|\eta| < 2.6$ , with leading lepton  $p_T > 15 \text{ GeV}$  and  
 169       subleading lepton  $p_T > 5 \text{ GeV}$

- 170 • OR at least one light lepton with  $p_T > 15$  GeV within a range  $|\eta| < 2.6$ , and at least two  
 171 hadronic taus with  $p_T > 15$  GeV.

172 Samples were then generated from these HIGG8D1 derivations with p-tag of p4134 for data  
 173 and p4133 for Monte Carlo using AnalysisBase version 21.2.127 modified to include custom  
 174 variables.

### 175 3.1 Data Samples

176 The study uses a sample of proton-proton collision data collected by the ATLAS detector from  
 177 2015 through 2018 at an energy of  $\sqrt{s} = 13$  TeV, which represents an integrated luminosity of  
 178  $139 \text{ fb}^{-1}$  [2]. This data set was collected with a bunch crossing rate of 25 ns. All data used in  
 179 this analysis was verified by data quality checks [3], having been included in the following Good  
 180 Run Lists:

- 181 • data15\_13TeV.periodAllYear\_DetStatus-v79-repro20-02\_DQDefects-00-02-02  
 182 \_PHYS\_StandardGRL\_All\_Good\_25ns.xml
- 183 • data16\_13TeV.periodAllYear\_DetStatus-v88-pro20-21\_DQDefects-00-02-04  
 184 \_PHYS\_StandardGRL\_All\_Good\_25ns.xml
- 185 • data17\_13TeV.periodAllYear\_DetStatus-v97-pro21-13\_Unknown\_PHYS\_StandardGRL  
 186 \_All\_Good\_25ns\_Triggerno17e33prim.xml
- 187 • data18\_13TeV.periodAllYear\_DetStatus-v102-pro22-04\_Unknown\_PHYS\_StandardGRL  
 188 \_All\_Good\_25ns\_Triggerno17e33prim.xml

189 Runs included from the AllYear period containers are included.

### 190 3.2 Monte Carlo Samples

191 Several different generators were used to produce Monte Carlo simulations of the signal and  
 192 background processes. For all samples, the response of the ATLAS detector is simulated using  
 193 GEANT4 [4]. The WZ signal samples are simulated using Sherpa 2.2.2 [5]. Signal events are  
 194 generated using NNPDF30NNLO PDF set with up to one parton at NLO and 2 to 3 partons at  
 195 LO [**Butterworth:2015oua**].

196 The tZ background is simulated at NLO with MADGRAPH5\_AMC@NLO, with PYTHIA8 used to  
 197 perform parton showering and fragmentation. The NNPDF30NNLO PDF set is used.

198 Specific information about the Monte Carlo samples being used can be found in Table 1. A list  
 199 of the specific samples used by data set ID is shown in Table 2.

Table 1: The configurations used for event generation of signal and background processes, including the event generator, matrix element (ME) order, parton shower algorithm, and parton distribution function (PDF).

Process	Event generator	ME order	Parton Shower	PDF
WZ, VV	SHERPA 2.2.2	MEPS NLO	SHERPA	CT10 [6]
tZ	MG5_AMC [7]	NLO	PYTHIA 8	CTEQ6L1
t̄W	MG5_AMC (SHERPA 2.1.1)	NLO (LO multileg)	PYTHIA 8 (SHERPA)	NNPDF 3.0 NLO (NNPDF 3.0 NLO)
t̄(Z/γ* → ll)	MG5_AMC	NLO	PYTHIA 8	NNPDF 3.0 NLO
t̄H	MG5_AMC (MG5_AMC)	NLO (NLO)	PYTHIA 8 (HERWIG++) [9]	NNPDF 3.0 NLO [8] (CT10 [6])
tHqb	MG5_AMC	LO	PYTHIA 8	CT10
tHW	MG5_AMC (SHERPA 2.1.1)	NLO (LO multileg)	HERWIG++ (SHERPA)	CT10 (NNPDF 3.0 NLO)
tWZ	MG5_AMC	NLO	PYTHIA 8	NNPDF 2.3 LO
t̄t, t̄t̄t̄	MG5_AMC	LO	PYTHIA 8	NNPDF 2.3 LO [10]
t̄tW+W-	MG5_AMC	LO	PYTHIA 8	NNPDF 2.3 LO
t̄t	POWHEG-BOX v2 [11]	NLO	PYTHIA 8	NNPDF 3.0 NLO
t̄t̄γ	MG5_AMC	LO	PYTHIA 8	NNPDF 2.3 LO
s-, t-channel, Wt single top	POWHEG-BOX v1 [12]	NLO	PYTHIA 6	CT10
qqVV, VVV Z → l+l-	SHERPA 2.2.1	MEPS NLO	SHERPA	NNPDF 3.0 NLO

Sample	DSID
WZ	364253, 364739-42
VV	364250, 364254, 364255, 363355-60, 364890
t̄W	410155
t̄Z	410156, 410157, 410218-20
low mass t̄Z	410276-8
Rare Top	410397, 410398, 410399
single Top	410658-9, 410644-5
three Top	304014
four Top	410080
t̄WW	410081
Z + jets	364100-41
low mass Z + jets	364198-215
W + jets	364156-97
Vγ	364500-35
tZ	412063-5
tW	410013-4
WtZ	410408
VVV	364242-9
VH	342284-5
WtH	341998
t̄tγ	410389
t̄t	410470
t̄tH	345873-5, 346343-5

Table 2: List of Monte Carlo samples by data set ID used in the analysis.

## 200 4 Object Reconstruction

201 All regions defined in this analysis share a common lepton, jet, and overall event preselection.  
 202 The selection applied to each physics object is detailed here; the event preselection, and the  
 203 selection used to define the various fit regions, is described in Section 5.

### 204 4.1 Trigger

205 Events are required to be selected by dilepton triggers, as summarized in Table 3.

Dilepton triggers (2015)	
$\mu\mu$ (asymm.)	HLT_mu18_mu8noL1
$ee$ (symm.)	HLT_2e12_lhloose_L12EM10VH
$e\mu, \mu e$ ( $\sim$ symm.)	HLT_e17_lhloose_mu14
Dilepton triggers (2016)	
$\mu\mu$ (asymm.)	HLT_mu22_mu8noL1
$ee$ (symm.)	HLT_2e17_lhvloose_nod0
$e\mu, \mu e$ ( $\sim$ symm.)	HLT_e17_lhloose_nod0_mu14
Dilepton triggers (2017)	
$\mu\mu$ (asymm.)	HLT_mu22_mu8noL1
$ee$ (symm.)	HLT_2e24_lhvloose_nod0
$e\mu, \mu e$ ( $\sim$ symm.)	HLT_e17_lhloose_nod0_mu14
Dilepton triggers (2018)	
$\mu\mu$ (asymm.)	HLT_mu22_mu8noL1
$ee$ (symm.)	HLT_2e24_lhvloose_nod0
$e\mu, \mu e$ ( $\sim$ symm.)	HLT_e17_lhloose_nod0_mu14

Table 3: List of lowest  $p_T$ -threshold, un-prescaled dilepton triggers used for 2015-2018 data taking.

## 4.2 Light leptons

- 207 Electron candidates are reconstructed from energy clusters in the electromagnetic calorimeter  
 208 that are associated with charged particle tracks reconstructed in the inner detector [13]. Electron  
 209 candidates are required to have  $p_T > 10$  GeV and  $|\eta_{\text{cluster}}| < 2.47$ . Muon candidates are  
 210 reconstructed by combining inner detector tracks with track segments or full tracks in the muon  
 211 spectrometer [14]. Muon candidates are required to have  $p_T > 10$  GeV and  $|\eta| < 2.5$ . Candidates  
 212 in the transition region between different electromagnetic calorimeter components,  $1.37 <$   
 213  $|\eta_{\text{cluster}}| < 1.52$ , are rejected. A multivariate likelihood discriminant combining shower shape  
 214 and track information is used to distinguish real electrons from hadronic showers (fake electrons).  
 215 To further reduce the non-prompt electron contribution, the track is required to be consistent  
 216 with originating from the primary vertex; requirements are imposed on the transverse impact  
 217 parameter significance ( $|d_0|/\sigma_{d_0} < 5$ ) and the longitudinal impact parameter ( $|\Delta z_0 \sin \theta_\ell| < 0.5$   
 218 mm). Electron candidates are required to pass TightLH identification.
- 219 Muon candidates are reconstructed by combining inner detector tracks with track segments or  
 220 full tracks in the muon spectrometer [14]. Muon candidates are required to have  $p_T > 10$  GeV  
 221 and  $|\eta| < 2.5$ . The longitudinal impact parameter is the same for both electrons and muons, while  
 222 muons are required to pass a slightly tighter transverse impact parameter,  $|d_0|/\sigma_{d_0} < 3$ . Muons  
 223 are also required to pass Medium ID requirements.

224 Leptons are additionally required to pass a non-prompt BDT selection developed by the  $t\bar{t}H$   
225 multilepton/ $t\bar{t}W$  analysis group. This BDT and the WPs used are summarized in Appendix A.1,  
226 and described in detail in [15]. Optimized working points and scale factors for this BDT are  
227 taken from that analysis.

### 228 4.3 Jets

229 Jets are reconstructed from calibrated topological clusters built from energy deposits in the  
230 calorimeters [16], using the anti- $k_t$  algorithm with a radius parameter  $R = 0.4$ . Particle Flow,  
231 or PFlow, jets are used in the analysis. Jets with energy contributions likely arising from noise  
232 or detector effects are removed from consideration [17], and only jets satisfying  $p_T > 25$  GeV  
233 and  $|\eta| < 2.5$  are used in this analysis. For jets with  $p_T < 60$  GeV and  $|\eta| < 2.4$ , a jet-track  
234 association algorithm is used to confirm that the jet originates from the selected primary vertex,  
235 in order to reject jets arising from pileup collisions [18].

### 236 4.4 B-tagged Jets

237 In order to make a measurement of  $WZ +$  heavy flavor it is necessary to distinguish these events  
238 from  $WZ +$  light jets. For this purpose, the DL1r b-tagging algorithm is used to distinguish  
239 heavy flavor jets from lighter ones. The DL1r algorithm uses jet kinematics, particularly jet  
240 vertex information, as input for a neural network which assigns each jet a score designed to  
241 reflect how likely that jet is to have originated from a b-quark.

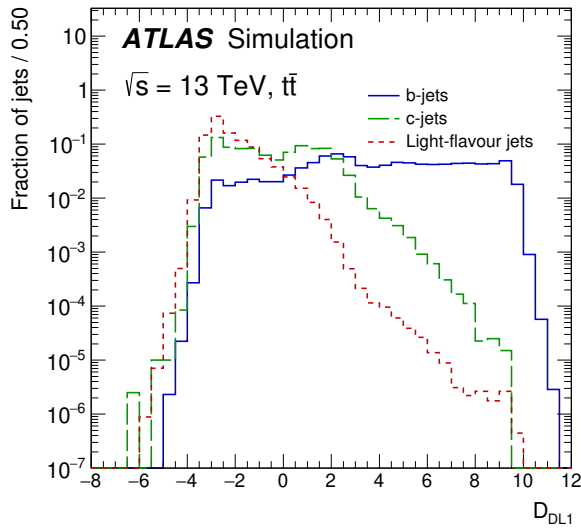


Figure 1: Output distribution of the DL1r algorithm for b-jets, charm jets, and light jets

242 From the output of the BDT, working points (WPs) are developed based on the efficiency of truth  
 243 b-jets at particular values of the DL1r algorithm. These WPs are taken from the March 2020 CDI  
 244 file, 2020-21-13TeV-MC16-CDI-2020-03-11\_v2.root. The working points used in this analysis  
 245 are summarized in Table 4.

WP	Rejection	
	b-jet eff.	c-jet
85%	2.6	29
77%	4.9	130
70%	9.4	390
60%	27	1300

Table 4: c-jet and light-flavor jet rejections corresponding to each b-tagging Working Point by b-jet efficiency, evaluated on  $t\bar{t}$  events.

246 As shown in table 4, a tighter WP will accept fewer b-jets, but reject a higher fraction of charm  
 247 and light jets. Generally, analyses that include b-jets will use a fixed working point, for example,  
 248 requiring that a jet pass the 70% threshold. By instead treating these working point as bins, e.g.  
 249 events with jets that fall between the 85% and 77% WPs fall into one bin, while events with jets  
 250 passing the 60% WP fall into another, additional information can be gained. This analysis uses  
 251 each of these working points to form orthogonal regions in order to provide separation between  
 252 WZ + b, WZ + c, and WZ + light.

#### 253 4.5 Missing transverse energy

254 Missing transverse momentum ( $E_T^{\text{miss}}$ ) is used as part of the event selection. The missing  
 255 transverse momentum vector is defined as the inverse of the sum of the transverse momenta of  
 256 all reconstructed physics objects as well as remaining unclustered energy, the latter of which is  
 257 estimated from low- $p_T$  tracks associated with the primary vertex but not assigned to a hard object,  
 258 with object definitions taken from [19]. Light leptons considered in the  $E_T^{\text{miss}}$  reconstruction are  
 259 required to have  $p_T > 10$  GeV, while jets are required to have  $p_T > 20$  GeV.

#### 260 4.6 Overlap removal

261 To avoid double counting objects and remove leptons originating from decays of hadrons, overlap  
 262 removal is performed in the following order: any electron candidate within  $\Delta R = 0.1$  of another  
 263 electron candidate with higher  $p_T$  is removed; any electron candidate within  $\Delta R = 0.1$  of a muon  
 264 candidate is removed; any jet within  $\Delta R = 0.3$  of an electron candidate is removed; if a muon  
 265 candidate and a jet lie within  $\Delta R = \min(0.4, 0.04 + 10[\text{GeV}] / p_T(\text{muon}))$  of each other, the jet  
 266 is kept and the muon is removed.

267 This algorithm is applied to the preselected objects. The overlap removal procedure is summarized  
 268 in Table 5.

Keep	Remove	Cone size ( $\Delta R$ )
electron	electron (low $p_T$ )	0.1
muon	electron	0.1
electron	jet	0.3
jet	muon	$\min(0.4, 0.04 + 10[\text{GeV}]/p_T(\text{muon}))$
electron	tau	0.2

Table 5: Summary of the overlap removal procedure between electrons, muons, and jets.

## 269 5 Event Selection and Signal Region Definitions

270 Event are required to pass a preselection described in Section 5.1 and summarized in Table 6.  
 271 Those that pass this preselection are divided into various fit regions described in Section 5.2,  
 272 based on the number of jets in the event, and the b-tag score of those jets.

### 273 5.1 Event Preselection

274 Events are required to include exactly three reconstructed light leptons passing the requirement  
 275 described in 4.2, which have a total charge of  $\pm 1$ .

276 The leptons are ordered in the analysis code as 0, 1, and 2. Lepton 0 is the lepton whose charge  
 277 is opposite the other two. Lepton 1 is the lepton closest to the opposite charge lepton, i.e. the  
 278 smallest  $\Delta R$ , leaving lepton 2 as the lepton further from the opposite charge lepton. Lepton 0  
 279 is required to have  $p_T > 10 \text{ GeV}$ , while the same sign leptons, 1 and 2, are required to have  
 280  $p_T > 20 \text{ GeV}$  to reduce the contribution of non-prompt leptons.

281 The invariant mass of at least one pair of opposite sign, same flavor leptons is required to fall  
 282 within 10 GeV of the mass of the Z boson, 91.2 GeV. Events where one of the opposite sign pairs  
 283 have an invariant mass less than 12 GeV are rejected in order to suppress low mass resonances.

284 An additional requirement is placed on the missing transverse energy,  $E_T^{\text{miss}} > 20 \text{ GeV}$ , and the  
 285 transverse mass of the W candidate,  $m(E_T^{\text{miss}} + l_{\text{other}}) > 30 \text{ GeV}$ , defined as  $\sqrt{2p_T^{\text{lep}} E_T^{\text{miss}} * (1 - \cos(\phi_{\text{lep}} - \phi_{E_T^{\text{miss}}}))}$ .  
 286 Here  $E_T^{\text{miss}}$  is the missing transverse energy, and  $l_{\text{other}}$  is the lepton not included in the Z-  
 287 candidate.

288 Events are required to have one or two reconstructed jets passing the selection described in  
 289 Section 4.3. Events with more than two jets are rejected in order to reduce the contribution of  
 290 backgrounds such as  $t\bar{t}Z$  and  $t\bar{t}W$ , which tend to have higher jet multiplicity.

Event Selection
Exactly three leptons with charge $\pm 1$
Two same-charge leptons with $p_T > 20$ GeV
One opposite charge lepton with $p_T > 10$ GeV
$m(l^+l^-)$ within 10 GeV of 91.2 GeV
Transverse mass of W-candidate, $\sqrt{2p_T^{lep}E_T^{\text{miss}} * (1 - \cos(\phi_{lep} - \phi_{E_T^{\text{miss}}}))} > 30$ GeV
Missing transverse energy, $E_T^{\text{miss}} > 20$ GeV
One or two jets with $p_T > 25$ GeV

Table 6: Summary of the selection applied to events for inclusion in the fit

291 The event yields in the preselection region for both data and Monte Carlo are summarized in  
 292 Table 5.1, which shows good agreement between data and Monte Carlo, and demonstrates that  
 293 this region consists primarily of WZ events. The WZ events are split into WZ + b, WZ + c, and  
 294 WZ + l based on the truth flavor of the associated jet in the event. Specifically, this determination  
 295 is made based on the HadronConeExclTruthLabelID of the jet, as recommended by the b-  
 296 tagging working group [20]. In this ordering b-jet supersedes charm, which supersedes light. That  
 297 is, WZ + l events contain no charm and no b jets at truth level, WZ + c contain at least one truth  
 298 charm and no b-jets, and WZ + b contains at least one truth b-jet.

Process	Events
WZ + b	$167.6 \pm 6.5$
WZ + c	$1080 \pm 40$
WZ + l	$7220 \pm 310$
Other VV	$850 \pm 140$
t̄tW	$16.8 \pm 2.3$
t̄tZ	$115 \pm 17$
rare Top	$2.2 \pm 0.1$
Single top	$0.10 \pm 0.45$
Three top	$0.01 \pm 0.01$
Four top	$0.02 \pm 0.01$
t̄tWW	$0.23 \pm 0.05$
Z + jets	$600 \pm 260$
V + $\gamma$	$37 \pm 54$
tZ	$190 \pm 70$
tW	$5.5 \pm 1.2$
WtZ	$25.8 \pm 1.1$
VVV	$26.2 \pm 0.9$
VH	$94 \pm 7$
t̄t	$108.68 \pm 8$
t̄tH	$4.3 \pm 0.5$
Total	$10600 \pm 530$
Data	10574

Table 7: Event yields in the preselection region at  $139.0 \text{ fb}^{-1}$ 

<sup>299</sup> Here Other VV represents diboson processes other than WZ, and consists predominantly of  
<sup>300</sup>  $ZZ \rightarrow ll\bar{l}\bar{l}$  events where one of the leptons is not reconstructed.

<sup>301</sup> Simulations are further validated by comparing the kinematic distributions of the Monte Carlo  
<sup>302</sup> with data, which are shown in Figure 2. Here, bins with 5% or more WZ+b are blinded.

## WZ Fit Region - Inclusive

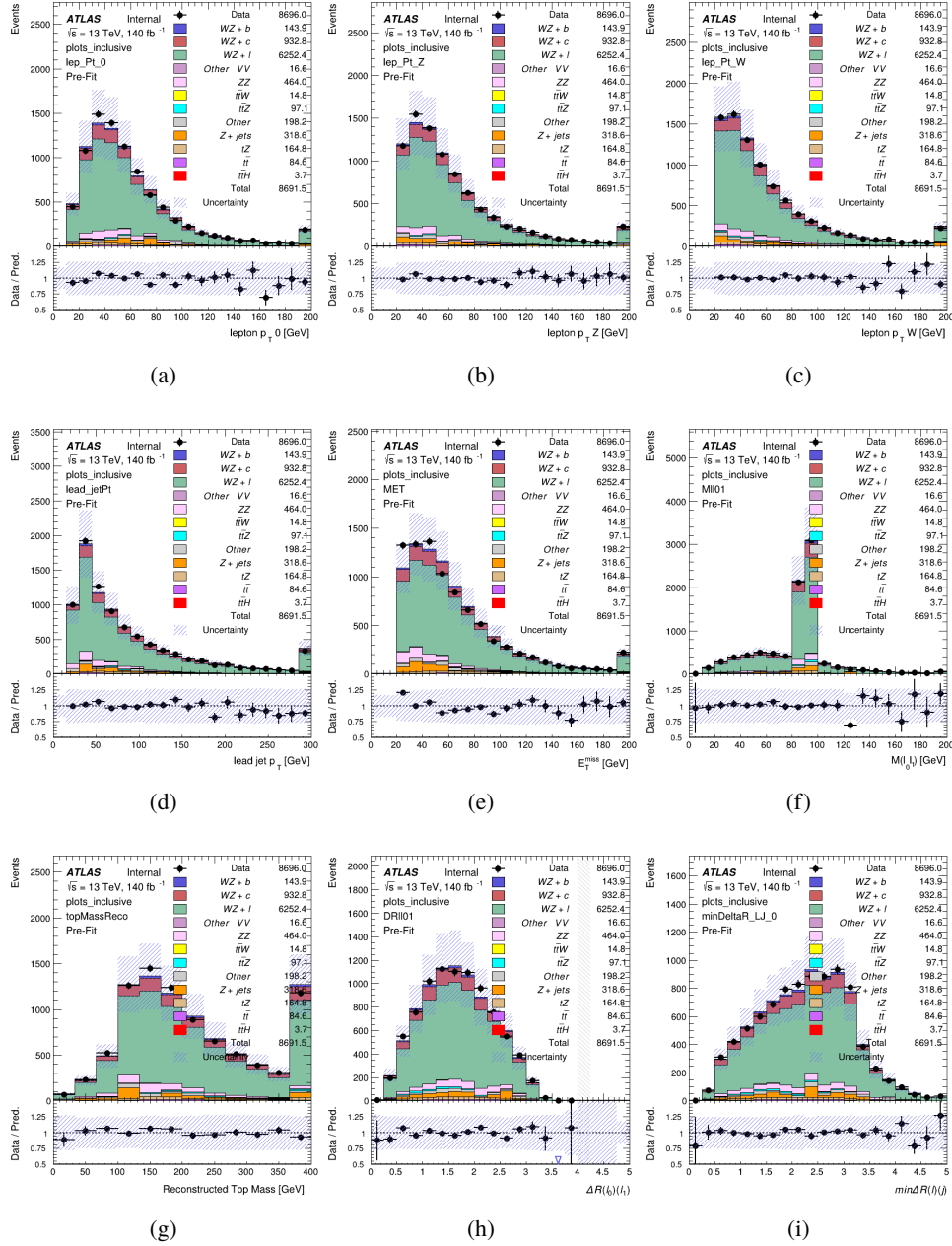


Figure 2: Comparisons between the data and MC distributions in the preselection region for (a) the  $p_T$  of the opposite sign lepton, (b) the  $p_T$  of the other lepton from the Z candidate, (c) the  $p_T$  of the lepton from the W candidate, (d) the leading jet  $p_T$ , (e) the  $E_T^{\text{miss}}$ , and (f) the invariant mass of leptons 0 and 1, (g) the reconstructed top mass, (h)  $\Delta(R)$  between lepton 0 and 1, (i) the  $\Delta(R)$  between the closest lepton and jet.

303 **5.2 Fit Regions**

304 Once preselection has been applied, the remaining events are categorized into one of twelve  
 305 orthogonal regions. The regions used in the fit are summarized in Table 8.

Table 8: A list of the regions used in the fit and the selection used for each.

Region	Selection
1j, <85%	$N_{\text{jets}} = 1, n_{\text{Jets\_DL1r\_85}} = 0$
1j, 85%-77%	$N_{\text{jets}} = 1, n_{\text{Jets\_DL1r\_85}} = 1, n_{\text{Jets\_DL1r\_77}} = 0$
1j, 77%-70%	$N_{\text{jets}} = 1, n_{\text{Jets\_DL1r\_77}} = 1, n_{\text{Jets\_DL1r\_70}} = 0$
1j, 70%-60%	$N_{\text{jets}} = 1, n_{\text{Jets\_DL1r\_70}} = 1, n_{\text{Jets\_DL1r\_60}} = 0$
1j, >60%	$N_{\text{jets}} = 1, n_{\text{Jets\_DL1r\_60}} = 1, tZ \text{ BDT} > 0.12$
1j tZ CR	$N_{\text{jets}} = 1, n_{\text{Jets\_DL1r\_60}} = 1, tZ \text{ BDT} < 0.12$
2j, <85%	$N_{\text{jets}} = 2, n_{\text{Jets\_DL1r\_85}} = 0$
2j, 85%-77%	$N_{\text{jets}} = 2, n_{\text{Jets\_DL1r\_85}} \geq 1, n_{\text{Jets\_DL1r\_77}} = 0$
2j, 77%-70%	$N_{\text{jets}} = 2, n_{\text{Jets\_DL1r\_77}} \geq 1, n_{\text{Jets\_DL1r\_70}} = 0$
2j, 70%-60%	$N_{\text{jets}} = 2, n_{\text{Jets\_DL1r\_70}} \geq 1, n_{\text{Jets\_DL1r\_60}} = 0$
2j, >60%	$N_{\text{jets}} = 2, n_{\text{Jets\_DL1r\_60}} \geq 1, tZ \text{ BDT} > 0.12$
2j tZ CR	$N_{\text{jets}} = 2, n_{\text{Jets\_DL1r\_60}} \geq 1, tZ \text{ BDT} < 0.12$

306 The working points discussed in Section 4.4 are used to separate events into fit regions based on  
 307 the highest working point reached by a jet in each event. Because the background composition  
 308 differs significantly based on the number of b-jets, events are further subdivided into 1-jet and  
 309 2-jet regions in order to minimize the impact of background uncertainties.

310 An unfolding procedure is performed to account for differences in the number of reconstructed  
 311 jets compared to the number of truth jets in each event. The `AntiKt4TruthDressedWZJets`  
 312 truth jet collection is used to make this determination. In order to account for migration of  
 313 WZ+1-jet and WZ+2-jet events between the 1-jet and 2-jet bins at reco level, the signal samples  
 314 are separated based on the number of truth jets. Events with 0 jets or more than 3 jets at truth  
 315 level, yet fall within one of the categories listed in Table 8, are categorized as WZ + other, and  
 316 treated as a background. The migration matrix in the number of jets at truth level versus reco  
 317 level is shown in Figure 3. The composition of the number of truth jets in each reco jet bin is  
 318 taken from MC, with uncertainties in these estimates described in detail in Section 7.

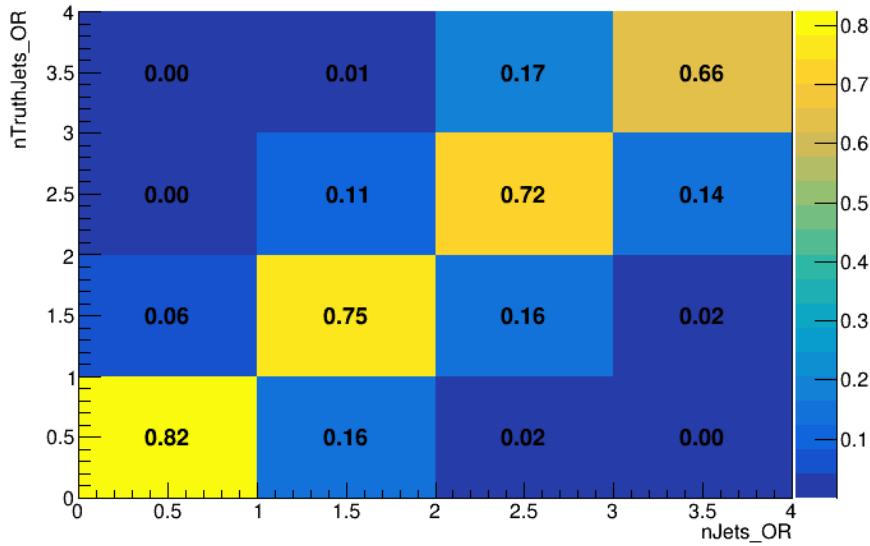


Figure 3: Number of truth jets compared to the number of reconstructed jets in each WZ event falling in the preselection region. Each row is normalized to unity.

319 An additional tZ control region is created based on the BDT described in Section 6. The region  
 320 with 1-jet passing the 60% working point is split in two - a signal enriched region of events with  
 321 a BDT score greater than 0.12, and a tZ control region including events with less than 0.12. This  
 322 cutoff is arrived at by performing an Asimov fit with a variety of cutoffs, and selecting the value  
 323 that produces the highest significance for the measurement of WZ + b.

324 The modeling in each region is validated by comparing data and MC predictions for various  
 325 kinematic distributions. These plot are shown in Figures 4-17.

## WZ Fit Region - 1j Inclusive

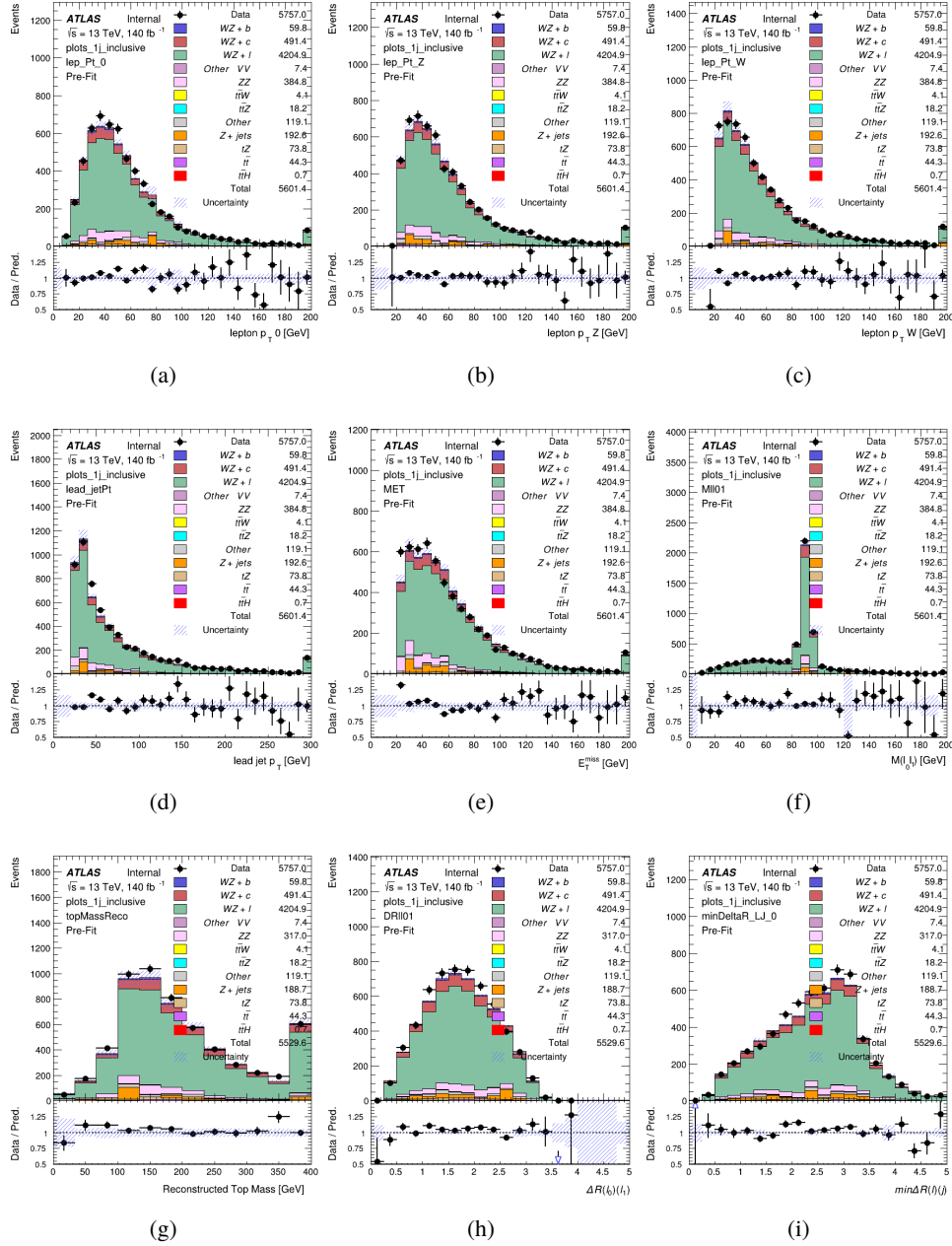


Figure 4: Comparisons between the data and MC distributions in the preselection region for (a) the  $p_T$  of the opposite sign lepton, (b) the  $p_T$  of the other lepton from the Z candidate, (c) the  $p_T$  of the lepton from the W candidate, (d) the leading jet  $p_T$ , (e) the  $E_T^{\text{miss}}$ , and (f) the invariant mass of leptons 0 and 1, (g) the reconstructed top mass, (h)  $\Delta(R)$  between lepton 0 and 1, (i) the  $\Delta(R)$  between the closest lepton and jet.

## WZ Fit Region - 1j &lt; 85% WP

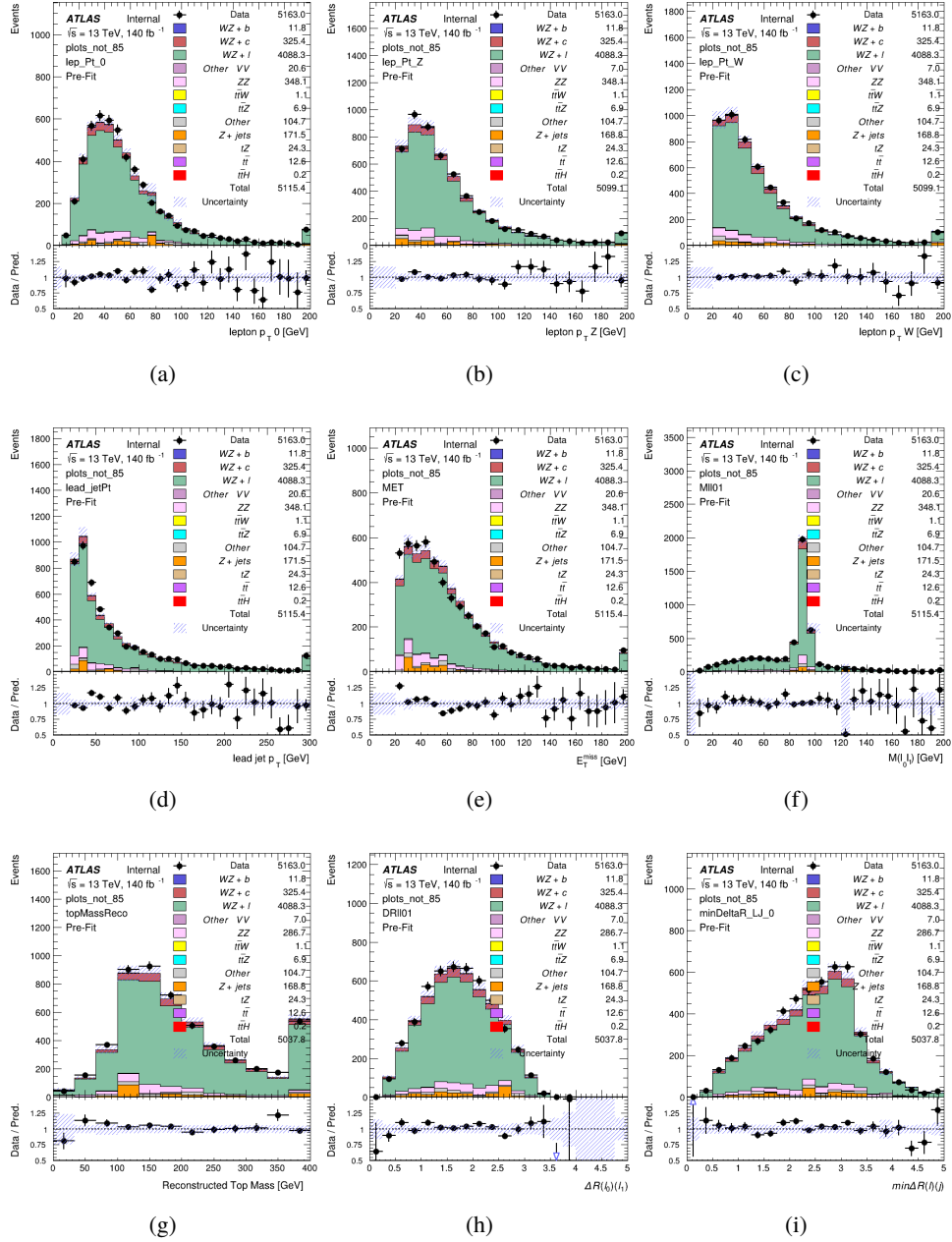


Figure 5: Comparisons between the data and MC distributions in the preselection region for (a) the  $p_T$  of the opposite sign lepton, (b) the  $p_T$  of the other lepton from the Z candidate, (c) the  $p_T$  of the lepton from the W candidate, (d) the leading jet  $p_T$ , (e) the  $E_T^{\text{miss}}$ , and (f) the invariant mass of leptons 0 and 1, (g) the reconstructed top mass, (h)  $\Delta(R)$  between lepton 0 and 1, (i) the  $\Delta(R)$  between the closest lepton and jet.

## WZ Fit Region - 1j 77-85% WP

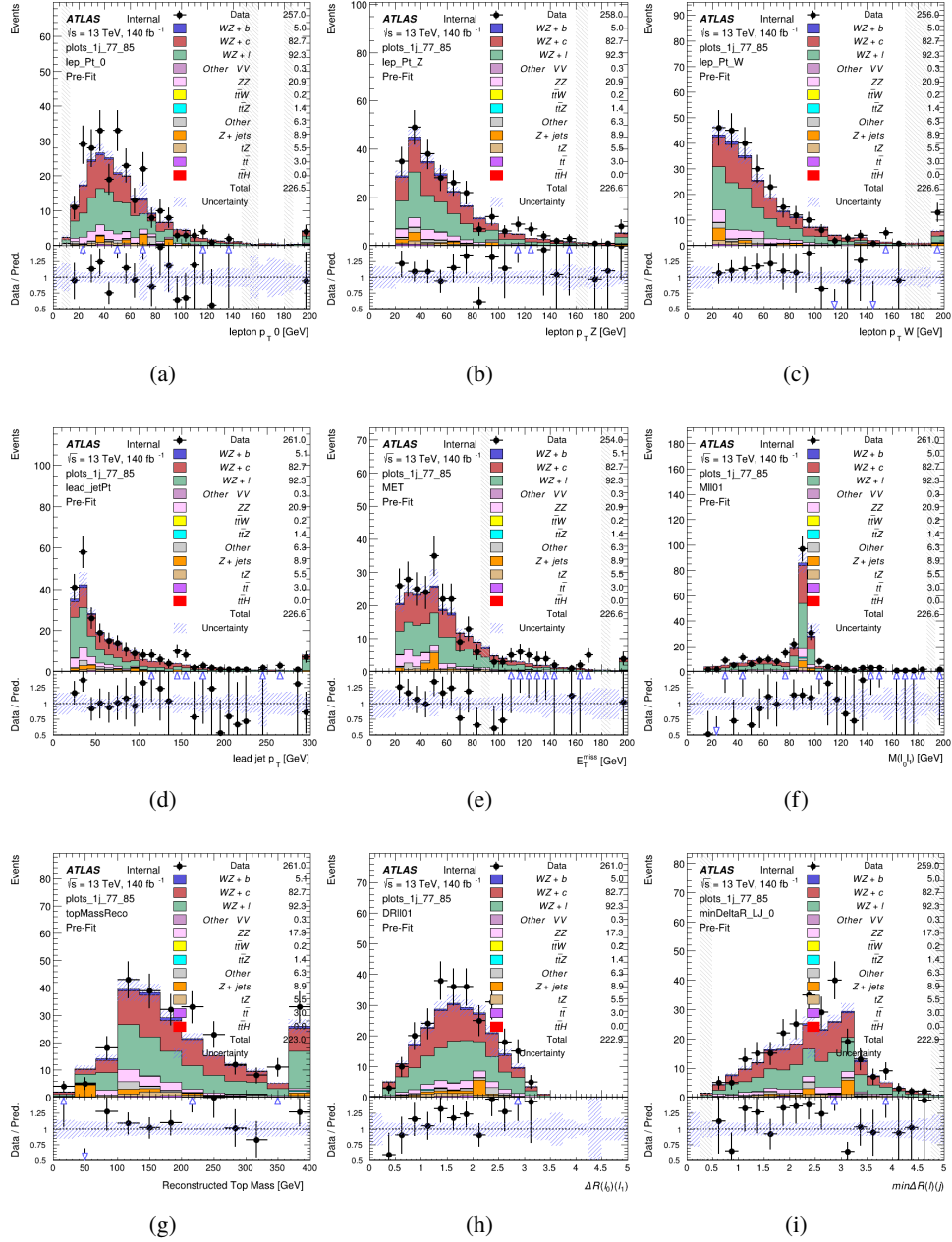


Figure 6: Comparisons between the data and MC distributions in the preselection region for (a) the  $p_T$  of the opposite sign lepton, (b) the  $p_T$  of the other lepton from the Z candidate, (c) the  $p_T$  of the lepton from the W candidate, (d) the leading jet  $p_T$ , (e) the  $E_T^{\text{miss}}$ , and (f) the invariant mass of leptons 0 and 1, (g) the reconstructed top mass, (h)  $\Delta(R)$  between lepton 0 and 1, (i) the  $\Delta(R)$  between the closest lepton and jet.

## WZ Fit Region - 1j 70-77% WP

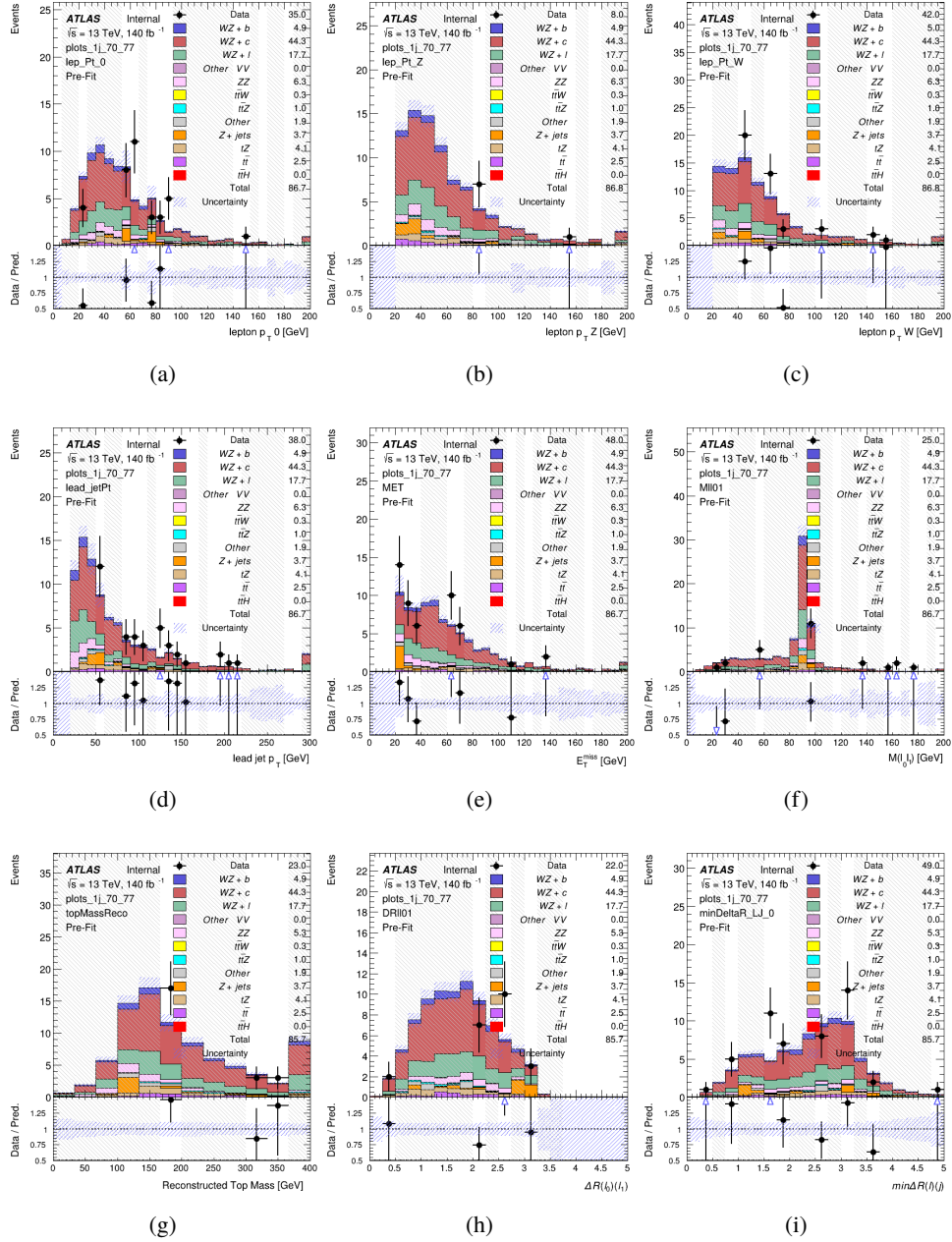


Figure 7: Comparisons between the data and MC distributions in the preselection region for (a) the  $p_T$  of the opposite sign lepton, (b) the  $p_T$  of the other lepton from the Z candidate, (c) the  $p_T$  of the lepton from the W candidate, (d) the leading jet  $p_T$ , (e) the  $E_T^{\text{miss}}$ , and (f) the invariant mass of leptons 0 and 1, (g) the reconstructed top mass, (h)  $\Delta(R)$  between lepton 0 and 1, (i) the  $\Delta(R)$  between the closest lepton and jet.

## WZ Fit Region - 1j 60-70% WP

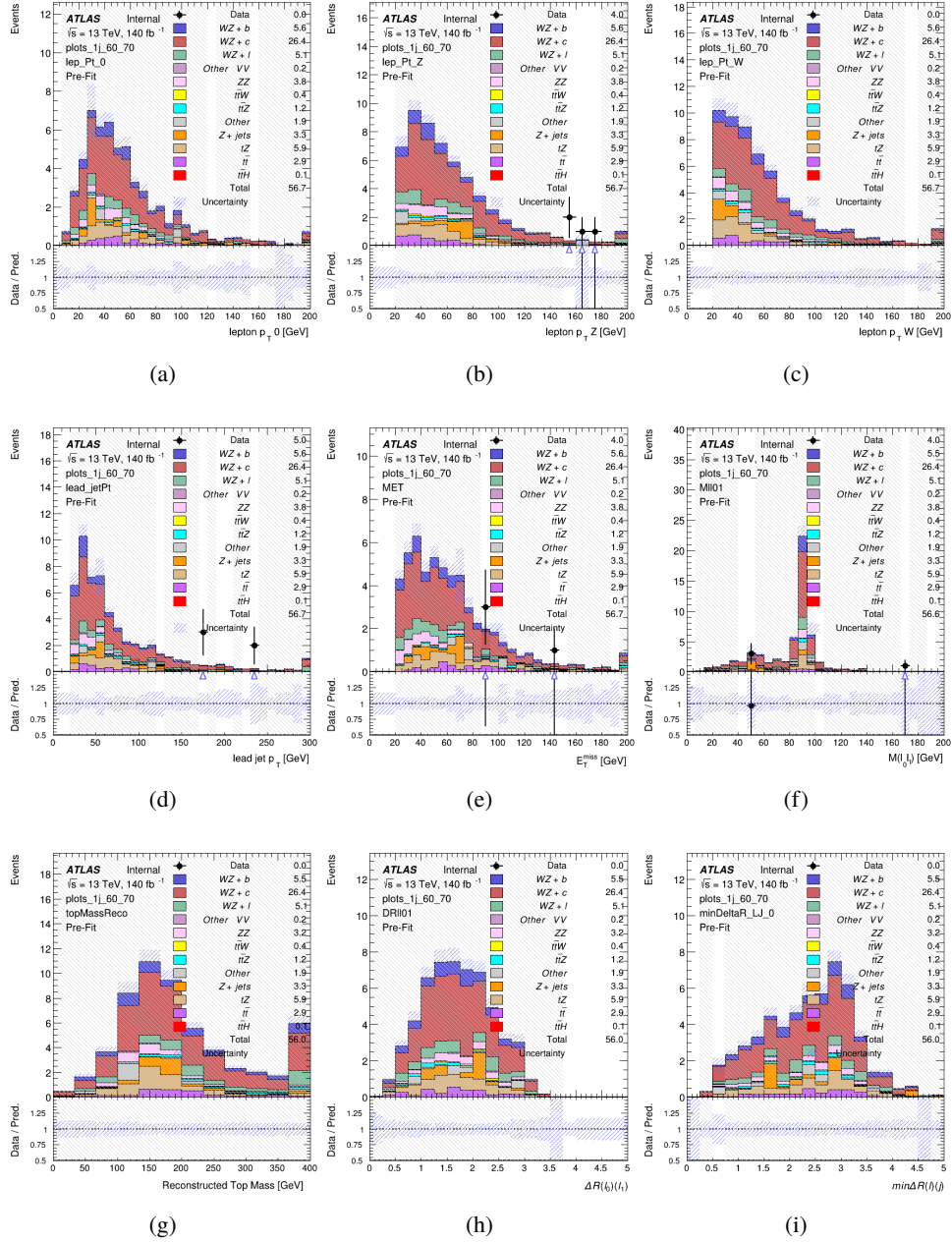


Figure 8: Comparisons between the data and MC distributions in the preselection region for (a) the  $p_T$  of the opposite sign lepton, (b) the  $p_T$  of the other lepton from the Z candidate, (c) the  $p_T$  of the lepton from the W candidate, (d) the leading jet  $p_T$ , (e) the  $E_T^{\text{miss}}$ , and (f) the invariant mass of leptons 0 and 1, (g) the reconstructed top mass, (h)  $\Delta(R)$  between lepton 0 and 1, (i) the  $\Delta(R)$  between the closest lepton and jet.

## WZ Fit Region - 1j 60% WP

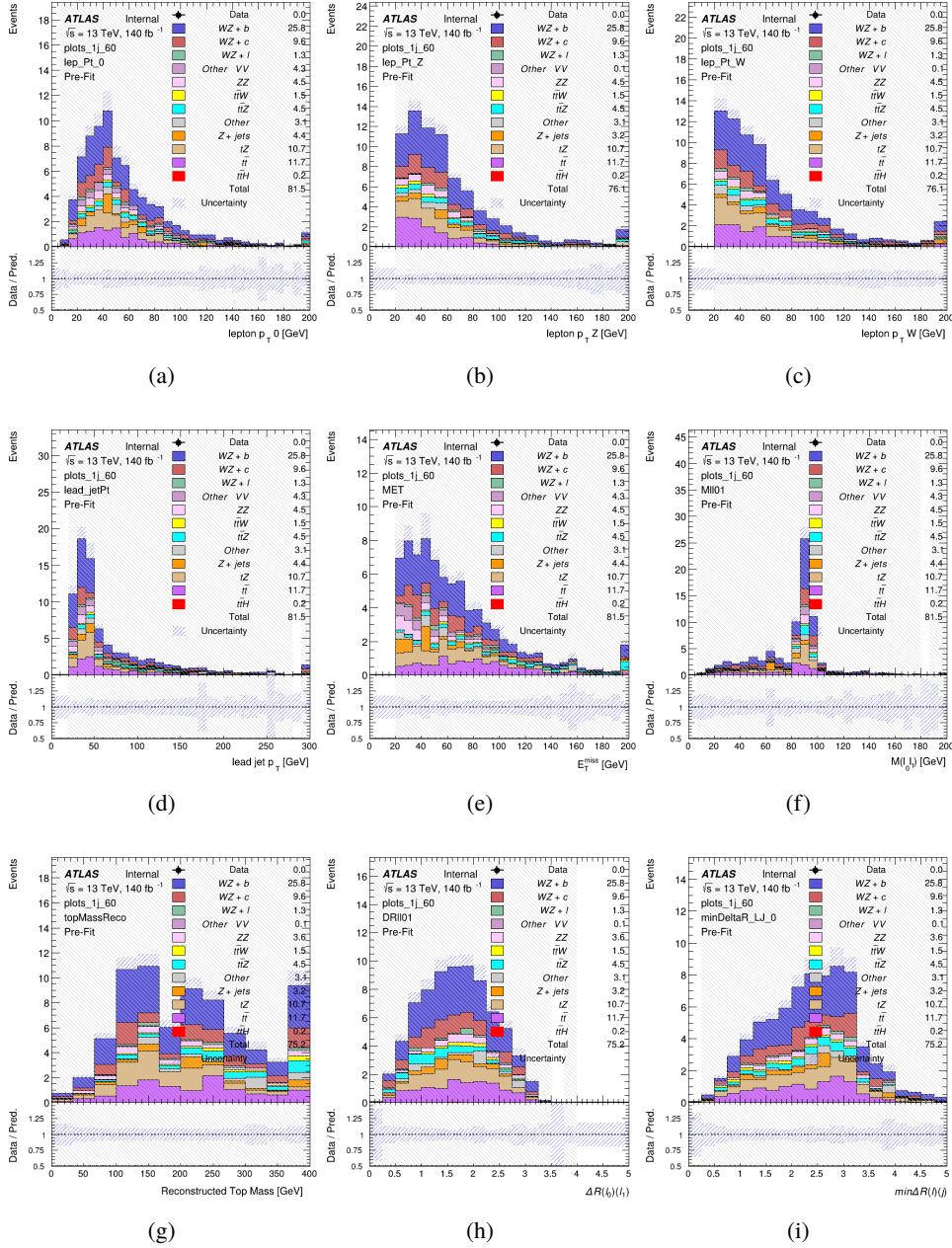


Figure 9: Comparisons between the data and MC distributions in the preselection region for (a) the  $p_T$  of the opposite sign lepton, (b) the  $p_T$  of the other lepton from the Z candidate, (c) the  $p_T$  of the lepton from the W candidate, (d) the leading jet  $p_T$ , (e) the  $E_T^{\text{miss}}$ , and (f) the invariant mass of leptons 0 and 1, (g) the reconstructed top mass, (h)  $\Delta(R)$  between lepton 0 and 1, (i) the  $\Delta(R)$  between the closest lepton and jet.

## WZ Fit Region - tZ-CR

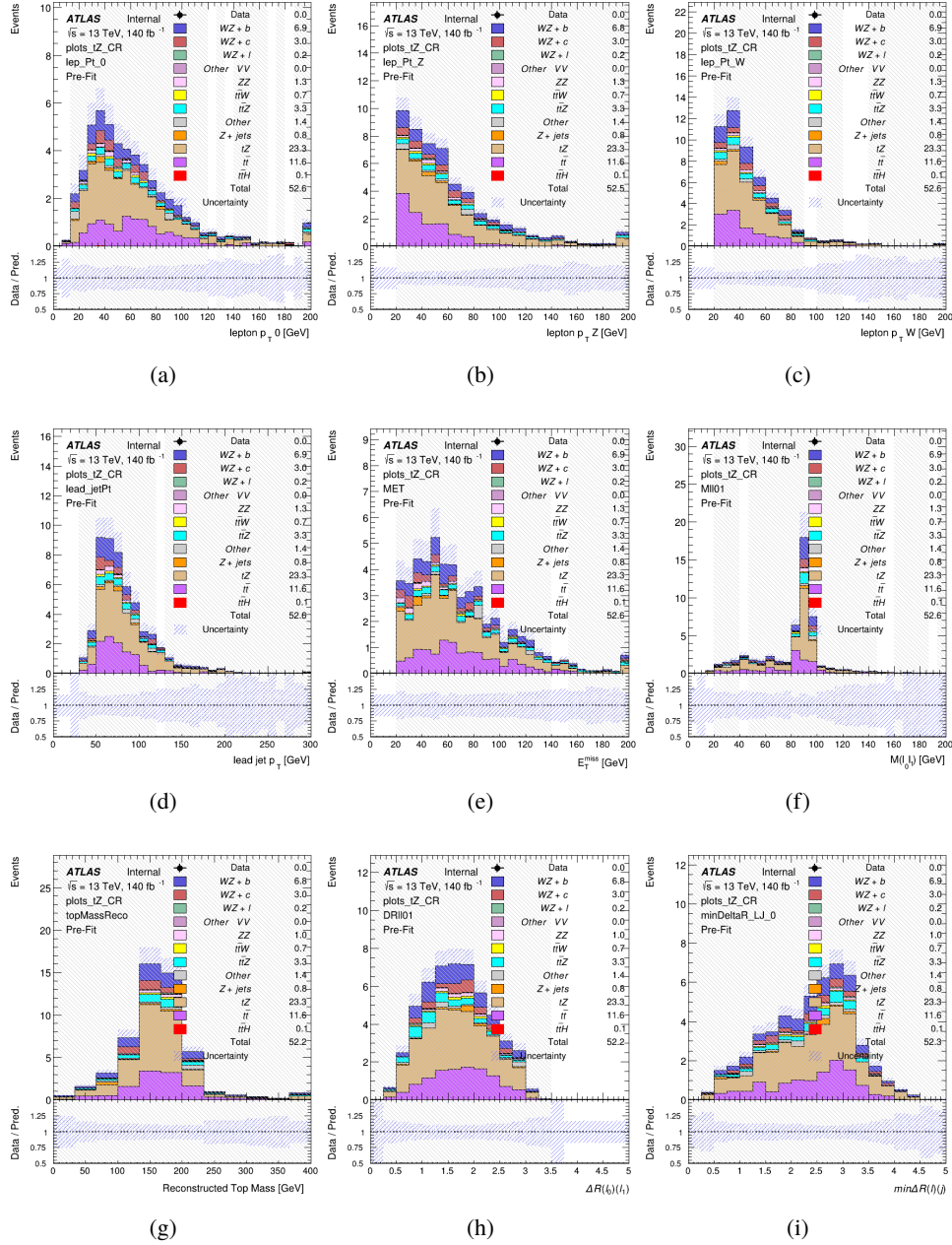


Figure 10: Comparisons between the data and MC distributions in the preselection region for (a) the  $p_T$  of the opposite sign lepton, (b) the  $p_T$  of the other lepton from the Z candidate, (c) the  $p_T$  of the lepton from the W candidate, (d) the leading jet  $p_T$ , (e) the  $E_T^{\text{miss}}$ , and (f) the invariant mass of leptons 0 and 1, (g) the reconstructed top mass, (h)  $\Delta(R)$  between lepton 0 and 1, (i) the  $\Delta(R)$  between the closest lepton and jet.

## WZ Fit Region - 2j Inclusive

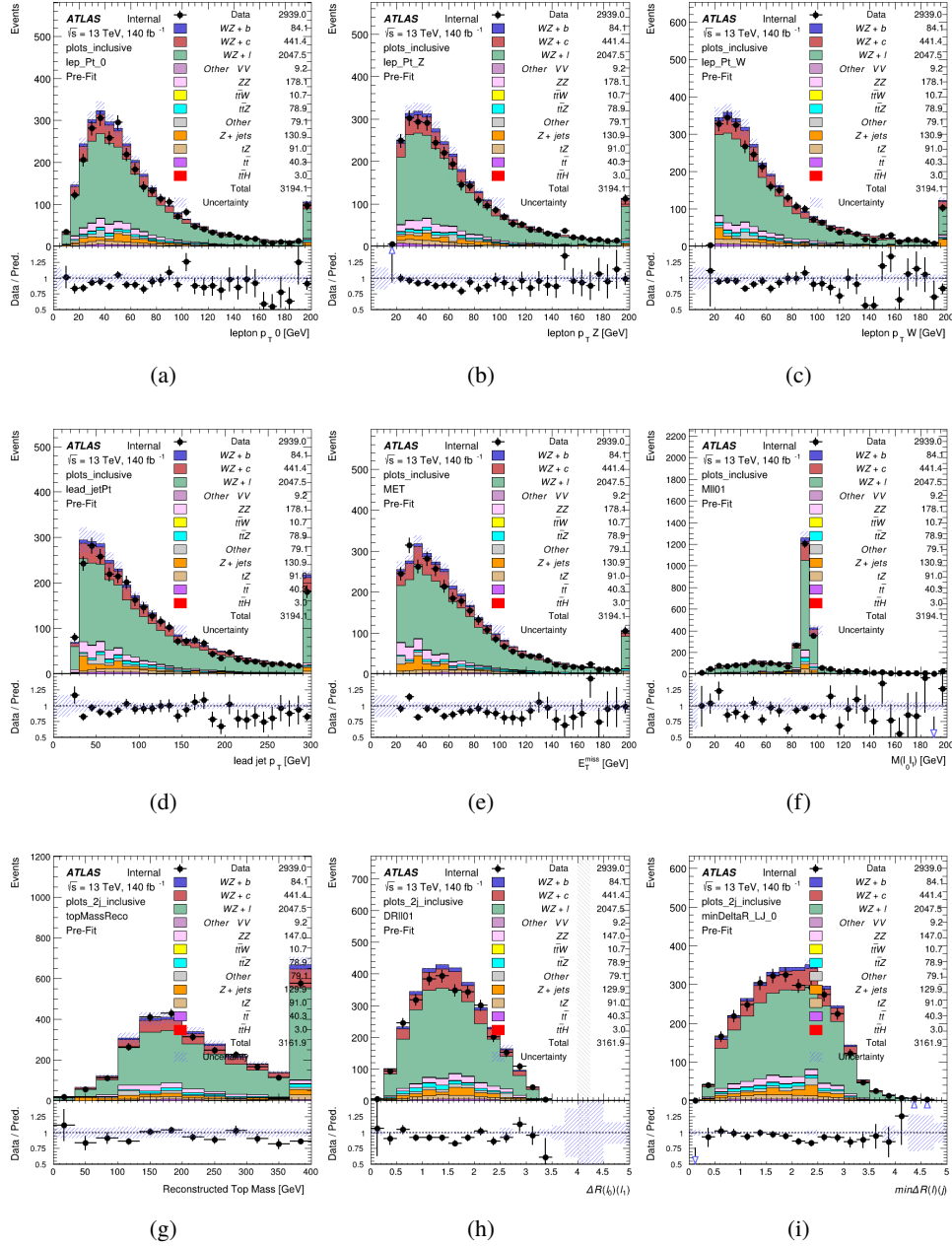


Figure 11: Comparisons between the data and MC distributions in the preselection region for (a) the  $p_T$  of the opposite sign lepton, (b) the  $p_T$  of the other lepton from the Z candidate, (c) the  $p_T$  of the lepton from the W candidate, (d) the leading jet  $p_T$ , (e) the  $E_T^{\text{miss}}$ , and (f) the invariant mass of leptons 0 and 1, (g) the reconstructed top mass, (h)  $\Delta(R)$  between lepton 0 and 1, (i) the  $\Delta(R)$  between the closest lepton and jet.

## WZ Fit Region - 2j &lt; 85% WP

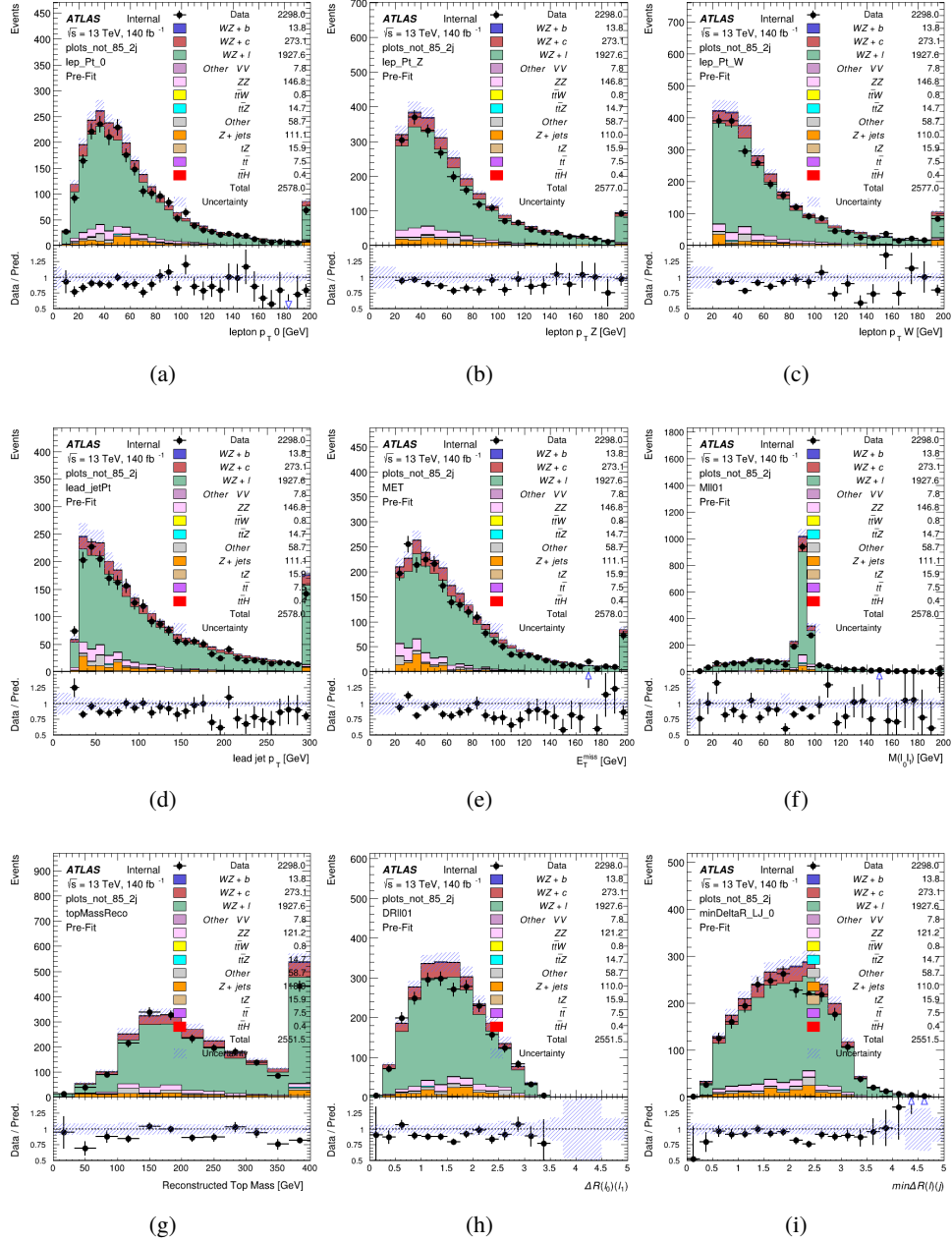


Figure 12: Comparisons between the data and MC distributions in the preselection region for (a) the  $p_T$  of the opposite sign lepton, (b) the  $p_T$  of the other lepton from the Z candidate, (c) the  $p_T$  of the lepton from the W candidate, (d) the leading jet  $p_T$ , (e) the  $E_T^{\text{miss}}$ , and (f) the invariant mass of leptons 0 and 1, (g) the reconstructed top mass, (h)  $\Delta(R)$  between lepton 0 and 1, (i) the  $\Delta(R)$  between the closest lepton and jet.

## WZ Fit Region - 2j 77-85% WP

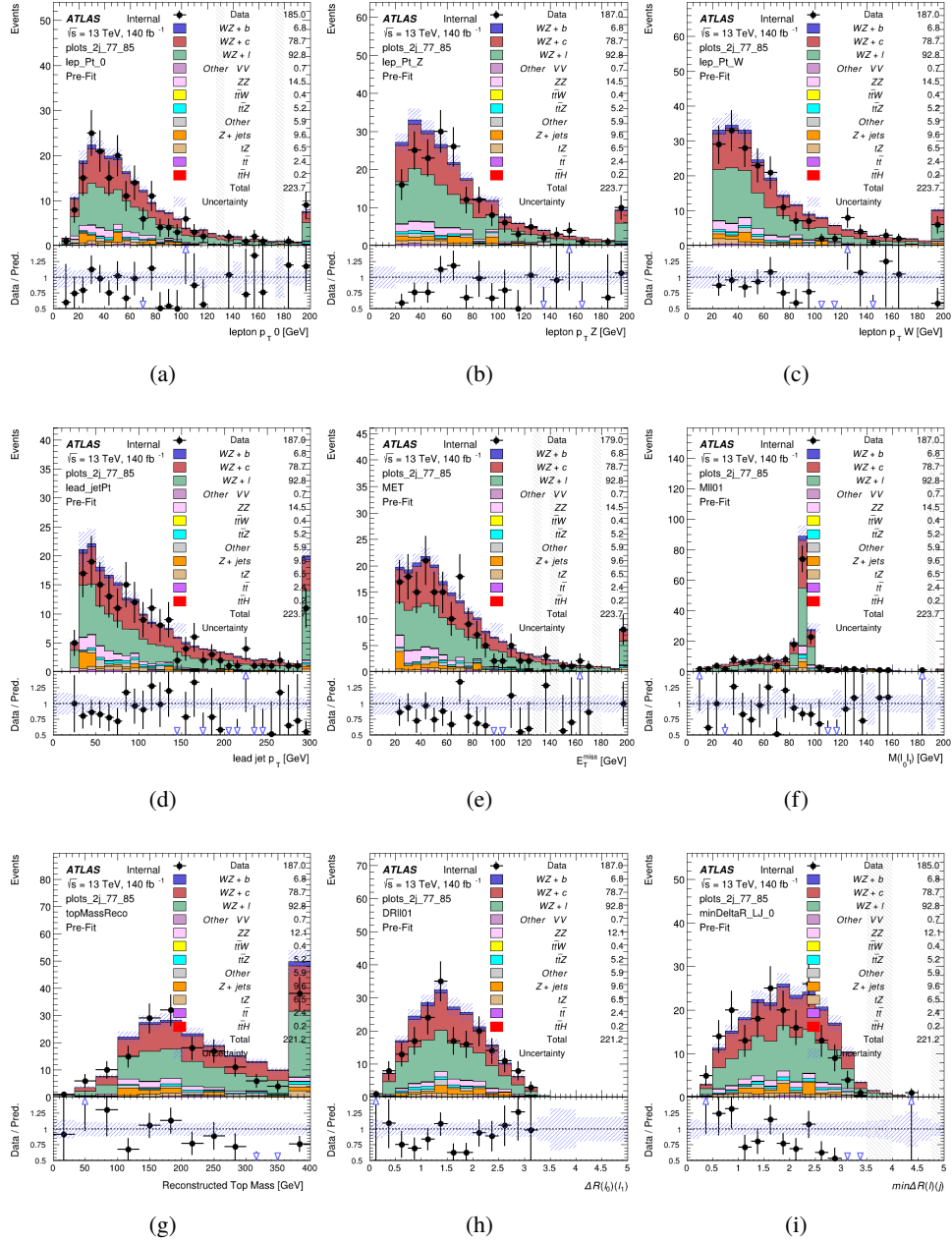


Figure 13: Comparisons between the data and MC distributions in the preselection region for (a) the  $p_T$  of the opposite sign lepton, (b) the  $p_T$  of the other lepton from the Z candidate, (c) the  $p_T$  of the lepton from the W candidate, (d) the leading jet  $p_T$ , (e) the  $E_T^{\text{miss}}$ , and (f) the invariant mass of leptons 0 and 1, (g) the reconstructed top mass, (h)  $\Delta(R)$  between lepton 0 and 1, (i) the  $\Delta(R)$  between the closest lepton and jet.

## WZ Fit Region - 2j 70-77% WP

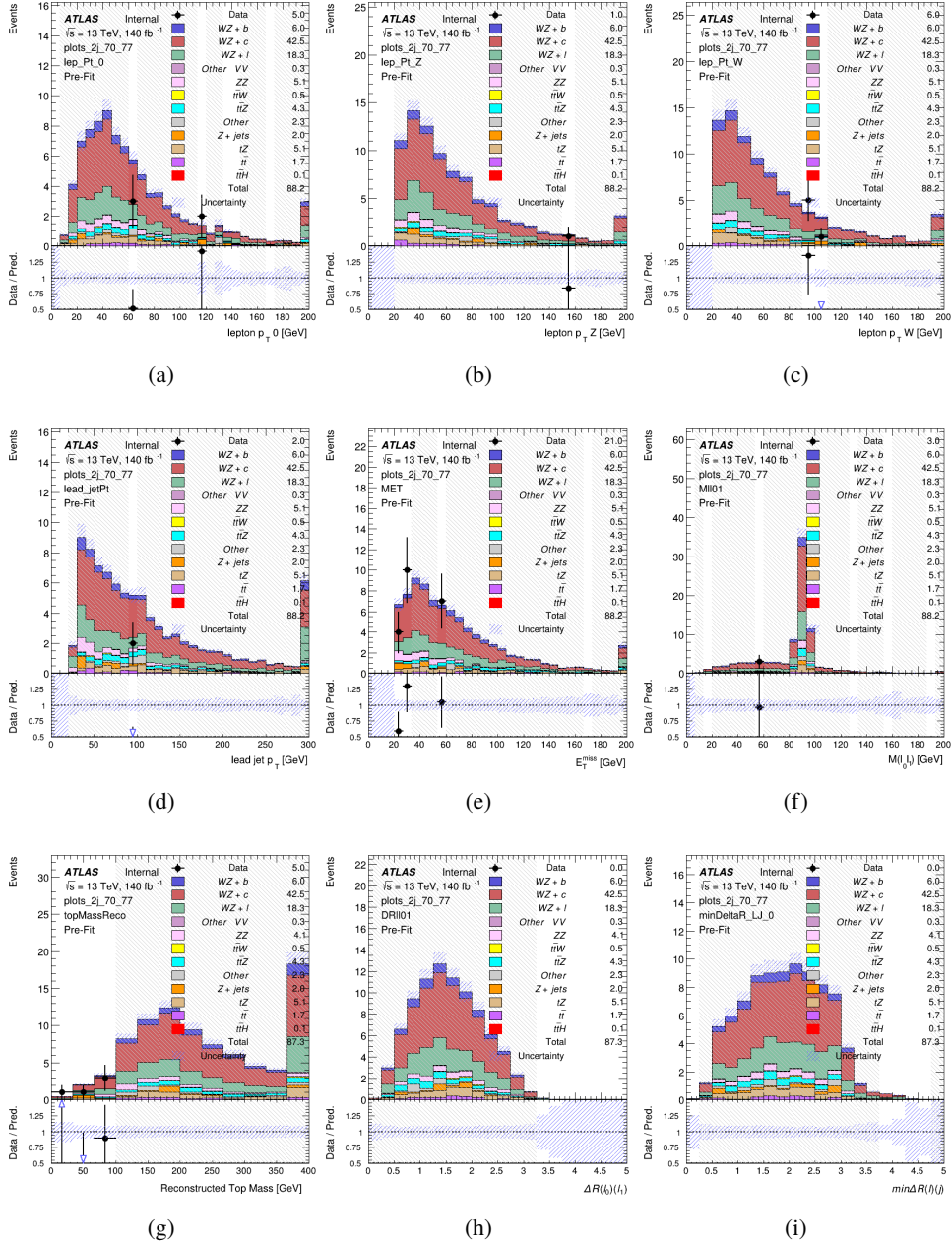


Figure 14: Comparisons between the data and MC distributions in the preselection region for (a) the  $p_T$  of the opposite sign lepton, (b) the  $p_T$  of the other lepton from the Z candidate, (c) the  $p_T$  of the lepton from the W candidate, (d) the leading jet  $p_T$ , (e) the  $E_T^{\text{miss}}$ , and (f) the invariant mass of leptons 0 and 1, (g) the reconstructed top mass, (h)  $\Delta(R)$  between lepton 0 and 1, (i) the  $\Delta(R)$  between the closest lepton and jet.

## WZ Fit Region - 2j 60-70% WP

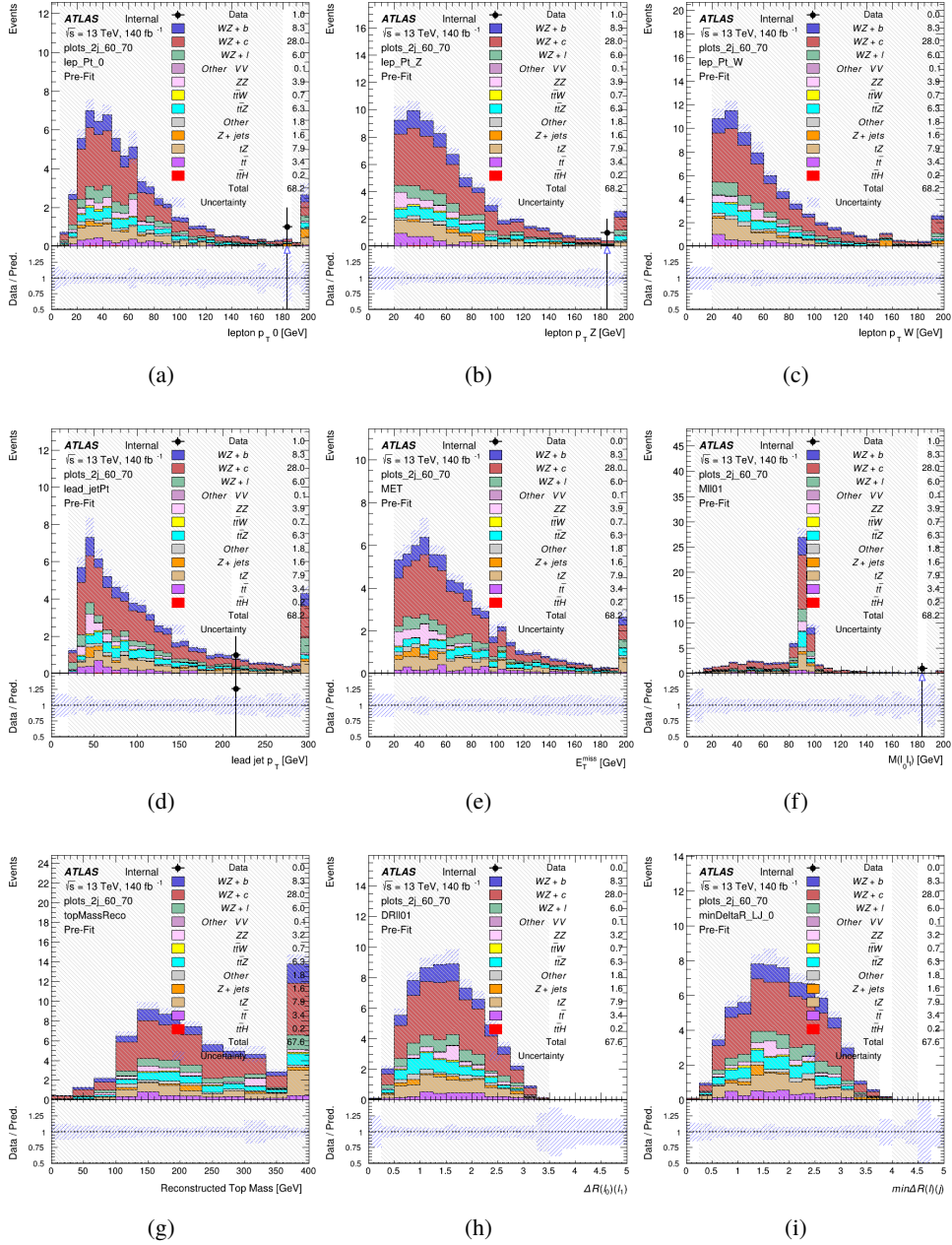


Figure 15: Comparisons between the data and MC distributions in the preselection region for (a) the  $p_T$  of the opposite sign lepton, (b) the  $p_T$  of the other lepton from the Z candidate, (c) the  $p_T$  of the lepton from the W candidate, (d) the leading jet  $p_T$ , (e) the  $E_T^{\text{miss}}$ , and (f) the invariant mass of leptons 0 and 1, (g) the reconstructed top mass, (h)  $\Delta(R)$  between lepton 0 and 1, (i) the  $\Delta(R)$  between the closest lepton and jet.

## WZ Fit Region - 2j 60% WP

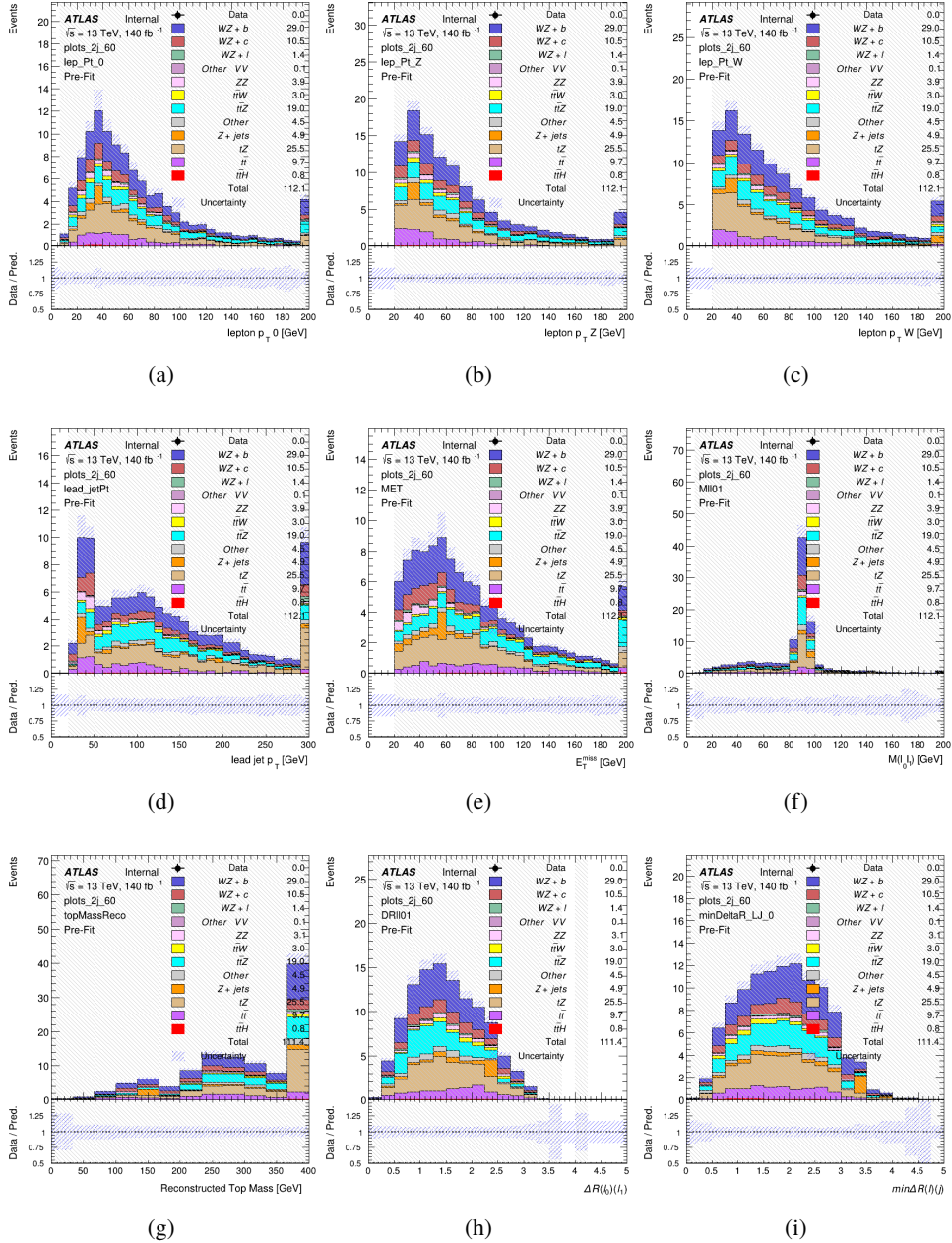


Figure 16: Comparisons between the data and MC distributions in the preselection region for (a) the  $p_T$  of the opposite sign lepton, (b) the  $p_T$  of the other lepton from the Z candidate, (c) the  $p_T$  of the lepton from the W candidate, (d) the leading jet  $p_T$ , (e) the  $E_T^{\text{miss}}$ , and (f) the invariant mass of leptons 0 and 1, (g) the reconstructed top mass, (h)  $\Delta(R)$  between lepton 0 and 1, (i) the  $\Delta(R)$  between the closest lepton and jet.

## WZ Fit Region - tZ-CR-2j

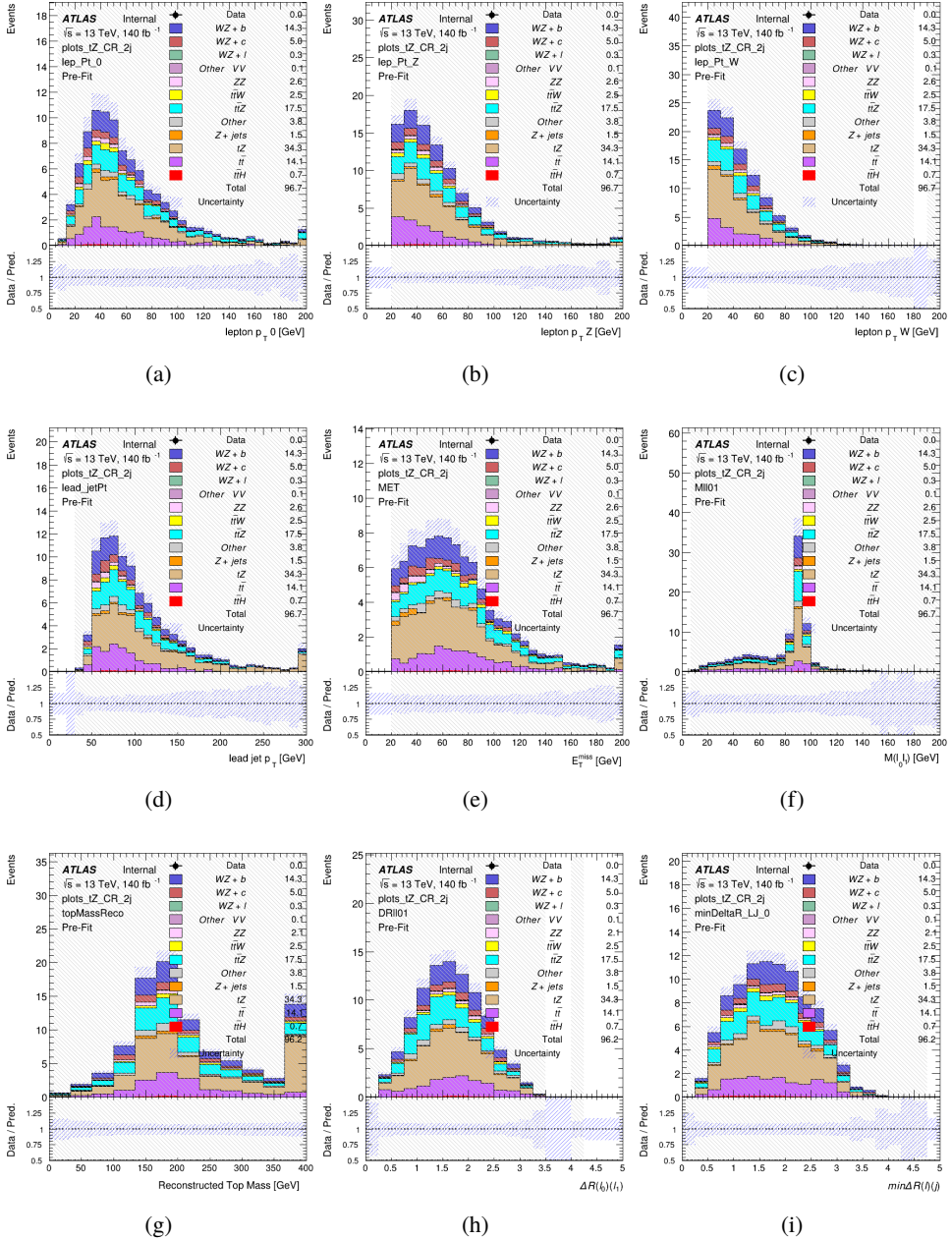


Figure 17: Comparisons between the data and MC distributions in the preselection region for (a) the  $p_T$  of the opposite sign lepton, (b) the  $p_T$  of the other lepton from the Z candidate, (c) the  $p_T$  of the lepton from the W candidate, (d) the leading jet  $p_T$ , (e) the  $E_T^{\text{miss}}$ , and (f) the invariant mass of leptons 0 and 1, (g) the reconstructed top mass, (h)  $\Delta(R)$  between lepton 0 and 1, (i) the  $\Delta(R)$  between the closest lepton and jet.

326 **5.3 Non-Prompt Lepton Estimation**

327 Two processes act as sources of non-prompt leptons appear in the analysis:  $t\bar{t}$  and  $Z+jet$   
328 production both produce two prompt leptons, and each contribute to the 31 region when an  
329 additional non-prompt lepton appears in the event. The contribution of these processes is  
330 estimated with Monte Carlo simulations, which are validated using enriched validation regions.

331 The modelling in the  $Z+jets$  and  $t\bar{t}$  CRs is further validated for each of the pseudo-continuous  
332 b-tag regions used in the analysis. The relevant lepton  $p_T$  spectrum in each b-tag region is shown  
333 in Appendix A.2 for these CRs after the correction factors derived below have been applied.

334 **5.3.1  $t\bar{t}$  Validation**

335  $t\bar{t}$  events can produce two prompt leptons from the decay of each of the tops. These top decays  
336 produce two b-quarks, the decay of which can produce additional non-prompt leptons, which  
337 occasionally pass the event preselection. In order to validate that the Monte Carlo accurately  
338 simulates this process accurately, the MC prediction in a non-prompt  $t\bar{t}$  enriched validation  
339 region is compared to data.

340 The  $t\bar{t}$  validation region is similar to the preselection region - three leptons meeting the criteria  
341 described in Section 5 are required, and the requirements on  $E_T^{\text{miss}}$  remain the same. However,  
342 the selection requiring a lepton pair form a  $Z$ -candidate are reversed. Events where the invariant  
343 mass of any two opposite sign, same flavor leptons falls within 10 GeV of 91.2 GeV are rejected.  
344 This ensures the  $t\bar{t}$  validation region is orthogonal to the preselection region.

345 Further, because the jet multiplicity of  $t\bar{t}$  events tends to be higher than  $WZ$ , the number of jets  
346 in each event is required to be greater than 1. As b-jets are almost invariably produced from top  
347 decays, at least one b-tagged jet passing the 70% DL1r WP in each event is required. Various  
348 kinematic plots of this region are shown in Figure 18.

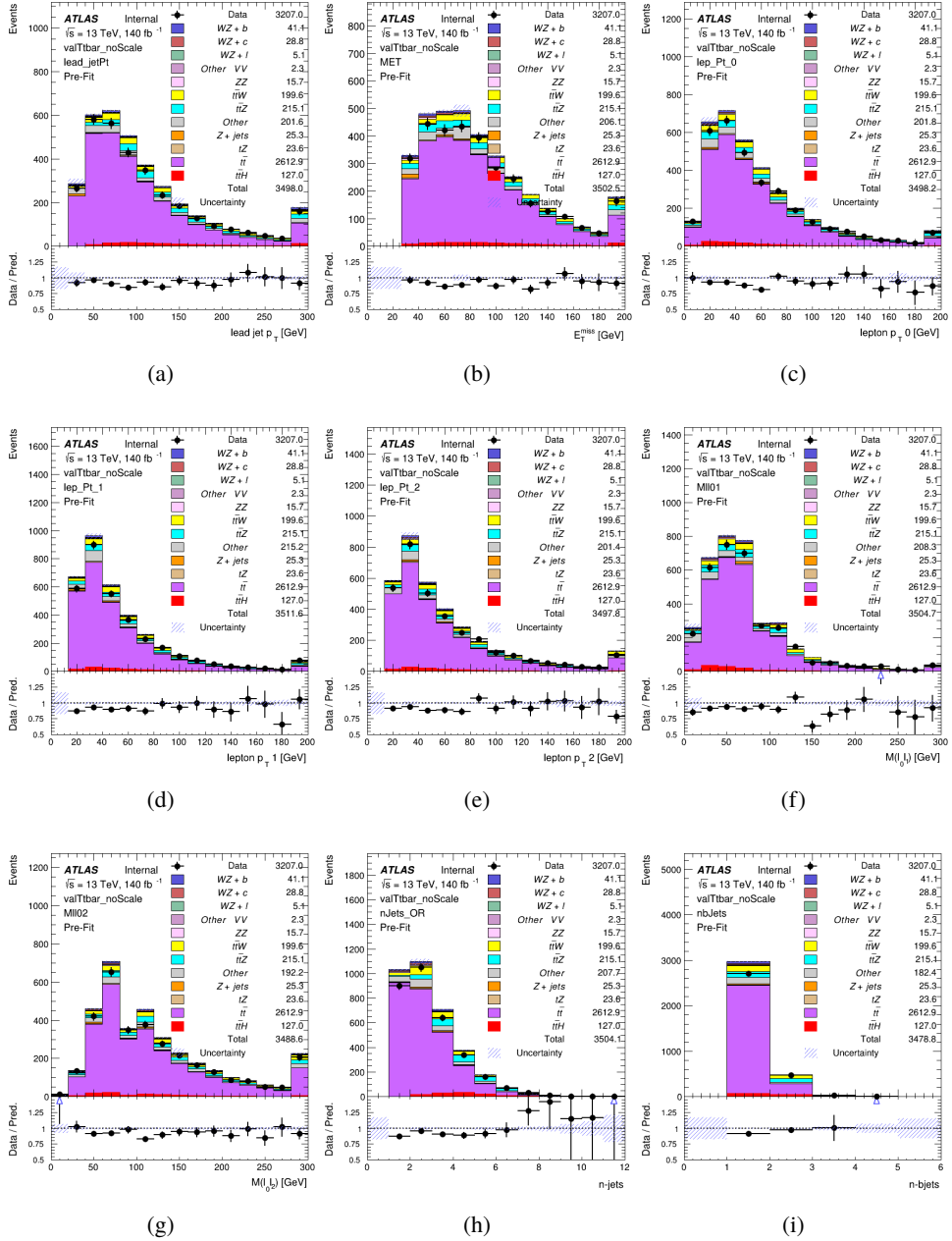


Figure 18: Comparisons between the data and MC distributions in the  $t\bar{t}$  validation region for (a) the  $p_T$  of the leading jet, (b) the missing transverse energy, (c) the  $p_T$  of lepton 0, (d)  $p_T$  of lepton 1, (e)  $p_T$  of lepton 2, (f) the invariant mass of leptons 0 and 1, (g) the invariant mass of leptons 0 and 2, (h) the number of jets, (i) the number of b-tagged jets.

349 The shape of each distribution agrees quite well between data and MC, with a constant offset  
 350 between the two. This is accounted for by applying a constant correction factor of 0.9 to the  $t\bar{t}$

351 MC prediction. Plots showing the kinematics of the  $t\bar{t}$  VR after this correction factor has been  
 352 applied are shown in Figure 19.

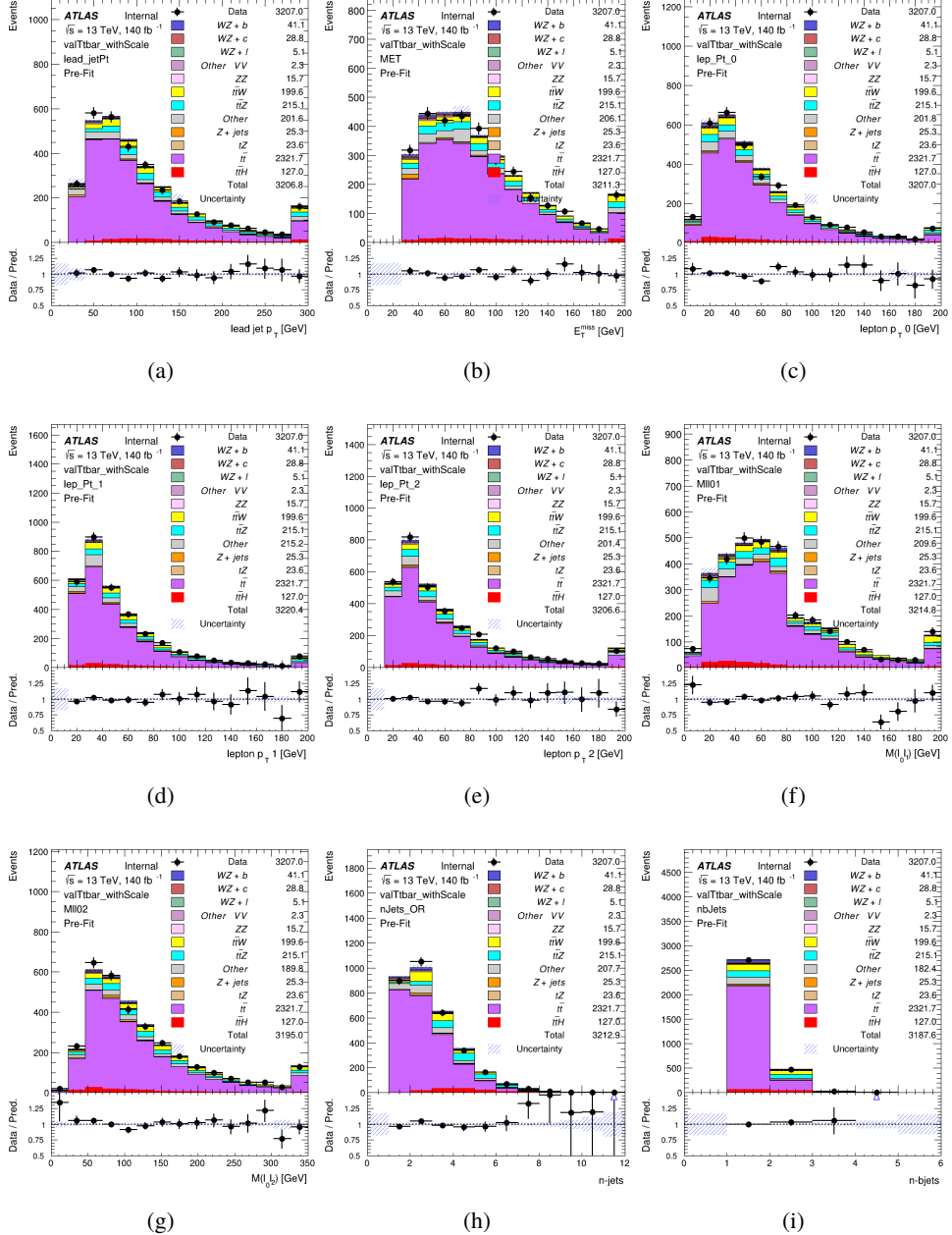


Figure 19: Comparisons between the data and MC distributions in the  $t\bar{t}$  validation region after the correction factor has been applied for (a) the  $p_T$  of the leading jet, (b) the missing transverse energy, (c) the  $p_T$  of lepton 0, (d)  $p_T$  of lepton 1, (e)  $p_T$  of lepton 2, (f) the invariant mass of leptons 0 and 1, (g) the invariant mass of leptons 0 and 2, (h) the number of jets, (i) the number of b-tagged jets.

353 The modeling is further validated by looking at the yield in the  $t\bar{t}$  VR for each DL1r WP, giving  
 354 a clearer correspondence to the signal regions used in the fit. For these plots, the requirement  
 355 that each event contain at least one b-tagged jet is removed. Each region shown in Figure 20  
 356 requires one or more jets pass the listed WP, with no jets passing the next highest WP.

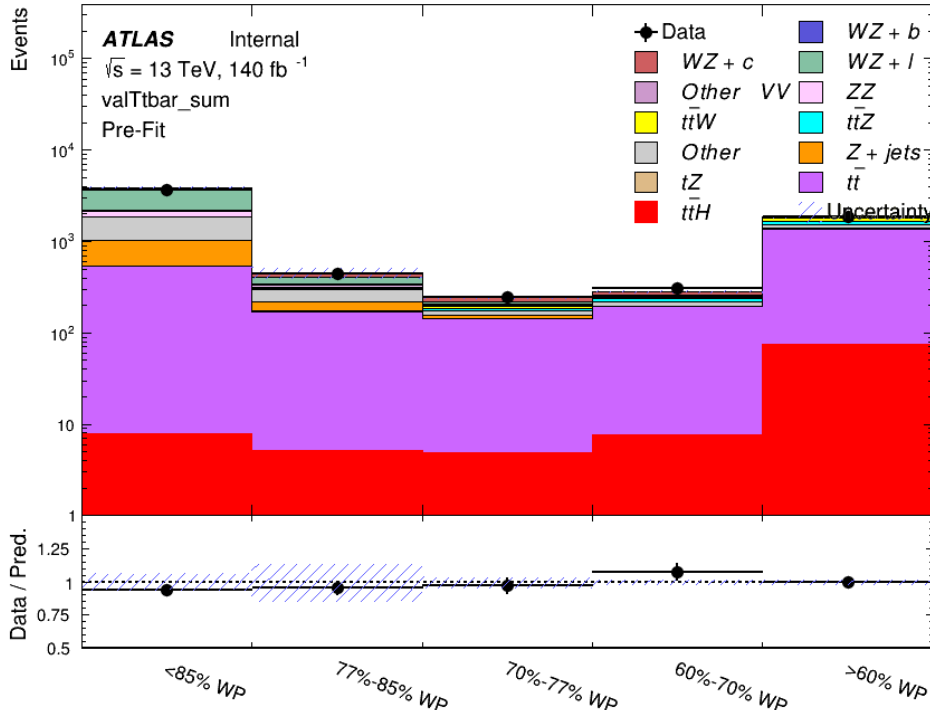


Figure 20: Data and MC comparisons for each DL1r WP for both 1-jet and 2-jet regions, after the  $t\bar{t}$  VR selection and correction factor have been applied

357 As data and MC are found to agree within 20% for each of these working points, a 20% systematic  
 358 uncertainty on the  $t\bar{t}$  prediction is included for the analysis.

### 359 5.3.2 Z+jets Validation

360 Similar to  $t\bar{t}$ , a non-prompt Z+jets validation region is produced in order to validate the MC  
 361 predictions. The lepton requirements remain the same as the preselection region. Because no  
 362 neutrinos are present for this process, the  $E_T^{\text{miss}}$  cut is reversed, requiring  $E_T^{\text{miss}} < 30$  GeV. This  
 363 also ensures this validation region is orthogonal to the preselection region. Further, the number  
 364 of jets in each event is required to be greater than or equal to one. Various kinematic plots of this  
 365 region are shown below. The general agreement between data and MC in each of these suggests  
 366 that the non-prompt contribution of Z+jets is well modeled by Monte Carlo.

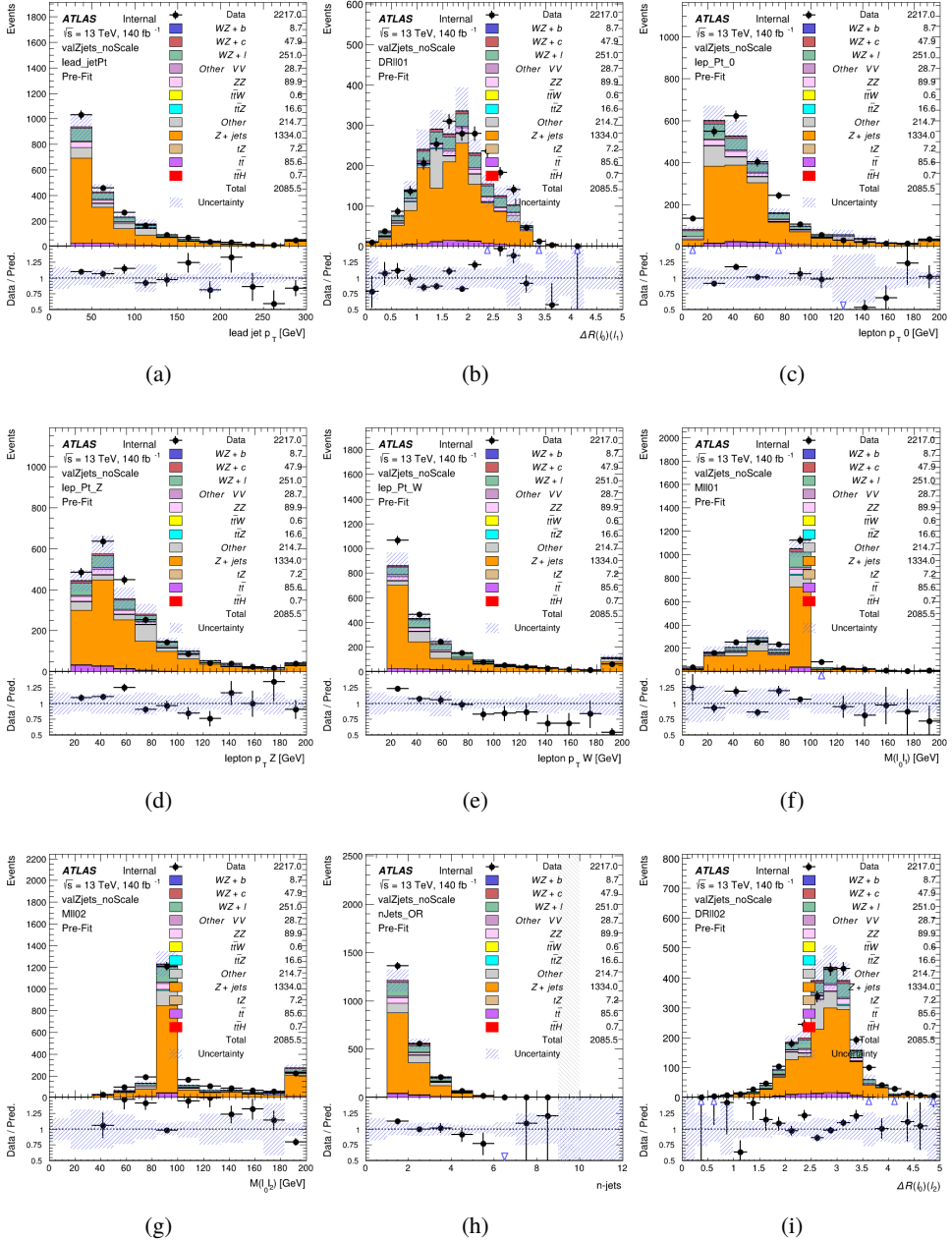


Figure 21: Comparisons between the data and MC distributions in the Z+jets validation region for (a) the  $p_T$  of the leading jet, (b)  $\Delta R$  between leptons 0 and 1, (c) the  $p_T$  of lepton 0, (d)  $p_T$  of SS lepton from the Z candidate, (e)  $p_T$  of the SS lepton from the W candidate, (f) the invariant mass of leptons 0 and 1, (g) the invariant mass of leptons 0 and 2, (h) the number of jets, (i)  $\Delta R$  between leptons 0 and 2. Includes only statistical uncertainties

367 While there is general agreement between data and MC within statistical uncertainty, the shape

<sup>368</sup> of the  $p_T$  spectrum of the lepton from the W is found to differ. To account for this discrepancy, a  
<sup>369</sup> variable correction factor is applied to Z+jets.  $\chi^2$  minimization of the W lepton  $p_T$  spectrum is  
<sup>370</sup> performed to derive a correction factor as a function of this  $p_T$ . Kinematic plots of the Z + jets  
<sup>371</sup> validation region after this correction factor has been aplied are shown in Figure 22.

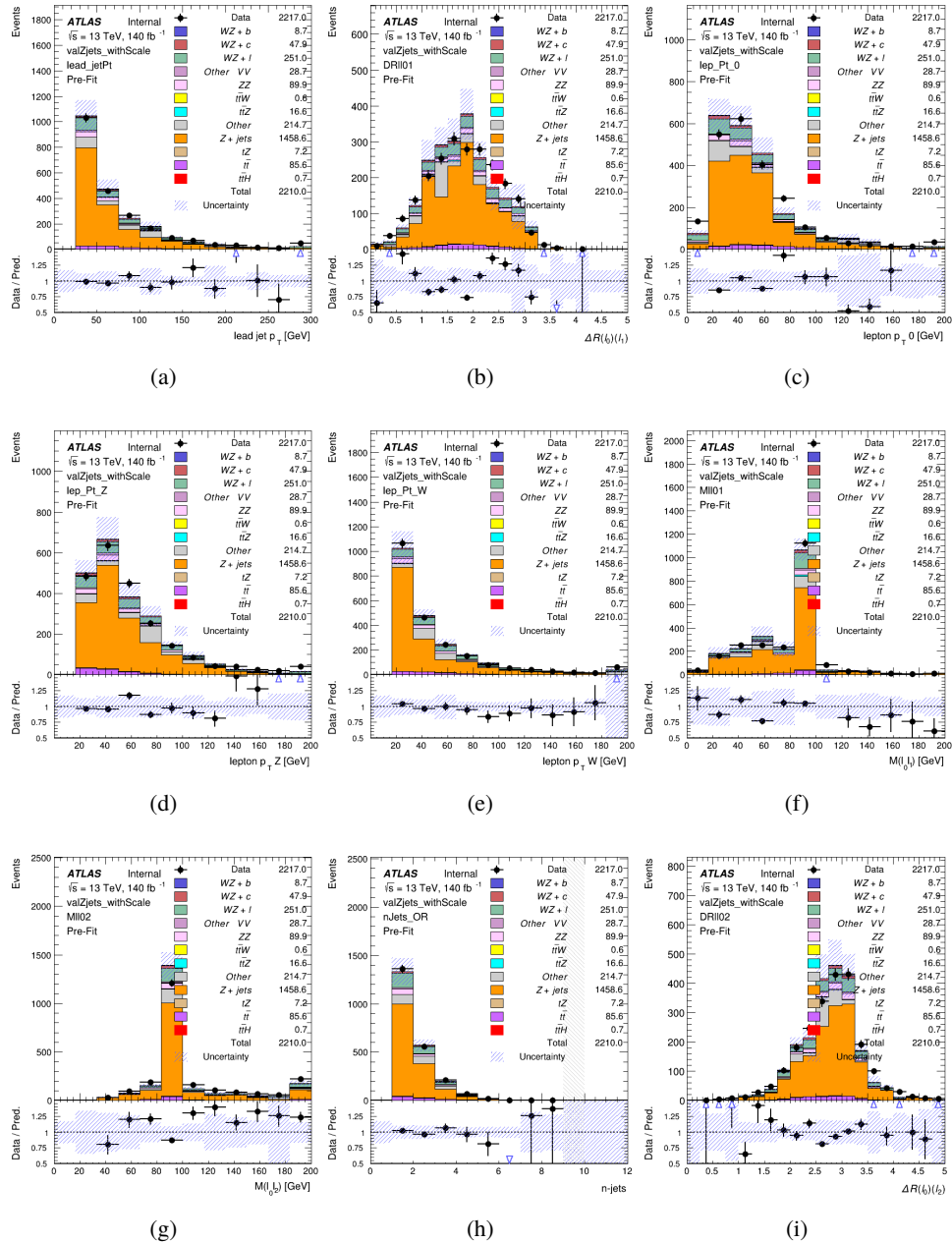


Figure 22: Comparisons between the data and MC distributions in the Z+jets validation region after the correction factor has been applied for (a) the  $p_T$  of the leading jet, (b)  $\Delta R$  between leptons 0 and 1, (c) the  $p_T$  of lepton 0, (d)  $p_T$  of SS lepton from the Z candidate, (e)  $p_T$  of the SS lepton from the W candidate, (f) the invariant mass of leptons 0 and 1, (g) the invariant mass of leptons 0 and 2, (h) the number of jets, (i)  $\Delta R$  between leptons 0 and 2

372 The modeling is further validated by looking at the yield in the Z+jets VR for each DL1r WP,

373 giving a clearer correspondence to the signal regions used in the fit. Each region shown in Figure  
 374 23 requires one or more jets pass the listed WP, with no jets passing the next highest WP.

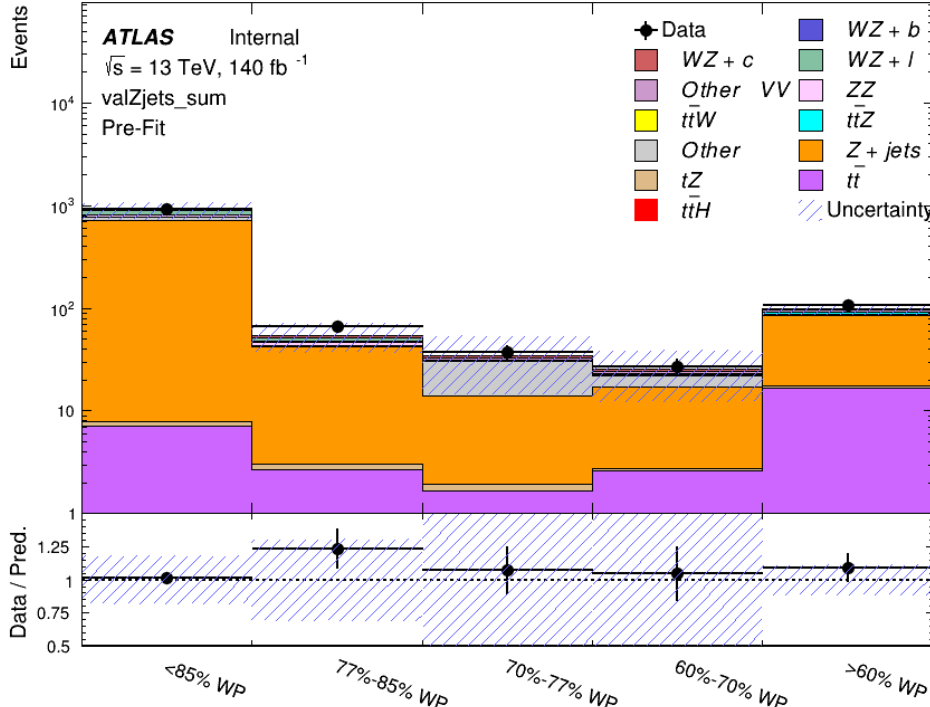


Figure 23: Data and MC comparisons for each DL1r WP for both 1-jet and 2-jet regions, after the Z+jets VR selection and correction factor have been applied

375 For each of the b-tagging working points considered, the data falls within 25% of the MC  
 376 prediction once this correction factor has been applied. Therefore, a 25% systematic uncertainty  
 377 is applied to Z + jets in the analysis.

## 378 6 tZ Separation Multivariate Analysis

379 Because tZ produces a final state identical to signal, it represents a predominant background in  
 380 the most signal enriched regions. That is, the region with one jet passing the 60% DL1r WP.  
 381 Therefore, a boosted decision tree (BDT) algorithm is trained to separate WZ + heavy flavor  
 382 from tZ.

383 Separation between tZ and WZ + heavy flavor is achieved in part by reconstructing the invariant  
 384 mass of the top candidate, which clusters more closely to the top mass for tZ than WZ + heavy  
 385 flavor. The result of this BDT is used to create a tZ enriched region in the fit, reducing its impact  
 386 on the measurement of WZ + heavy flavor.

387 **6.1 Top Mass Reconstruction**

388 The reconstruction of the top mass follows the procedure described in detail in section 6.1 of  
 389 [21]. The mass of the top quark candidate is reconstructed from the jet, the lepton not included  
 390 in the Z-candidate, and a reconstructed neutrino. In the case that there is one jet in the event,  
 391 there is only possible b-jet candidate. For events with two jets, the jet with the highest DL1r  
 392 score is used.

393 The neutrino from the W decay is expected to be the only source of  $E_T^{\text{miss}}$ . Therefore, the  $E_T$   
 394 and  $\phi$  of the neutrino are taken from the  $E_T^{\text{miss}}$  measurement. This leaves the z-component of  
 395 the neutrino momentum,  $p_{\nu z}$  as the only unknown.

396 This unknown is solved for by taking the combined invariant mass of the lepton and neutrino to  
 397 give the invariant mass of the W boson:

$$398 \quad (p_l + p_\nu)^2 = m_W^2$$

399 Expanding this out into components, this equation gives:

$$400 \quad \sqrt{p_{T\nu}^2 + p_{z\nu}^2} E_l = \frac{m_w^2 - m_l^2}{2} + p_{T\nu}(p_{lx}\cos\phi_\nu + p_{ly}\sin\phi_\nu) + p_{lz}p_{\nu z}$$

401 This equation gives two solutions for  $p_{\nu z}$ . For cases where only one of these solutions is real,  
 402 that is taken as the value of  $p_{\nu z}$ . For instances with two real solutions, the one which is shown  
 403 to be correct in the largest fraction of simulations is taken. For cases when no real solution is  
 404 found, often because of detector effects, the value of  $E_T^{\text{miss}}$  is varied in decreasing increments of  
 405 100 MeV until a real solution is found.

406 The reconstructed top mass distribution for tZ and WZ + b can be seen in figure 24.

407 **6.2 tZ BDT**

408 A Boosted Decision Tree (BDT), specifically XGBoost [22], is used to provide separation between  
 409 tZ and WZ+b. The following kinematic variables are used as inputs:

- 410 • The invariant mass of the reconstructed top candidate
- 411 •  $p_T$  of each of the leptons, jet
- 412 • The invariant mass of each combination of lepton pairs,  $M(l\bar{l})$
- 413 •  $E_T^{\text{miss}}$
- 414 • Distance between each combination of leptons,  $\Delta R(l\bar{l})$
- 415 • Distance between each lepton and the jet,  $\Delta R(lj)$

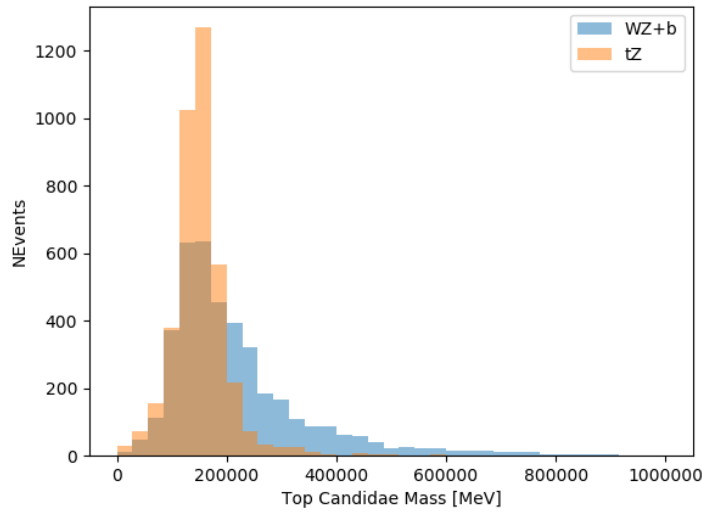


Figure 24: Reconstructed top mass distributions for tZ and WZ + b, measured in MeV.

416 The training samples included only events meeting the requirements of the 1-jet, >60% region,  
 417 i.e. passing all the selection described in section 5 and having exactly one jet which passes the  
 418 tightest (60%) DL1r working point.

419 The distributions of a few of these features for both signal and background is shown in figure  
 420 25.

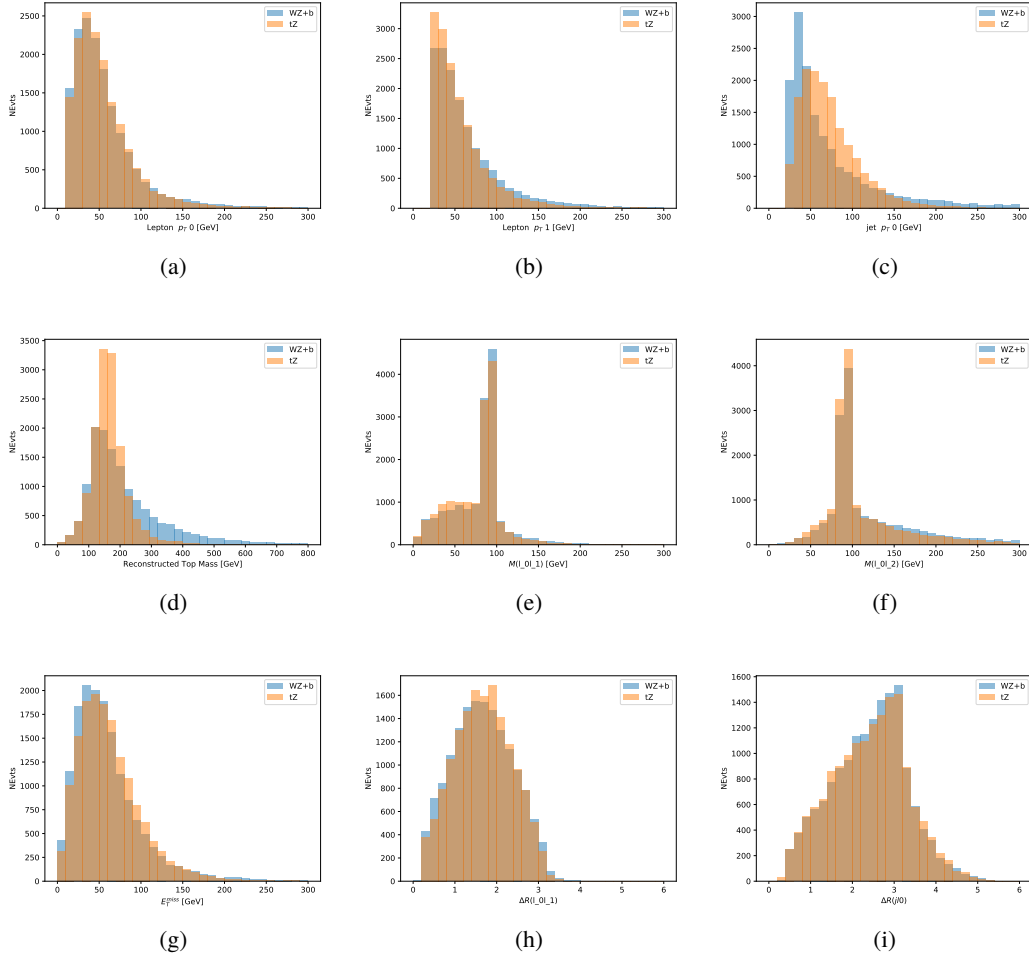


Figure 25: Distribution of input features of the BDT for signal (WZ) and background (tZ). Both are scaled to an equal number of events. (a), (b) and (c) show the  $p_T$  of lepton 0, lepton 1, and the jet, (d) show the reconstructed top mass, (e) and (f) show the invariant mass of leptons 0 and 1, leptons 0 and 2. (g) shows the  $E_T^{\text{miss}}$  of each event. (h) and (i) show the  $\Delta R$  between lepton 0 and lepton 1, and the jet.

421 A sample of 20,000 background (tZ) and signal (WZ+b) Monte Carlo events are used to train  
 422 the BDT. And additional 5,000 events are reserved for testing the model, in order to prevent  
 423 over-fitting. A total of 750 decision trees with a maximum depth of 6 branches are used to build  
 424 the model. These parameters are chosen empirically, by training several models with different  
 425 parameters and selecting the one that gave the best separation for the test sample.

426 The results of the BDT training are shown in figure 26. The output scores for both signal and  
 427 background events is shown on the left. The right shows the receiving operating characteristic  
 428 (ROC) curve that results from the MVA. The ROC curve represents the background rejection  
 429 as a function of signal efficiency, where each point on the curve represents a different response

430 score.

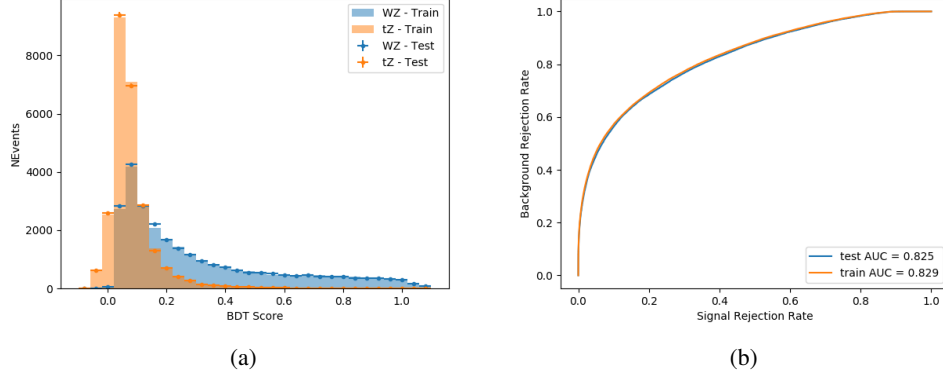


Figure 26: Distribution of the BDT response for signal and background events on the left, the ROC curve for the BDT on the right.

431 The relative important of each input feature in the model, measured by how often they appeared  
432 in the decision trees, is shown in figure 27.

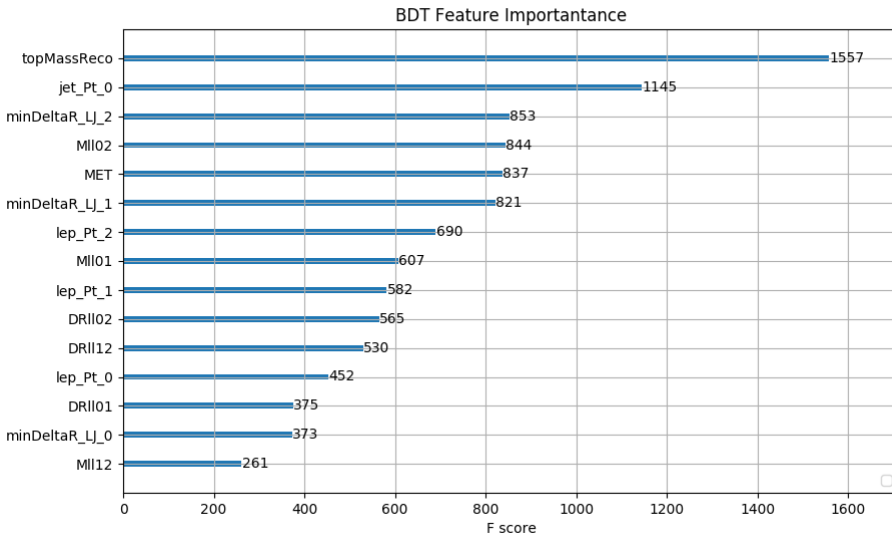


Figure 27: Relative importance of each input feature in the model.

433 These results suggest that some amount of separation can be achieved between these two pro-  
434 cesses, with a high BDT score selecting a set of events that is pure in WZ + b. A BDT score

435 of 0.725 is selected as a cutoff, where events with scores higher than this form a signal enriched  
436 region, and events with scores lower than this form a tZ control region. This cutoff is selected by  
437 varying the value of this cutoff in stat-only Asimov fits, and selecting the value that minimizes  
438 the statistical uncertainty on WZ + b.

439 **6.3 tZ Interference Studies**

440 Because it includes an on-shell Z boson as well as a b-jet and W from the top decay, tZ  
441 production represents an identical final state to WZ + b-jet. This implies the possibility of matrix  
442 level interference between these two processes not accounted for in the Monte Carlo simulations,  
443 which consider the two processes independently. Truth level studies are performed in order to  
444 estimate the impact of these interference effects.

445 In order to estimate the matrix level interference effects between tZ and WZ + b-jet, two different  
446 sets of simulations are produced using MadGraph 5 [Madgraph] - one which simulates these  
447 two processes independently, and another where they are produced simultaneously, such that  
448 interference effects are present. These two sets of samples are then compared, and the difference  
449 between them can be taken to represent any interference effects.

450 MadGraph simulations of 10,000 tZ and 10,000 WZ + b-jet events are produced, along with  
451 20,000 events where both are present, in the fiducial region where three leptons and at least one  
452 jet are produced.

453 A selection mimicking the preselection used in the main analysis is applied to the samples: The  
454 SS leptons are required to have  $p_T > 20$  GeV, and  $> 10$  GeV is required for the OS lepton. The  
455 associated b-jet is required to have  $p_T > 25$  GeV, and all physics objects are required to fall in a  
456 range of  $|\eta| < 2.5$ .

457 The kinematics of these samples after the selection has been applied are shown below:

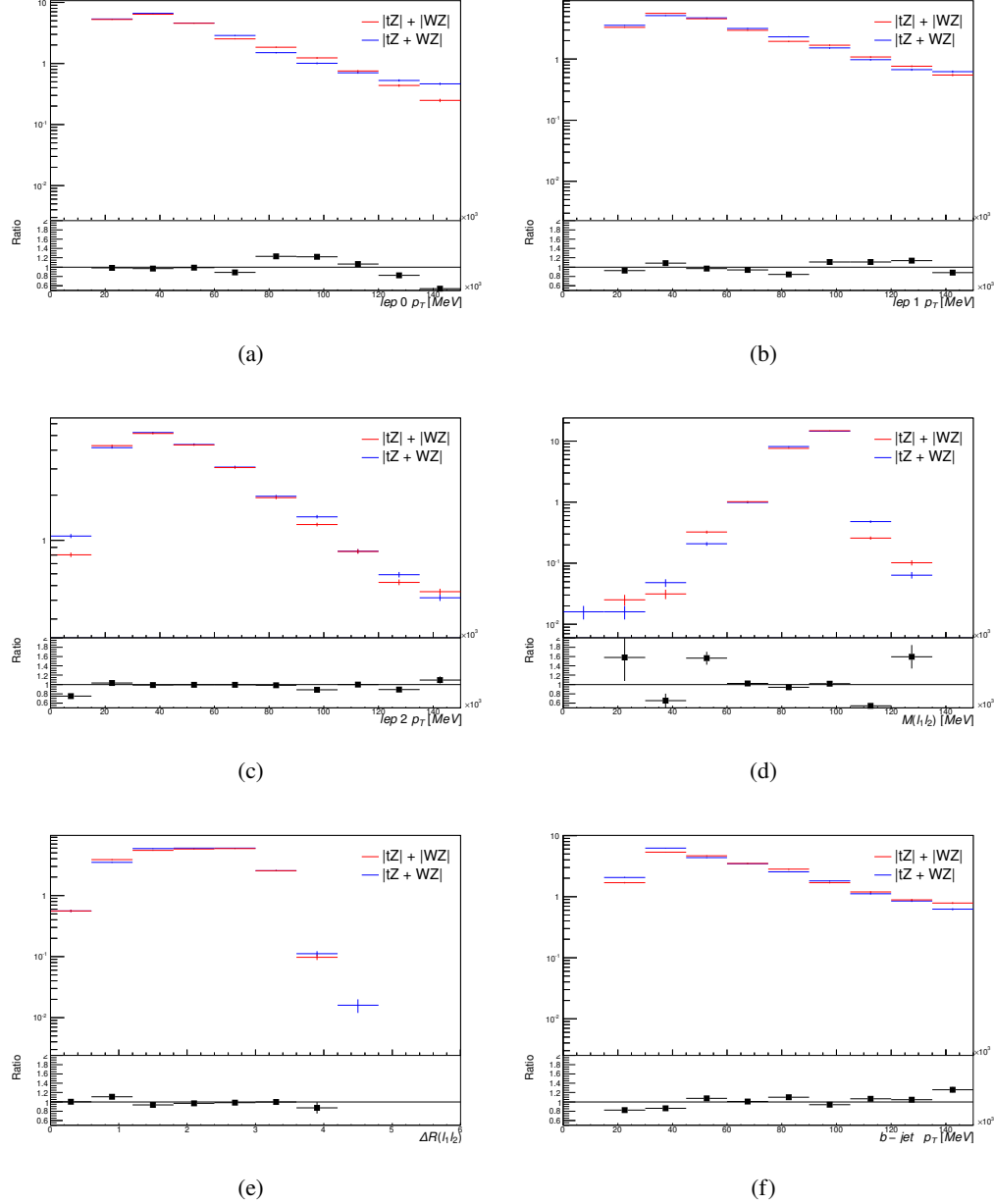


Figure 28: Comparisons between (a) the  $p_T$  of the lepton from the W, (b) and (c) show the  $p_T$  of the lepton from the Z, (d) the invariant mass of the Z-candidate, (e)  $\Delta R$  of the leptons from the Z, and (f) the  $p_T$  of the b-jet, for WZ and tZ events generated with interference effects (blue) and without interference effects (red).

458 The overall cross-section of the two methods agree within error, and no significant differences  
459 in the kinematic distributions are seen. It is therefore concluded that interference effects do not

460 significantly impact the results.

## 461 7 Systematic Uncertainties

462 The systematic uncertainties that are considered are summarized in Table 9. These are imple-  
463 mented in the fit either as a normalization factors or as a shape variation or both in the signal  
464 and background estimations. The numerical impact of each of these uncertainties is outlined in  
465 Section 8.

Table 9: Sources of systematic uncertainty considered in the analysis.

Systematic uncertainty	Components
Luminosity	1
Pileup reweighting	1
<b>Physics Objects</b>	
Electron	6
Muon	15
Jet energy scale	28
Jet energy resolution	8
Jet vertex fraction	1
Jet flavor tagging	131
$E_T^{\text{miss}}$	3
Total (Experimental)	194
<b>Signal Modeling</b>	
Shape modelling	3
Renormalization and factorization scales	5
nJet Migration	5
<b>Background Modeling</b>	
Cross section	15
Renormalization and factorization scales	12
Parton shower and hadronization model	2
Shower tune	4
Total (Signal and background modeling)	41
Total (Overall)	236

466 The uncertainty in the combined 2015–2018 integrated luminosity is 1.7% [23], obtained using  
467 the LUCID-2 detector [24] for the primary luminosity measurements.

468 The experimental uncertainties are related to the reconstruction and identification of light  
469 leptons and b-tagging of jets, and to the reconstruction of  $E_T^{\text{miss}}$ . The TOTAL electron ID

470 correlation model is used, corresponding to 1 electron ID systematic. Electron ID is found to be  
471 a subleading systematic that is unconstrained by the fit, making it an appropriate choice for this  
472 analysis.

473 The sources which contribute to the uncertainty in the jet energy scale (JES) [25] are decom-  
474 posed into uncorrelated components and treated as independent sources in the analysis. The  
475 CategoryReduction model is used to account for JES uncertainties, which decomposes the uncer-  
476 tainties into 30 nuisance parameters included in the fit. The SimpleJER model is used to account  
477 for jet energy resolution (JER) uncertainties, and 8 JER uncertainty components included as NPs  
478 in the fit.

479 The uncertainties in the b-tagging efficiencies measured in dedicated calibration analyses  
480 [26] are also decomposed into uncorrelated components. The large number of components for  
481 b-tagging is due to the calibration of the distribution of the MVA discriminant.

482 The full list of systematic uncertainties considered in the analysis is summarized in Tables 10,  
483 11 and 12.

484

<b>Experimental Systematics on Leptons and <math>E_T^{\text{miss}}</math></b>			
Type	Description	Systematics Name	Application
<b>Trigger</b>			
Scale Factors	Trigger Efficiency	lepSFTrigTight_MU(EL)_SF_Trigger_STAT(SYST)	Event Weight
<b>Muons</b>			
Efficiencies	Reconstruction and Identification	lepSFObjTight_MU_SF_ID_STAT(SYST)	Event Weight
	Isolation	lepSFObjTight_MU_SF_Isol_STAT(SYST)	Event Weight
	Track To Vertex Association	lepSFObjTight_MU_SF_TTVA_STAT(SYST )	Event Weight
$p_T$ Scale	$p_T$ Scale	MUONS_SCALE	$p_T$ Correction
Resolution	Inner Detector Energy Resolution	MUONS_ID	$p_T$ Correction
	Muon Spectrometer Energy Resolution	MUONS_MS	$p_T$ Correction
<b>Electrons</b>			
Efficiencies	Reconstruction	lepSFObjTight_EL_SF_ID	Event Weight
	Identification	lepSFObjTight_EL_SF_Reco	Event Weight
	Isolation	lepSFObjTight_EL_SF_Isol	Event Weight
Scale Factor	Energy Scale	EG_SCALE_ALL	Energy Correction
Resolution	Energy Resolution	EG_RESOLUTION_ALL	Energy Correction
<b><math>E_T^{\text{miss}}</math></b>			
Soft Tracks Terms	Resolution	MET_SoftTrk_ResoPerp	$p_T$ Correction
	Resolution	MET_SoftTrk_ResoPara	$p_T$ Correction
	Scale	MET_SoftTrk_ScaleUp	$p_T$ Correction
	Scale	MET_SoftTrk_ScaleDown	$p_T$ Correction

Table 10: Summary of experimental systematics considered for leptons and  $E_T^{\text{miss}}$ . Includes type, description, name of systematic as used in the fit, and mode of application. The mode of application indicates the systematic evaluation, e.g. as an overall event re-weighting (Event Weight) or rescaling ( $p_T$  Correction).

Experimental Systematics on Jets			
Type	Origin	Systematics Name	Application
Jet Vertex Tagger		JVT	Event Weight
Energy Scale	Calibration Method	JET_21NP_ JET_EffectiveNP_1-19	$p_T$ Correction $p_T$ Correction
	$\eta$ inter-calibration	JET_EtaIntercalibration_Modelling JET_EtaIntercalibration_NonClosure JET_EtaIntercalibration_TotalStat	$p_T$ Correction $p_T$ Correction $p_T$ Correction
	High $p_T$ jets	JET_SingleParticle_HighPt	$p_T$ Correction
	Pile-Up	JET_Pileup_OffsetNPV JET_Pileup_OffsetMu JET_Pileup_PtTerm JET_Pileup_RhoTopology	$p_T$ Correction $p_T$ Correction $p_T$ Correction $p_T$ Correction
	Non Closure	JET_PunchThrough_MC15	$p_T$ Correction
	Flavour	JET_Flavor_Response JET_BJES_Response JET_Flavor_Composition	$p_T$ Correction $p_T$ Correction $p_T$ Correction
Resolution		JET_JER_SINGLE_NP	Event Weight

Table 11: Jet systematics take into account effects of jets calibration method,  $\eta$  inter-calibration, high  $p_T$  jets, pile-up, and flavor response. They are all diagonalised into effective parameters.

Experimental Systematics on b-tagging		
Type	Origin	Systematic Name
Scale Factors	DL1r b-tagger efficiency on b originated jets in bins of $\eta$	DL1r_Continuous_EventWeight_B0-29
	DL1r b-tagger efficiency on c originated jets in bins of $\eta$	DL1r_Continuous_EventWeight_C0-19
	DL1r b-tagger efficiency on light flavoured originated jets in bins of $\eta$ and $p_T$	DL1r_Continuous_EventWeight_Light0-79
	DL1r b-tagger extrapolation efficiency	DL1r_Continuous_EventWeight_extrapolation DL1r_Continuous_EventWeight_extrapolation_from_charm

Table 12: Summary of experimental systematics to be included for b-tagging of jets in the analysis, using the continuous DL1r tagging algorithm. All of the b-tagging related systematics are applied as event weights. From left: type, description, and the name of systematic used in the fit.

485     Theoretical uncertainties applied to MC predictions, including cross section, PDF, and scale  
 486     uncertainties are taken from theory calculations, with the exception of non-prompt and diboson  
 487     backgrounds. The cross-section uncertainty on tZ is taken from [27]. Derivation of the non-  
 488     prompt background uncertainties, Z+jets and tt}, are explained in detail in Section 5.3. These  
 489     normalization uncertainties are chosen so as to account for the complete uncertainty in the  
 490     non-prompt contribution, and therefore no additional modelling uncertainties are considered for  
 491     Z+jets and tt}.

492     The other VV + heavy flavor processes (namely VV+b and VV+charm, which primarily consist  
 493     of ZZ events) are also poorly understood, because these processes involve the same physics as  
 494     WZ + heavy flavor, and have also not been measured. Therefore, a conservative 50% uncertainty  
 495     is applied to those samples. While this uncertainty is large, it is found to have little impact on  
 496     the significance of the final result.

497     The theory uncertainties applied to the predominate background estimates are summarized in  
 498     Table 13.

Process	X-section [%]
tZ	X-sec: $\pm 15.2$ QCD Scale: $^{+5.2}_{-1.3}$ PDF( $+\alpha_S$ ): $\pm 1.2$
t <bar>t} H (aMC@NLO+Pythia8)</bar>	QCD Scale: $^{+5.8}_{-9.2}$ PDF( $+\alpha_S$ ): $\pm 3.6$
t <bar>t} Z (aMC@NLO+Pythia8)</bar>	QCD Scale: $^{+9.6}_{-11.3}$ PDF( $+\alpha_S$ ): $\pm 4$
t <bar>t} W (aMC@NLO+Pythia8)</bar>	QCD Scale: $^{+12.9}_{-11.5}$ PDF( $+\alpha_S$ ): $\pm 3.4$
VV + b/charm (Sherpa 2.2.1)	$\pm 50$
VV + light (Sherpa 2.2.1)	$\pm 6$
t <bar>t}</bar>	$\pm 20$
Z + jets	$\pm 25$
Others	$\pm 50$

Table 13: Summary of theoretical uncertainties for MC predictions in the analysis.

499     The fit involves varying the overall normalization of signal templates over the regions de-  
500     scribed in Section 5.2, which are defined by the flavor and number of associated jets at truth-  
501     level. The modelling of these template shapes therefore significantly impacts the final result.  
502     Additional signal uncertainties, probing the shape of the signal templates as well as the rate of  
503     migrations between the number of truth-jets and reconstructed jets, are estimated by comparing  
504     estimates from the nominal Sherpa WZ samples with alternate WZ samples generated with  
505     POWHEG+PYTHIA8 (DSID 361601). Separate systematics are included in the fit for WZ + b, WZ  
506     + c and WZ + light, where the distribution among each of the fit regions is varied based on the  
507     prediction of the Powheg sample.

508     The variations in the signal templates are shown in Figures 29 and 30. Each of these plots are  
509     normalized to unity in order to capture the relevant differences in shape.

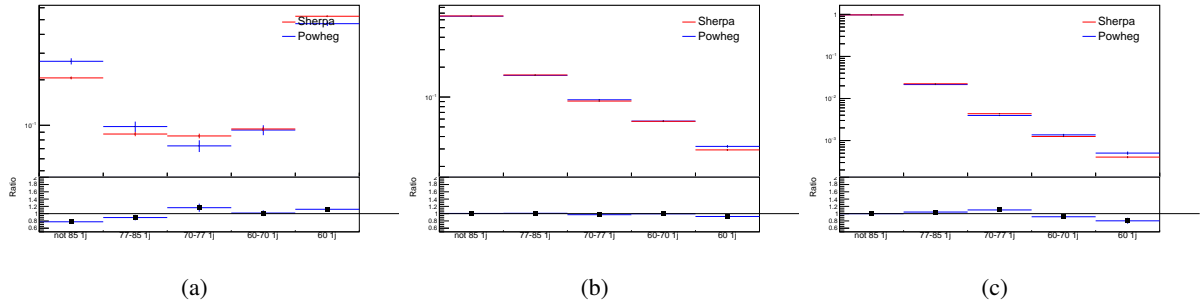


Figure 29: Comparison between Sherpa and Powheg predictions of the distribution of (a) WZ + b, (b) WZ + charm, and (c) WZ + light among the various b-tag WPs used in the 1-jet fit.

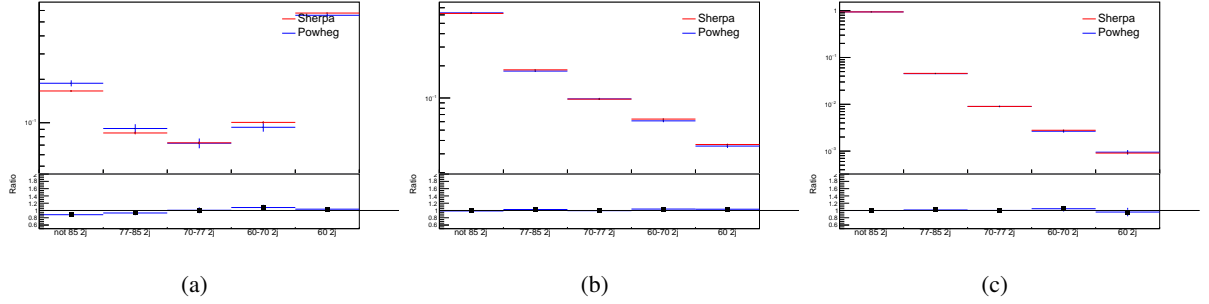


Figure 30: Comparison between Sherpa and Powheg predictions of the distribution of (a) WZ + b, (b) WZ + charm, and (c) WZ + light among the various b-tag WPs used in the 2-jet fit.

510 Separate systematics are included in the fit for WZ + b, WZ + charm and WZ + light, where  
 511 the distribution among each of the fit regions is varied based on the prediction of the Powheg  
 512 sample.

513 A similar approach is taken to account for uncertainties in migrations between the number of  
 514 reco and truth jets. The fraction of events with 1 truth jet which fall into the 1 jet bin versus the  
 515 2 jet bin at reco level is compared for Sherpa and Powheg. The same is done for events with 2  
 516 truth jets. This comparison is shown in figure 31.

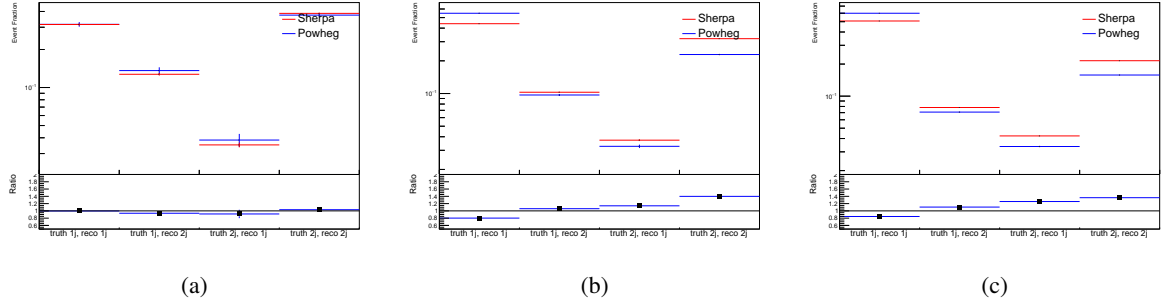


Figure 31: Comparison between Sherpa and Powheg predictions for truth jet migrations between the 1 and 2 jet reco bins for (a) WZ + b, (b) WZ + charm, and (c) WZ + light

517 A systematic is included where events are shifted between the 1-jet and 2-jet regions based on  
 518 the differences between these two shapes. This is done independently for each of the WZ + b,  
 519 WZ + charm, and WZ + light templates.

520 Additional systematics are included to account for the uncertainty in the contamination of 0 jet  
 521 and 3 or more jet events (at truth level) in the 1 and 2 reco jet bins. Because these events fall

522 outside the scope of this measurement, these events are included as a background. As such, a  
 523 normalization, rather than a shape, uncertainty is applied for this background.

524 The number of WZ events with 0-jets and  $>=3$ -jets in the reconstructed 1-jet and 2-jet regions  
 525 are compared for Sherpa and Powheg, as seen in figure 32. These differences are taken as separate  
 526 normalization systematics on the yield of WZ+0-jet and WZ+ $>=3$ -jet events.

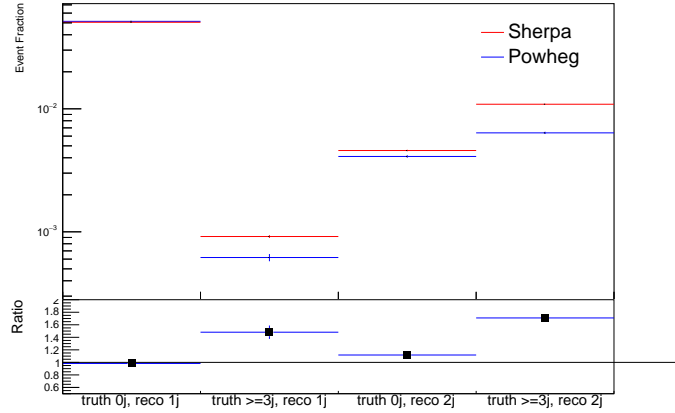


Figure 32: Comparison between Sherpa and Powheg predictions for 0 and  $>=3$  truth jet contributions in the 1 and 2 jet reco bins

## 527 8 Results

### 528 8.1 Fit Procedure

529 A maximum-likelihood fit is performed over the various fit regions described in Section 5 in  
 530 order to extract the best-fit value of the WZ + b-jet and WZ + charm jet contributions for events  
 531 with both 1 and 2 associated jets.

532 Because the fit regions are defined by the number of associated jets at reco-level, an unfolding  
 533 procedure is applied to the signal in order to account for differences in the number of truth jets  
 534 compared to the number of reco-jets. The WZ + b, WZ + charm and WZ + light contributions  
 535 are separated into independent samples based on the number of truth jets in each event. WZ + 1  
 536 truth-jet and WZ + 2 truth-jets are treated as signal samples, while WZ + 0 truth-jets and WZ +  
 537  $>=3$  truth-jets are treated as an additional background.

538 A maximum likelihood fit to data is performed simultaneously in the regions described in Section  
 539 5, summarized in figure 33. The six signal templates, which include WZ+b 1-jet, WZ+c 1-jet,  
 540 WZ+l 1-jet, WZ+b 2-jets, WZ+c 2-jets, WZ+l 2-jets, are allowed to float, while the remaining  
 541 background contributions are held fixed. The parameters  $\mu_{WZ+b-1-jet}$ ,  $\mu_{WZ+charm1-jet}$ ,

542  $\mu_{WZ+\text{light}-1\text{-jet}}$ ,  $\mu_{WZ+b-2\text{-jet}}$ ,  $\mu_{WZ+\text{charm}2\text{-jet}}$ ,  $\mu_{WZ+\text{light}-2\text{-jet}}$ , where  $\mu = \sigma_{\text{observed}}/\sigma_{\text{SM}}$ ,  
 543 are extracted from the fit. A simultaneous fit is performed over all 1-jet and 2-jet regions.

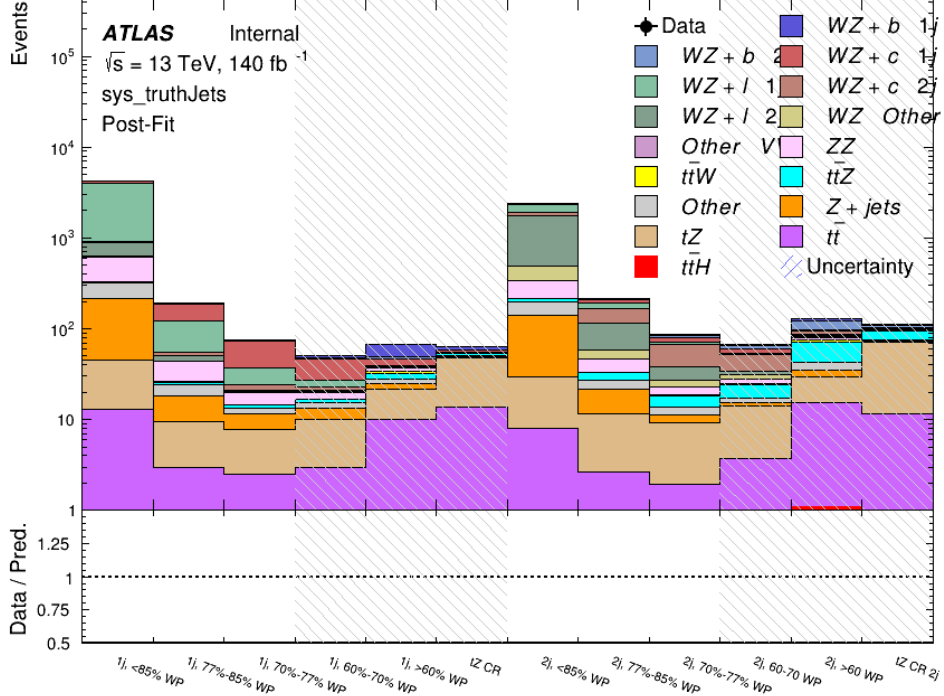


Figure 33: Post-fit summary of the fit regions.

544 As described in Section 7, there are 230 systematic uncertainties that are considered as NPs in  
 545 the fit. These NPs are constrained by Gaussian or log-normal probability density functions. The  
 546 latter are used for normalisation factors to ensure that they are always positive. The expected  
 547 number of signal and background events are functions of the likelihood. The prior for each NP  
 548 is added as a penalty term, decreasing the likelihood as it is shifted away from its nominal value.  
 549 The correlations between these nuisance parameters are summarized in Figure 34.

550 Several alternate fit strategies are documented in Appendices 8.3-8.4.1. These include a mea-  
 551 surement of  $WZ + 1$  or  $2$  jets inclusively, a fit where  $tZ$  is allowed to float, and a case where  $tZ$  is  
 552 included as part of the signal.

## 553 8.2 Results of the Simultaneous Fit

554 The Asimov fit for 1-jet events gives an expected  $\mu$  value of  $1.00^{+0.47}_{-0.43}(\text{stat})^{+0.30}_{-0.27}(\text{sys})$  for  $WZ$   
 555 +  $b$ . The fitted cross-section modifiers for  $WZ + \text{charm}$  and  $WZ + \text{light}$  are  $1.00 \pm 0.17 \pm 0.17$   
 556 and  $1.00 \pm 0.06 \pm 0.14$ , respectively.

557 The expected cross-section of WZ+b with 1-jet is  $1.74^{+0.82}_{-0.75}(\text{stat})^{+0.53}_{-0.48}(\text{sys})$  fb, and  $14.6 \pm$   
 558  $2.5(\text{stat}) \pm 2.3(\text{sys})$  fb for WZ + charm, with a correlation of -0.15 between them. An expected  
 559 significance of 2.0 is observed for WZ + b in this region.

560 For 2-jet events, the fit gives an expected  $\mu$  value of  $1.00^{+0.53}_{-0.51}(\text{stat})^{+0.39}_{-0.34}(\text{sys})$  for WZ + b.  
 561 The fitted cross-section modifiers for WZ + charm and WZ + light are  $1.00 \pm 0.25 \pm 0.21$  and  
 562  $1.00 \pm 0.06 \pm 0.16$ , respectively.

563 The expected WZ + b cross-section in the 2-jet region is  $2.5^{+1.3}_{-1.3}(\text{stat})^{+0.95}_{-0.83}(\text{sys})$  fb with an  
 564 expected significance of  $1.7\sigma$ . The 2-jet expected cross-section of WZ + charm is  $12.7 \pm$   
 565  $3.2(\text{stat}) \pm 2.7(\text{sys})$  fb, and the correlation between WZ + charm and WZ + b is -0.22.

566 A summary of the correlation between the various WZ components is summarized in Table 14.

567

	WZ + b - 1-jet	WZ + c - 1-jet	WZ + l - 1-jet	WZ + b - 2-jet	WZ + c - 2-jet	WZ + l - 2-jet
WZ + b - 1-jet	1.00	-0.15	0.28	-0.13	-0.22	0.17
WZ + c - 1-jet	-	1.00	0.36	0.13	-0.14	-0.16
WZ + l - 1-jet	-	-	1.00	0.10	-0.20	-0.39
WZ + b - 2-jet	-	-	-	1.00	-0.22	0.17
WZ + c - 2-jet	-	-	-	-	1.00	0.23
WZ + l - 2-jet	-	-	-	-	-	1.00

Table 14: Correlations between the various components of WZ

568 The correlations between the all of the nuisance parameters considered in the fit are summarized  
 569 in Figure 34.a

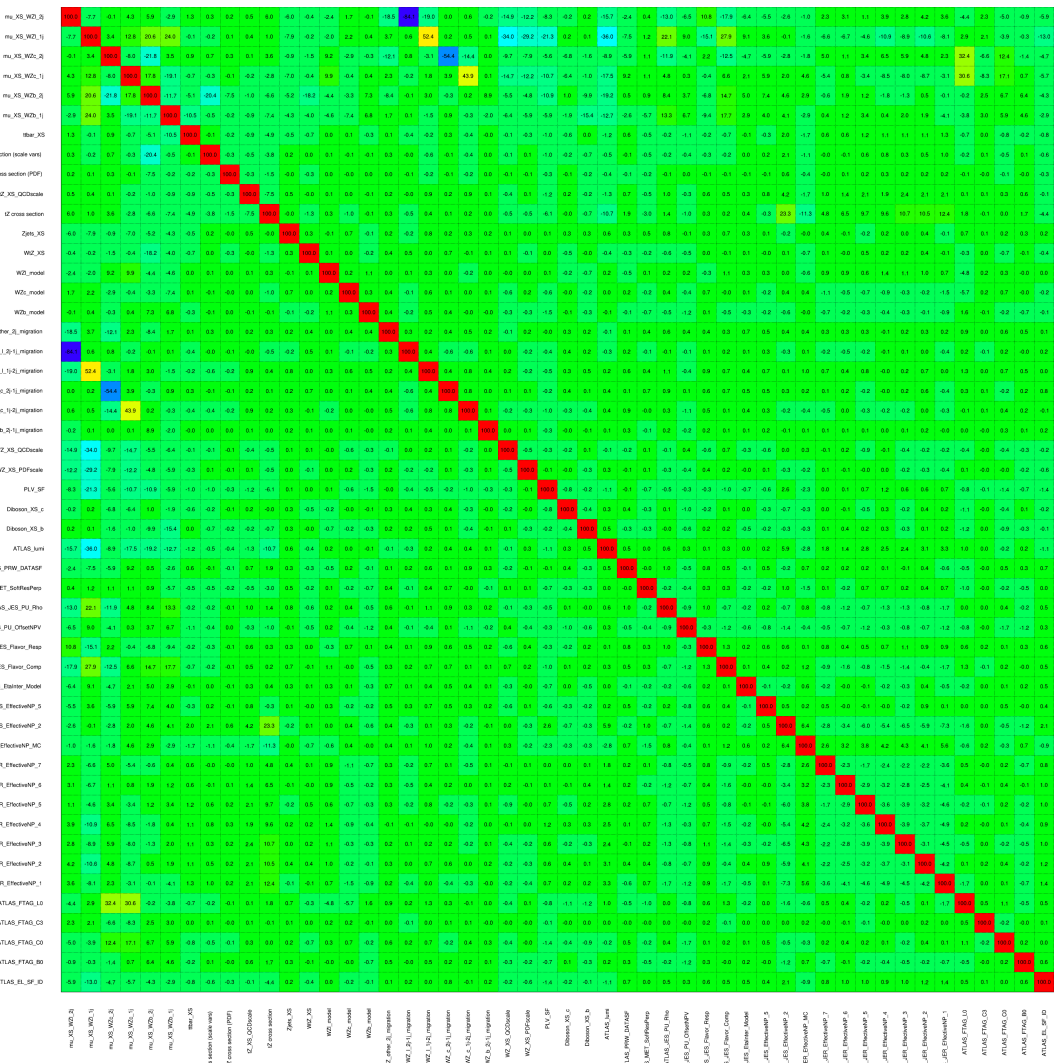


Figure 34: Correlations between nuisance parameters

The pre-fit yields in each of the 1-jet regions used in the fit are shown in Table 8.2.

Sample	1j, <85% WP	1j, 77%-85% WP	1j, 70%-77% WP	1j, 60%-70% WP	1j, >60% WP	tZ CR
WZ + b – 1j	$8.1 \pm 1.6$	$4.7 \pm 0.5$	$4.6 \pm 0.4$	$5.1 \pm 0.4$	$18.1 \pm 2.4$	$5.0 \pm 0.6$
WZ + c – 1j	$260 \pm 22$	$81 \pm 6$	$43.1 \pm 3.6$	$25.8 \pm 2.6$	$9.4 \pm 1.8$	$2.9 \pm 0.6$
WZ + l – 1j	$3090 \pm 250$	$91 \pm 13$	$17 \pm 3$	$4.9 \pm 1.6$	$1.3 \pm 0.4$	$0.2 \pm 0.1$
WZ + b – 2j	$1.10 \pm 0.37$	$0.44 \pm 0.11$	$0.39 \pm 0.06$	$0.62 \pm 0.14$	$2.1 \pm 0.5$	$0.59 \pm 0.14$
WZ + c – 2j	$21 \pm 5$	$5.6 \pm 1.2$	$3.0 \pm 0.7$	$2.0 \pm 0.5$	$0.70 \pm 0.20$	$0.30 \pm 0.08$
WZ + l – 2j	$250 \pm 60$	$5.7 \pm 1.6$	$0.73 \pm 0.53$	$0.31 \pm 0.15$	$0.07 \pm 0.06$	$0.01 \pm 0.01$
WZ – Other	$13 \pm 5$	$1.4 \pm 0.4$	$0.42 \pm 0.08$	$0.2 \pm 0.01$	$0.30 \pm 0.05$	$0.67 \pm 0.15$
Other VV	$6.2 \pm 0.6$	$0.2 \pm 0.4$	$0.2 \pm 0.04$	$0.07 \pm 0.1$	$0.1 \pm 0.1$	$0.1 \pm 0.2$
ZZ	$336 \pm 26$	$17.8 \pm 2.1$	$4.3 \pm 0.6$	$1.7 \pm 0.5$	$0.36 \pm 0.08$	$0.10 \pm 0.03$
t <bar>t&gt;W</bar>	$1.1 \pm 0.2$	$0.2 \pm 0.1$	$0.3 \pm 0.1$	$0.4 \pm 0.1$	$1.5 \pm 0.3$	$0.7 \pm 0.2$
t <bar>t&gt;Z</bar>	$6.8 \pm 1.2$	$1.4 \pm 0.3$	$1.0 \pm 0.2$	$1.2 \pm 0.2$	$4.4 \pm 0.8$	$3.2 \pm 0.6$
Z + jets	$169 \pm 38$	$8.9 \pm 1.9$	$3.7 \pm 0.8$	$3.3 \pm 0.7$	$3.2 \pm 0.7$	$0.8 \pm 0.17$
V + $\gamma$	$45 \pm 28$	$1.9 \pm 2.4$	$0.1 \pm 0.1$	$0.02 \pm 0.01$	$1.0 \pm 0.9$	$0.02 \pm 0.03$
tZ	$31.8 \pm 4.3$	$6.4 \pm 1.1$	$5.3 \pm 0.8$	$7.2 \pm 1.1$	$11.8 \pm 2.0$	$33.9 \pm 4.5$
tW	$1.4 \pm 0.8$	$0.2 \pm 0.5$	$0.0 \pm 0.2$	$0.7 \pm 0.6$	$0.26 \pm 0.42$	$0.39 \pm 0.41$
WtZ	$2.3 \pm 1.2$	$0.6 \pm 0.3$	$0.3 \pm 0.21$	$0.27 \pm 0.2$	$1.1 \pm 0.7$	$0.6 \pm 0.5$
VVV	$12.4 \pm 0.5$	$0.93 \pm 0.06$	$0.35 \pm 0.03$	$0.13 \pm 0.02$	$0.14 \pm 0.03$	$0.02 \pm 0.01$
VH	$40 \pm 6$	$2.6 \pm 1.4$	$0.9 \pm 0.8$	$0.7 \pm 0.8$	$0.5 \pm 0.6$	$0.0 \pm 0.0$
t <bar>t&gt;</bar>	$12.1 \pm 1.6$	$2.9 \pm 0.6$	$2.5 \pm 0.5$	$2.8 \pm 0.5$	$11.2 \pm 1.4$	$10.9 \pm 1.5$
t <bar>t&gt;H</bar>	$0.24 \pm 0.03$	$0.05 \pm 0.01$	$0.04 \pm 0.01$	$0.06 \pm 0.01$	$0.20 \pm 0.03$	$0.13 \pm 0.02$
Total	$5010 \pm 260$	$227 \pm 24$	$88 \pm 12$	$57 \pm 8$	$76 \pm 16$	$53 \pm 8$

Table 15: Pre-fit yields in each of the 1-jet regions.

<sup>572</sup> The post-fit yields in each region are summarized in Figure 8.2.

<sup>573</sup>

	1j, <85% WP	1j, 77%-85% WP	1j, 70%-77% WP	1j, 60%-70% WP	1j, >60% WP	tZ CR
WZ + b – 1j	$8.1 \pm 4.9$	$4.7 \pm 2.0$	$4.6 \pm 2.0$	$5.1 \pm 2.1$	$18 \pm 10$	$5.0 \pm 2.5$
WZ + c – 1j	$260 \pm 60$	$80 \pm 14$	$43 \pm 7$	$26 \pm 5$	$7.4 \pm 2.3$	$2.1 \pm 0.7$
WZ + l – 1j	$3090 \pm 130$	$90 \pm 11$	$17.3 \pm 2.8$	$4.9 \pm 1.6$	$1.3 \pm 0.4$	$0.23 \pm 0.13$
WZ + b – 2j	$1.10 \pm 0.37$	$0.44 \pm 0.11$	$0.39 \pm 0.06$	$0.62 \pm 0.14$	$2.1 \pm 0.5$	$0.59 \pm 0.14$
WZ + c – 2j	$21 \pm 5$	$5.6 \pm 1.2$	$3.0 \pm 0.7$	$2.0 \pm 0.5$	$0.70 \pm 0.20$	$0.30 \pm 0.08$
WZ + l – 2j	$250 \pm 60$	$5.7 \pm 1.6$	$0.73 \pm 0.53$	$0.31 \pm 0.15$	$0.07 \pm 0.06$	$0.01 \pm 0.01$
WZ – Other	$13 \pm 5$	$1.4 \pm 0.4$	$0.42 \pm 0.08$	$0.2 \pm 0.01$	$0.30 \pm 0.05$	$0.67 \pm 0.15$
Other VV	$6.2 \pm 0.6$	$0.92 \pm 0.07$	$0.02 \pm 0.01$	$0.01 \pm 0.01$	$0.01 \pm 0.01$	$0.01 \pm 0.01$
ZZ	$346 \pm 57$	$19 \pm 5$	$4.3 \pm 0.8$	$2.7 \pm 0.5$	$2.4 \pm 0.1$	$2.1 \pm 0.6$
t̄W	$1.09 \pm 0.21$	$0.2 \pm 0.1$	$0.1 \pm 0.1$	$0.4 \pm 0.1$	$1.5 \pm 0.3$	$0.1 \pm 0.2$
t̄Z	$6.8 \pm 1.2$	$1.4 \pm 0.3$	$1.0 \pm 0.2$	$1.2 \pm 0.2$	$4.4 \pm 0.7$	$3.2 \pm 0.5$
rare Top	$0.14 \pm 0.04$	$0.04 \pm 0.02$	$0.04 \pm 0.0$	$0.1 \pm 0.03$	$0.14 \pm 0.04$	$0.15 \pm 0.05$
t̄WW	$0.04 \pm 0.03$	$0.01 \pm 0.02$	$0.01 \pm 0.01$	$0.01 \pm 0.01$	$0.01 \pm 0.02$	$0.01 \pm 0.01$
Z + jets	$169 \pm 37$	$8.9 \pm 1.9$	$3.7 \pm 0.8$	$3.3 \pm 0.7$	$3.2 \pm 0.7$	$0.8 \pm 0.2$
W + jets	$0.01 \pm 0.01$					
V + $\gamma$	$46 \pm 28$	$1.9 \pm 2.4$	$0.1 \pm 0.1$	$0.0 \pm 0.2$	$1.0 \pm 0.9$	$0.0 \pm 0.0$
tZ	$31 \pm 4$	$6.0 \pm 1.0$	$5.3 \pm 0.8$	$7.2 \pm 1.0$	$11.8 \pm 1.8$	$33.9 \pm 4.5$
tW	$1.37 \pm 0.82$	$0.18 \pm 0.26$	$0.01 \pm 0.12$	$0.67 \pm 0.64$	$0.26 \pm 0.42$	$0.39 \pm 0.41$
WtZ	$2.3 \pm 1.2$	$0.6 \pm 0.3$	$0.3 \pm 0.2$	$0.3 \pm 0.2$	$1.1 \pm 0.6$	$0.6 \pm 0.3$
VVV	$12.4 \pm 0.4$	$0.9 \pm 0.1$	$0.4 \pm 0.1$	$0.13 \pm 0.02$	$0.14 \pm 0.03$	$0.02 \pm 0.01$
VH	$40 \pm 6$	$2.6 \pm 1.4$	$0.9 \pm 0.8$	$0.7 \pm 0.8$	$0.4 \pm 0.6$	$0.01 \pm 0.01$
t̄t	$12.1 \pm 1.6$	$2.9 \pm 0.6$	$2.5 \pm 0.5$	$2.8 \pm 0.5$	$11.2 \pm 1.5$	$10.9 \pm 1.4$
t̄tH	$0.24 \pm 0.03$	$0.05 \pm 0.01$	$0.04 \pm 0.01$	$0.06 \pm 0.01$	$0.20 \pm 0.03$	$0.13 \pm 0.02$
Total	$5100 \pm 110$	$227 \pm 12$	$87 \pm 6$	$56.7 \pm 4.4$	$76 \pm 9$	$52.5 \pm 4.2$

Table 16: Post-fit yields in each of the 1-jet regions.

<sup>574</sup> The impact of each NP is calculated by performing the fit with the parameter of interest held  
<sup>575</sup> fixed, varied from its fitted value by its uncertainty, and calculating  $\Delta\mu$  relative to the baseline  
<sup>576</sup> fit. The impact of the most significant sources of systematic uncertainties on WZ + b with one  
<sup>577</sup> associated jet is summarized in Table 17.

Uncertainty Source	$\Delta\mu$	
WZ + 1-jet light cross-section	0.13	-0.15
WZ + 1-jet charm cross-section	-0.10	0.12
Jet Energy Scale	0.1	-0.13
Other Diboson + b cross-section	-0.09	0.09
tZ cross-section	-0.08	0.08
WZ 1-jet/2-jet Migration	0.08	-0.07
Jet Energy Resolution	-0.07	0.08
Luminosity	-0.06	0.07
Flavor tagging	0.05	0.05
t <bar>t} cross-section</bar>	-0.05	0.05
Total Systematic Uncertainty	0.28	0.33

Table 17: Summary of the most significant sources of systematic uncertainty on the measurement of WZ + b with exactly one associated jet.

Uncertainty Source	$\Delta\sigma/\sigma_{\text{nominal}}$	
WZ + c 1j/2j migration	0.12	-0.09
Flavor Tagging	0.09	0.08
WZ + b, 1-jet cross-section	-0.04	0.05
Luminosity	-0.04	0.04
Jet Energy Resolution	0.04	0.04
WZ + b, 2-jet cross-section	0.04	-0.03
WZ cross-section - QCD scale	-0.04	0.04
Jet Energy Scaling	0.04	0.02
WZ cross-section - PDF	-0.03	0.03
WZ + light, 1-jet cross-section	0.03	-0.03
total	0.1879	0.1753

Table 18: Summary of the most significant sources of systematic uncertainty on the measurement of WZ + c with exactly one associated jet.

578 The ranking and impact of those nuisance parameters with the largest contribution to the overall  
 579 uncertainty is shown in Figure 35.

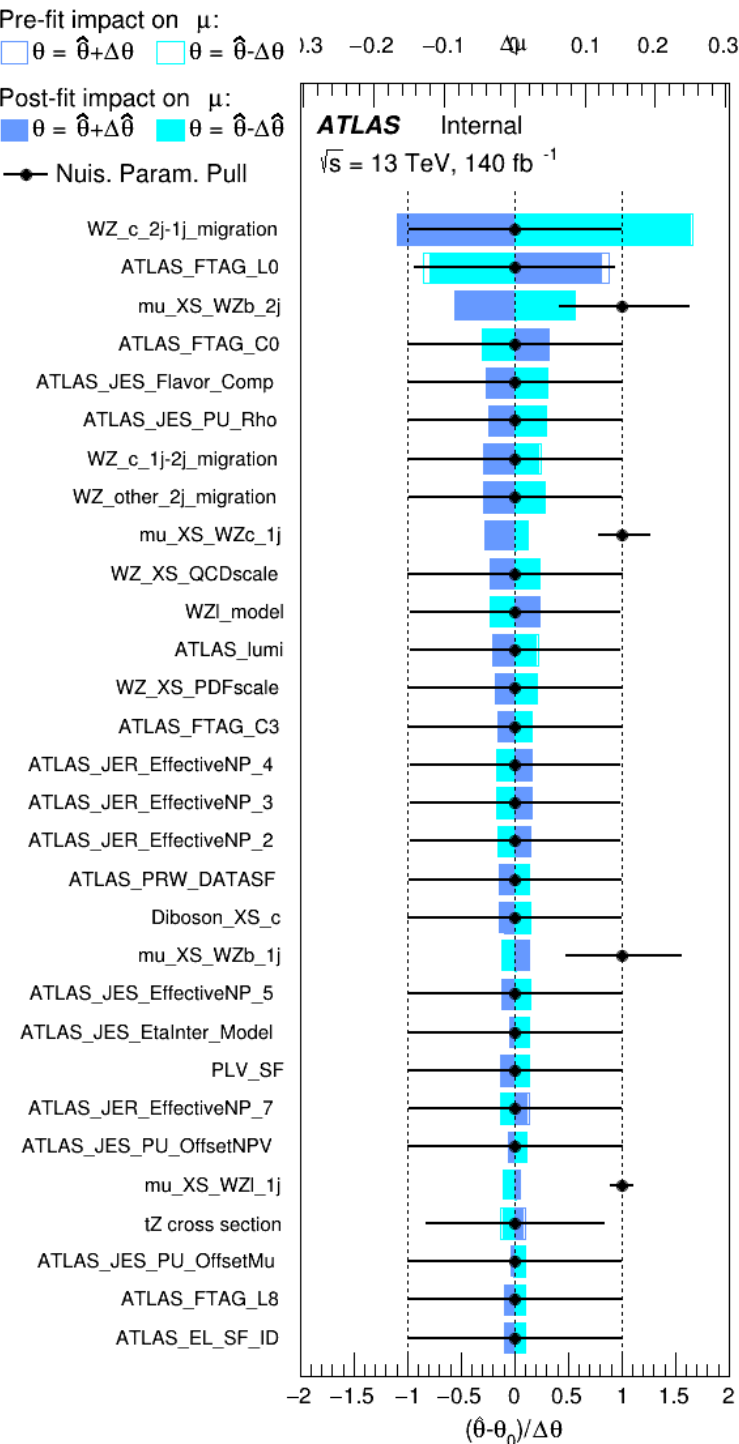


Figure 35: Impact of systematic uncertainties on the signal-strength of  $WZ + b$  for events with exactly one jet

580 The large impact of the Jet Energy Scale and Jet Flavor Tagging is unsurprising, as the shape of  
 581 the fit regions depends heavily on the modeling of the jets. The other major sources of uncertainty  
 582 come from background modelling and cross-section uncertainty.

583 Pre-fit yields in each of the 2-jet fit are shown in Figure 8.2.

	2j, <85% WP	2j, 77%-85% WP	2j, 70%-77% WP	2j, 60%-70% WP	2j, >60% WP	tZ CR 2j
WZ + b - 2j	$3.1 \pm 1.6$	$6.7 \pm 0.5$	$5.6 \pm 0.4$	$8.0 \pm 0.6$	$24 \pm 2$	$5 \pm 1$
WZ + c - 2j	$180 \pm 20$	$54 \pm 6$	$41 \pm 3$	$24 \pm 3$	$17 \pm 2$	$7.0 \pm 0.6$
WZ + l - 2j	$1250 \pm 150$	$90 \pm 14$	$18 \pm 3$	$5.8 \pm 1.4$	$1.4 \pm 0.4$	$0.25 \pm 0.15$
WZ + b - 1j	$3.4 \pm 0.6$	$1.52 \pm 0.35$	$1.58 \pm 0.23$	$1.95 \pm 0.39$	$7.8 \pm 1.1$	$0.8 \pm 0.6$
WZ + c - 1j	$56 \pm 14$	$17.6 \pm 4.0$	$8.6 \pm 2.2$	$6.3 \pm 1.8$	$3.0 \pm 0.9$	$0.7 \pm 0.2$
WZ + l - 1j	$427 \pm 120$	$24 \pm 7$	$4.7 \pm 2.3$	$1.6 \pm 0.7$	$0.3 \pm 0.2$	$0.01 \pm 0.01$
WZ - Other	$129 \pm 29$	$6.1 \pm 4.6$	$1.2 \pm 0.3$	$0.3 \pm 0.2$	$2.9 \pm 0.5$	$3.6 \pm 0.6$
Other VV	$7.63 \pm 0.63$	$0.6 \pm 0.5$	$0.16 \pm 0.03$	$0.01 \pm 0.01$	$0.1 \pm 0.1$	$0.1 \pm 0.1$
ZZ	$135 \pm 20$	$14.1 \pm 3.2$	$4.7 \pm 0.8$	$4.0 \pm 0.6$	$4.1 \pm 0.7$	$3.1 \pm 0.5$
t̄tW	$0.8 \pm 0.2$	$0.4 \pm 0.1$	$0.5 \pm 0.1$	$0.7 \pm 0.2$	$4.3 \pm 0.6$	$3.9 \pm 0.6$
t̄tZ	$14.7 \pm 2.2$	$5.6 \pm 0.8$	$4.5 \pm 0.7$	$6.5 \pm 1.1$	$25.4 \pm 4.0$	$21.9 \pm 3.4$
rare Top	$0.14 \pm 0.04$	$0.07 \pm 0.03$	$0.03 \pm 0.02$	$0.09 \pm 0.03$	$0.37 \pm 0.07$	$0.6 \pm 0.1$
t̄tWW	$0.04 \pm 0.03$	$0.02 \pm 0.02$	$0.01 \pm 0.01$	$0.01 \pm 0.00$	$0.03 \pm 0.03$	$0.01 \pm 0.01$
Z + jets	$110.0 \pm 22.9$	$9.6 \pm 2.0$	$2.1 \pm 0.50$	$1.6 \pm 0.4$	$5.1 \pm 1.1$	$1.5 \pm 0.3$
W + jets	$0.0 \pm 0.0$	$0.0 \pm 0.0$	$0.0 \pm 0.0$	$0.0 \pm 0.0$	$0.0 \pm 0.0$	$0.0 \pm 0.0$
V + γ	$25 \pm 18$	$0.5 \pm 0.2$	$0.1 \pm 0.1$	$0.1 \pm 0.1$	$0.0 \pm 0.02$	$0.05 \pm 0.07$
tZ	$21.9 \pm 2.9$	$9.6 \pm 1.3$	$9.1 \pm 1.0$	$10.0 \pm 1.5$	$14.7 \pm 3.2$	$60 \pm 6$
tW	$0.9 \pm 0.7$	$0.2 \pm 0.3$	$0.0 \pm 0.1$	$0.0 \pm 0.0$	$0.8 \pm 0.6$	$0.2 \pm 0.2$
WtZ	$4.9 \pm 2.5$	$1.5 \pm 0.8$	$1.1 \pm 0.6$	$1.3 \pm 0.7$	$4.6 \pm 2.4$	$3.3 \pm 1.7$
VVV	$7.4 \pm 0.3$	$1.0 \pm 0.1$	$0.4 \pm 0.1$	$0.2 \pm 0.1$	$0.13 \pm 0.03$	$0.04 \pm 0.01$
VH	$19.5 \pm 4.2$	$2.8 \pm 1.6$	$0.7 \pm 0.7$	$0.1 \pm 0.2$	$0.0 \pm 0.0$	$0.0 \pm 0.0$
t̄t	$0.7 \pm 0.4$	$0.1 \pm 0.1$	$0.05 \pm 0.06$	$0.15 \pm 0.13$	$0.8 \pm 0.5$	$2.3 \pm 1.2$
t̄t	$6.8 \pm 1.0$	$2.4 \pm 0.5$	$1.8 \pm 0.4$	$3.3 \pm 0.6$	$8.4 \pm 1.2$	$13.6 \pm 1.7$
t̄tH	$0.4 \pm 0.1$	$0.2 \pm 0.1$	$0.16 \pm 0.02$	$0.23 \pm 0.03$	$0.94 \pm 0.11$	$1.03 \pm 0.12$
Total	$2580 \pm 160$	$229 \pm 24$	$89 \pm 13$	$69 \pm 11$	$120 \pm 15$	$108 \pm 11$

Table 19: Pre-fit yields in each of the 2-jet regions.

584 The post-fit yields in each region are summarized in Figure 8.2.

	2j, <85% WP	2j, 77%-85% WP	2j, 70%-77% WP	2j, 60%-70% WP	2j, >60% WP	tZ CR 2j
WZ + b	$13 \pm 6$	$6.7 \pm 2.9$	$5.8 \pm 2.5$	$8.0 \pm 3.5$	$31 \pm 13$	$14 \pm 5$
WZ + c	$260 \pm 60$	$77 \pm 15$	$41 \pm 8$	$26 \pm 5$	$10.9 \pm 2.4$	$4.8 \pm 1.1$
WZ + l	$1860 \pm 90$	$90 \pm 12$	$17.6 \pm 2.8$	$5.8 \pm 1.3$	$1.4 \pm 0.4$	$0.3 \pm 0.2$
WZ + b - 1j	$3.4 \pm 0.6$	$1.52 \pm 0.35$	$1.58 \pm 0.23$	$1.95 \pm 0.39$	$6.7 \pm 1.1$	$1.9 \pm 0.6$
WZ + c - 1j	$56 \pm 14$	$17.6 \pm 4.0$	$8.6 \pm 2.2$	$6.3 \pm 1.8$	$3.0 \pm 0.9$	$0.7 \pm 0.2$
WZ + l - 1j	$427 \pm 120$	$24 \pm 7$	$4.7 \pm 2.3$	$1.6 \pm 0.7$	$0.3 \pm 0.2$	$0.01 \pm 0.01$
WZ - Other	$129 \pm 29$	$6.1 \pm 4.6$	$1.2 \pm 0.3$	$0.3 \pm 0.2$	$2.9 \pm 0.5$	$3.6 \pm 0.6$
Other VV	$7.6 \pm 0.6$	$0.3 \pm 0.3$	$0.3 \pm 0.1$	$0.1 \pm 0.06$	$0.03 \pm 0.02$	$0.1 \pm 0.1$
ZZ	$145 \pm 30$	$11.3 \pm 4.4$	$2.7 \pm 1.6$	$1.0 \pm 0.3$	$4.0 \pm 0.1$	$2.4 \pm 0.1$
t̄tW	$0.8 \pm 0.2$	$0.4 \pm 0.1$	$0.54 \pm 0.12$	$0.74 \pm 0.15$	$4.3 \pm 0.6$	$3.9 \pm 0.6$
t̄tZ	$14.7 \pm 2.2$	$5.6 \pm 0.8$	$4.5 \pm 0.7$	$6.5 \pm 1.0$	$25.4 \pm 3.9$	$21.9 \pm 3.3$
rare Top	$0.14 \pm 0.04$	$0.07 \pm 0.03$	$0.03 \pm 0.02$	$0.09 \pm 0.03$	$0.4 \pm 0.1$	$0.6 \pm 0.1$
t̄tWW	$0.04 \pm 0.03$	$0.02 \pm 0.02$	$0.01 \pm 0.01$	$0.01 \pm 0.01$	$0.03 \pm 0.03$	$0.01 \pm 0.01$
Z + jets	$110 \pm 23$	$9.6 \pm 2.0$	$2.1 \pm 0.5$	$1.6 \pm 0.4$	$5.1 \pm 1.1$	$1.5 \pm 0.3$
W + jets	$0.0 \pm 0.0$					
V + $\gamma$	$25 \pm 19$	$0.5 \pm 0.2$	$0.1 \pm 0.1$	$0.13 \pm 0.14$	$0.0 \pm 0.02$	$0.05 \pm 0.07$
tZ	$21.9 \pm 2.7$	$9.6 \pm 1.2$	$7.1 \pm 0.9$	$10.0 \pm 1.4$	$14.7 \pm 3.0$	$60 \pm 6$
tW	$0.1 \pm 0.7$	$0.2 \pm 0.3$	$0.0 \pm 0.1$	$0.0 \pm 0.0$	$0.8 \pm 0.6$	$0.2 \pm 0.2$
WtZ	$4.9 \pm 2.5$	$1.5 \pm 0.8$	$1.1 \pm 0.6$	$1.3 \pm 0.7$	$4.6 \pm 2.3$	$3.3 \pm 1.7$
VVV	$7.4 \pm 0.3$	$1.0 \pm 0.1$	$0.36 \pm 0.03$	$0.19 \pm 0.03$	$0.13 \pm 0.03$	$0.04 \pm 0.01$
VH	$19 \pm 4$	$2.8 \pm 1.6$	$0.7 \pm 0.7$	$0.1 \pm 0.2$	$0.0 \pm 0.0$	$0.0 \pm 0.0$
t̄t	$6.8 \pm 1.0$	$2.4 \pm 0.5$	$1.8 \pm 0.4$	$3.3 \pm 0.6$	$8.4 \pm 1.2$	$13.6 \pm 1.7$
t̄tH	$0.40 \pm 0.05$	$0.19 \pm 0.03$	$0.16 \pm 0.02$	$0.23 \pm 0.03$	$0.94 \pm 0.11$	$1.03 \pm 0.11$
Total	$2580 \pm 60$	$229 \pm 11$	$89 \pm 6$	$69.1 \pm 4.1$	$120 \pm 10$	$108 \pm 6$

Table 20: Post-fit yields in each of the 2-jet regions.

585 The same set of systematic uncertainties consider for the 1-jet fit are included in the 2-jet fit as  
 586 well. The impact of the most significant systematic uncertainties is summarized in Table 21.

Uncertainty Source	$\Delta\mu$	
WZ + c 2-jet cross-section	-0.13	0.16
WZ + l 2-jet cross-section	0.12	-0.09
ttZ cross-section - QCD scale	-0.10	0.13
WZ + b 1-jet cross-section	-0.11	0.10
Jet Energy Scale	-0.11	0.11
Luminosity	-0.11	0.12
tZ cross-section	-0.11	0.11
WtZ cross-section	-0.07	0.07
Flavor tagging	0.05	0.05
Other VV + b cross-section	-0.05	0.05
Total	0.35	0.37

Table 21: Summary of the most significant sources of systematic uncertainty on the measurement of WZ + b 2-jet events.

Uncertainty Source	$\Delta\sigma/\sigma_{\text{nominal}}$	
WZ + c 1j/2j migration	-0.17	0.25
Flavor Tagging	0.14	0.13
WZ + b, 1-jet cross-section	-0.09	0.09
Jet Energy Scale	0.06	0.08
Jet Energy Resolution	0.05	0.05
WZ $\geq 3j/2j$ migration	-0.04	0.04
WZ + c 2j/1j migration	-0.04	0.04
WZ cross-section - QCD scale	-0.04	0.04
WZ + light modelling	0.04	-0.03
Luminosity	-0.03	0.03
total	0.2694	0.3274

Table 22: Summary of the most significant sources of systematic uncertainty on the measurement of WZ + c with 2 associated jets.

587 The ranking and impact of those nuisance parameters with the largest contribution to the overall  
 588 uncertainty is shown in Figure 36.

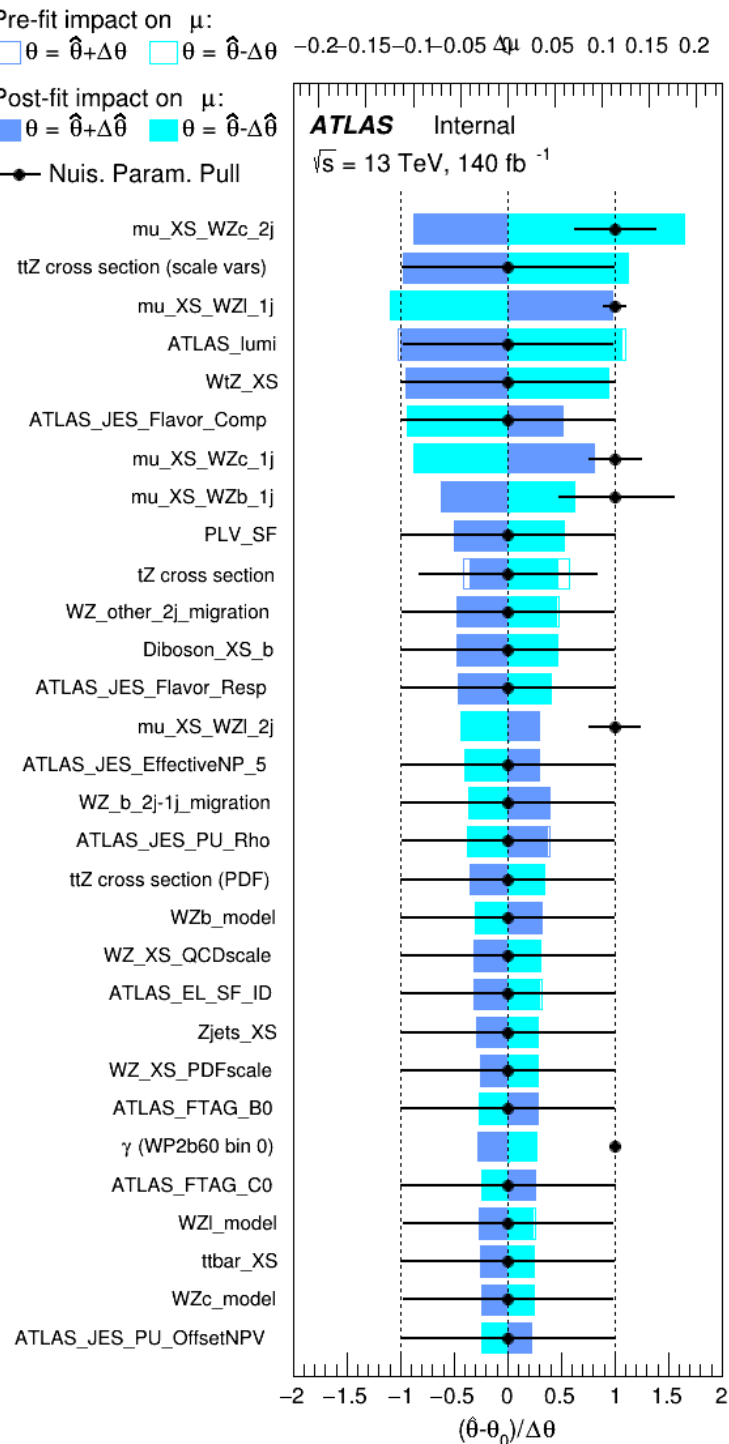


Figure 36: Impact of systematic uncertainties on the signal-strength of  $WZ + b$  in 2-jet events.

589 The large impact of the Jet Energy Scale and Jet Flavor Tagging is unsurprising, as the shape of  
590 the fit regions depends heavily on the modeling of the jets. The other major sources of uncertainty  
591 come from background modelling and cross-section uncertainty.

592 **8.3 Inclusive 1+2 Jet Fit**

593 An alternate fit is performed which combines the WZ + 1-jet and WZ + 2-jet samples rather than  
594 fitting them independently. This is done primarily as a cross-check of the nominal analysis, to  
595 see if measuring 1-jet and 2-jet events separately and combining them gives drastically different  
596 results than measuring them together.

597 For this study, three signal templates, WZ + b, WZ + charm and WZ + light, are fit to data, and  
598 the systematics accounting for migrations between 1-jet and 2-jet bins are removed. All other  
599 background and nuisance parameters remain the same as the nominal fit.

600 The measured  $\mu$  value for WZ + b is  $\mu = 1.00^{+0.30}_{-0.29}(\text{stat})^{+0.25}_{-23}(\text{sys})$ , with a significance of  $2.8\sigma$ ,  
601 and the uncertainty on WZ + charm is  $\mu = 1.00 \pm 0.12(\text{stat}) \pm 0.13(\text{sys})$ . This is compared to  
602 combined uncertainty of  $\mu = 1.00^{+0.32}_{-0.30}(\text{stat})^{+0.24}_{-23}(\text{sys})$  for WZ + b when 1-jet and 2-jet events  
603 are measured separately and then combined.

604 A post-fit summary plot of the fit regions is shown in Figure 37:

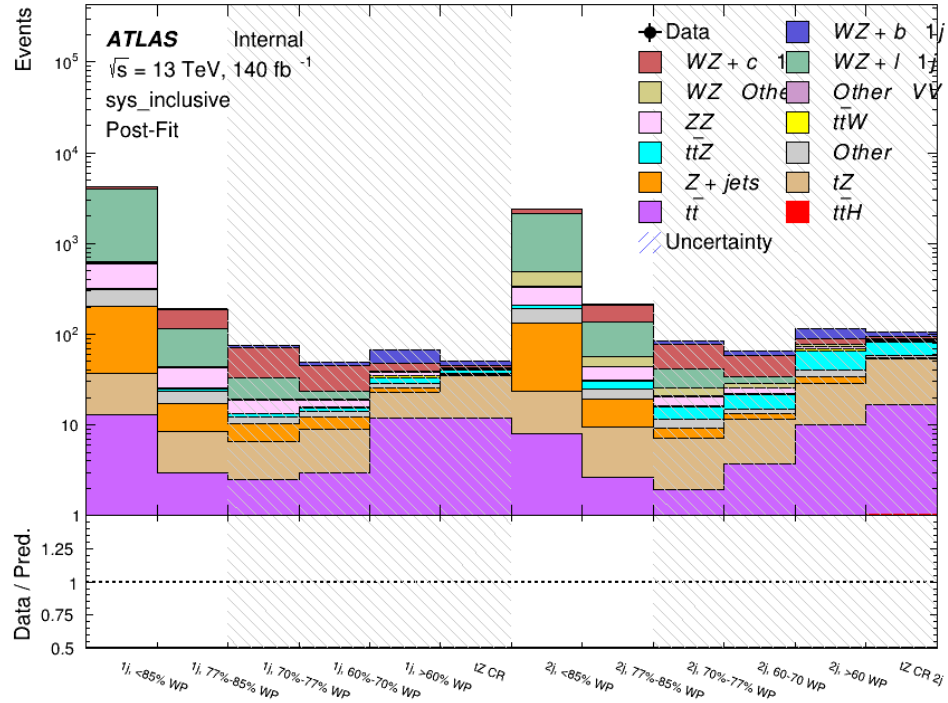


Figure 37: Post-fit summary of the 1-jet fit regions.

605 The impact of the most significant sources of systematic uncertainties on the measurement of  
 606 WZ+b is summarized in Table 23.

Uncertainty Source	$\Delta\mu$	
WZ + light cross-section	0.13	-0.12
WZ + charm cross-section	-0.10	0.12
Jet Energy Scale	0.08	0.13
tZ cross-section	-0.10	0.10
Jet Energy Resolution	-0.10	0.10
Luminosity	-0.08	0.09
Other Diboson + b cross-section	-0.07	0.07
Flavor tagging	0.05	0.05
t̄t cross-section	-0.05	0.05
WZ cross-section - QCD scale	-0.04	0.03
Total Systematic Uncertainty	0.28	0.32

Table 23: Summary of the most significant sources of systematic uncertainty on the measurement of WZ + b with one or two associated jets.

607 The ranking and impact of those nuisance parameters with the largest contribution to the overall  
608 uncertainty is shown in Figure 38.

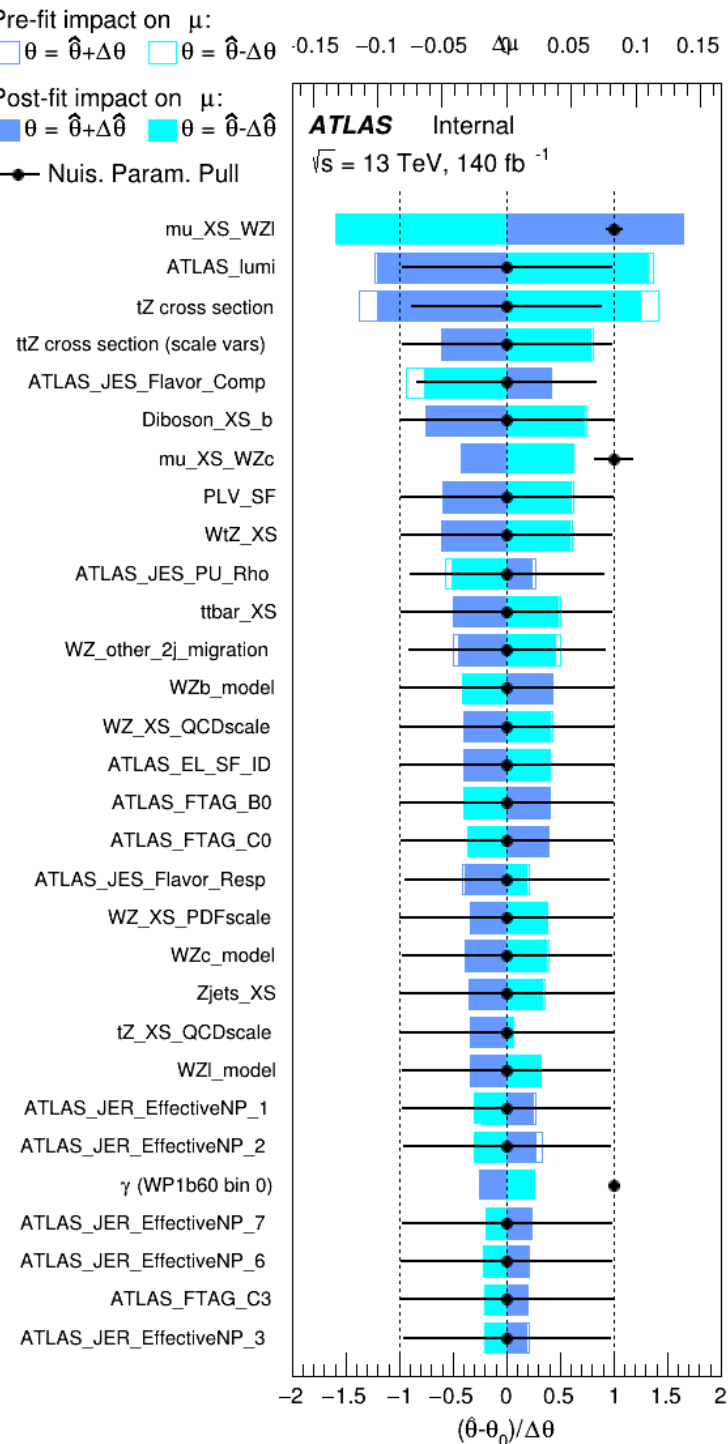


Figure 38: Impact of systematic uncertainties on the signal-strength of  $WZ + b$  for events with one or two jets

609 **8.4 Alternate tZ Inclusive Fit**

610 **8.4.1 tZ Inclusive Fit**

611 While tZ is often considered as a distinct process from WZ + b, this could also be considered part  
 612 of the signal. Alternate studies are performed where, using the same framework as the nominal  
 613 analysis, a measurement of WZ + b is performed that includes tZ as part of WZ+b.

614 Because of this change, the tZ CR is no longer necessary, and only the five pseudo-continuous  
 615 b-tag regions are used in the fit. Further, systematics related to the tZ cross-section are removed  
 616 from the fit, as they are now encompassed by the normalization measurement of WZ + b. All  
 617 other systematic uncertainties are carried over from the nominal analysis.

618 An expected WZ + b cross-section of  $4.1^{+0.78}_{-0.74}(\text{stat})^{+0.53}_{-0.52}(\text{sys}) \text{ fb}$  is extracted from the fit, with  
 619 an expected significance of  $4.0\sigma$ .

620 The impact of the predominate systematics are summarized in Table 24.

Uncertainty Source	$\Delta\mu$	
WZ + light cross-section	0.08	-0.08
Jet Energy Scale	-0.06	0.08
Luminosity	-0.05	0.06
WZ + charm cross-section	-0.04	0.05
Other Diboson + b cross-section	-0.04	0.04
WZ cross-section - QCD scale	-0.04	0.03
t̄t cross-section	-0.03	0.03
Jet Energy Resolution	-0.03	0.03
Flavor tagging	-0.03	0.03
Z+jets cross section	-0.02	0.02
Total Systematic Uncertainty	-0.15	0.16

Table 24: Summary of the most significant sources of systematic uncertainty on the measurement of WZ + b with exactly one associated jet.

621 **8.4.2 Floating tZ**

622 In order to quantify the impact of the tZ uncertainty on the fit, an alternate fit strategy is used  
 623 where the tZ normalization is allowed to float. This normalization factor replaces the cross-  
 624 section uncertainty on tZ, and all other parameters of the fit remain the same.

625 An uncertainty of 17% on the normalization of tZ is extracted from the fit, compared to a theory  
 626 uncertainty of 15% applied to the tZ cross-section. The measured uncertainties on WZ remain  
 627 the same.

## 628 9 Conclusion

629 A measurement of WZ + heavy flavor is performed using  $140 \text{ fb}^{-1}$  of  $\sqrt{s} = 13 \text{ TeV}$  proton-  
 630 proton collision data collected by the ATLAS detector at the LHC. The expected cross-section  
 631 of WZ+b with 1-jet is  $1.74^{+0.82}_{-0.75}(\text{stat})^{+0.53}_{-0.48}(\text{sys}) \text{ fb}$ , and  $14.6 \pm 2.5(\text{stat}) \pm 2.3(\text{sys}) \text{ fb}$  for WZ  
 632 + charm, with a correlation of -0.22 between them. An expected significance of 2.0 is observed  
 633 for WZ + b in this region.

634 For the 2-jet regions, an expected significance of 1.7 is observed for WZ + b, with an ex-  
 635 pected cross-section of  $2.5^{+1.3}_{-1.3}(\text{stat})^{+0.95}_{-0.83}(\text{sys}) \text{ fb}$ . For WZ + charm, a cross-section of  
 636  $12.7 \pm 3.2(\text{stat}) \pm 2.7(\text{sys}) \text{ fb}$  is expected for 2-jet events. A correlation of -0.26 is observed  
 637 for WZ+b and WZ + charm.

638 **This section will be include final results once unblinded.**

## 639 References

- 640 [1] ATLAS Collaboration. ‘Observation of electroweak  $W^\pm Z$  boson pair production in asso-  
 641 ciation with two jets in pp collisions at  $\sqrt{s} = 13 \text{ TeV}$  with the ATLAS detector’. In: *Phys.*  
 642 *Lett.* B793 (2019), pp. 469–492. doi: [10.1016/j.physletb.2019.05.012](https://doi.org/10.1016/j.physletb.2019.05.012). arXiv:  
 643 [1812.09740 \[hep-ex\]](https://arxiv.org/abs/1812.09740).
- 644 [2] ATLAS Collaboration. ‘Luminosity determination in pp collisions at  $\sqrt{s} = 7 \text{ TeV}$  using  
 645 the ATLAS detector at the LHC’. In: *Eur. Phys. J. C* 71 (2011), p. 1630. doi: [10.1140/epjc/s10052-011-1630-5](https://doi.org/10.1140/epjc/s10052-011-1630-5). arXiv: [1101.2185 \[hep-ex\]](https://arxiv.org/abs/1101.2185).
- 647 [3] ATLAS Collaboration. ‘Performance of the ATLAS detector using first collision data’.  
 648 In: *JHEP* 09 (2010), p. 056. doi: [10.1007/JHEP09\(2010\)056](https://doi.org/10.1007/JHEP09(2010)056). arXiv: [1005.5254 \[hep-ex\]](https://arxiv.org/abs/1005.5254).
- 650 [4] S. Agostinelli et al. ‘GEANT4: A Simulation toolkit’. In: *Nucl. Instrum. Meth.* A506  
 651 (2003), pp. 250–303. doi: [10.1016/S0168-9002\(03\)01368-8](https://doi.org/10.1016/S0168-9002(03)01368-8).
- 652 [5] T. Gleisberg et al. ‘Event generation with SHERPA 1.1’. In: *JHEP* 02 (2009), p. 007. doi:  
 653 [10.1088/1126-6708/2009/02/007](https://doi.org/10.1088/1126-6708/2009/02/007). arXiv: [0811.4622 \[hep-ph\]](https://arxiv.org/abs/0811.4622).
- 654 [6] H.-L. Lai et al. ‘New parton distributions for collider physics’. In: *Phys. Rev. D* 82 (2010),  
 655 p. 074024. doi: [10.1103/PhysRevD.82.074024](https://doi.org/10.1103/PhysRevD.82.074024). arXiv: [1007.2241 \[hep-ph\]](https://arxiv.org/abs/1007.2241).
- 656 [7] J. Alwall et al. ‘The automated computation of tree-level and next-to-leading order dif-  
 657 ferential cross sections, and their matching to parton shower simulations’. In: *JHEP* 07  
 658 (2014), p. 079. doi: [10.1007/JHEP07\(2014\)079](https://doi.org/10.1007/JHEP07(2014)079). arXiv: [1405.0301 \[hep-ph\]](https://arxiv.org/abs/1405.0301).
- 659 [8] R. D. Ball et al. ‘Parton distributions for the LHC Run II’. In: *JHEP* 04 (2015), p. 040.  
 660 doi: [10.1007/JHEP04\(2015\)040](https://doi.org/10.1007/JHEP04(2015)040). arXiv: [1410.8849 \[hep-ph\]](https://arxiv.org/abs/1410.8849).
- 661 [9] M. Bahr et al. ‘Herwig++ Physics and Manual’. In: *Eur. Phys. J. C* 58 (2008), p. 639. doi:  
 662 [10.1140/epjc/s10052-008-0798-9](https://doi.org/10.1140/epjc/s10052-008-0798-9). arXiv: [0803.0883 \[hep-ph\]](https://arxiv.org/abs/0803.0883).

- 663 [10] R. D. Ball et al. ‘Parton distributions with LHC data’. In: *Nucl. Phys. B* 867 (2013), p. 244.  
 664 doi: [10.1016/j.nuclphysb.2012.10.003](https://doi.org/10.1016/j.nuclphysb.2012.10.003). arXiv: [1207.1303 \[hep-ph\]](https://arxiv.org/abs/1207.1303).
- 665 [11] S. Frixione, G. Ridolfi and P. Nason. ‘A positive-weight next-to-leading-order Monte Carlo  
 666 for heavy flavour hadroproduction’. In: *JHEP* 09 (2007), p. 126. doi: [10.1088/1126-  
 6708/2007/09/126](https://doi.org/10.1088/1126-6708/2007/09/126). arXiv: [0707.3088 \[hep-ph\]](https://arxiv.org/abs/0707.3088).
- 668 [12] E. Re. ‘Single-top Wt-channel production matched with parton showers using the POWHEG  
 669 method’. In: *Eur. Phys. J. C* 71 (2011), p. 1547. doi: [10.1140/epjc/s10052-011-  
 670 1547-z](https://doi.org/10.1140/epjc/s10052-011-1547-z). arXiv: [1009.2450 \[hep-ph\]](https://arxiv.org/abs/1009.2450).
- 671 [13] ATLAS Collaboration. *Electron efficiency measurements with the ATLAS detector using  
 672 the 2015 LHC proton–proton collision data*. ATLAS-CONF-2016-024. 2016. URL: <https://cds.cern.ch/record/2157687>.
- 674 [14] ATLAS Collaboration. ‘Measurement of the muon reconstruction performance of the  
 675 ATLAS detector using 2011 and 2012 LHC proton–proton collision data’. In: *Eur. Phys.  
 676 J. C* 74 (2014), p. 3130. doi: [10.1140/epjc/s10052-014-3130-x](https://doi.org/10.1140/epjc/s10052-014-3130-x). arXiv: [1407.3935  
 677 \[hep-ex\]](https://arxiv.org/abs/1407.3935).
- 678 [15] R. Narayan et al. *Measurement of the total and differential cross sections of a top-quark-  
 679 antiquark pair in association with a W boson in proton-proton collisions at a centre-of-  
 680 mass energy of 13 TeV with ATLAS detector at the Large Hadron Collider*. Tech. rep.  
 681 ATL-COM-PHYS-2020-217. Geneva: CERN, Mar. 2020. URL: <https://cds.cern.ch/record/2712986>.
- 683 [16] ATLAS Collaboration. *Jet Calibration and Systematic Uncertainties for Jets Reconstruc-  
 684 ted in the ATLAS Detector at  $\sqrt{s} = 13$  TeV*. ATL-PHYS-PUB-2015-015. 2015. URL:  
 685 <https://cds.cern.ch/record/2037613>.
- 686 [17] ATLAS Collaboration. *Selection of jets produced in 13 TeV proton–proton collisions with  
 687 the ATLAS detector*. ATLAS-CONF-2015-029. 2015. URL: <https://cds.cern.ch/record/2037702>.
- 689 [18] ATLAS Collaboration. ‘Performance of pile-up mitigation techniques for jets in pp col-  
 690 lisions at  $\sqrt{s} = 8$  TeV using the ATLAS detector’. In: *Eur. Phys. J. C* 76 (2016), p. 581.  
 691 doi: [10.1140/epjc/s10052-016-4395-z](https://doi.org/10.1140/epjc/s10052-016-4395-z). arXiv: [1510.03823 \[hep-ex\]](https://arxiv.org/abs/1510.03823).
- 692 [19] ATLAS Collaboration. ‘Performance of missing transverse momentum reconstruction  
 693 with the ATLAS detector using proton–proton collisions at  $\sqrt{s} = 13$  TeV’. In: *The  
 694 European Physical Journal C* 78.11 (Nov. 2018). ISSN: 1434-6052. doi: [10.1140/epjc/s10052-018-  
 695 6288-9](https://doi.org/10.1140/epjc/s10052-018-6288-9). URL: [http://dx.doi.org/10.1140/epjc/s10052-018-  
 696 6288-9](http://dx.doi.org/10.1140/epjc/s10052-018-6288-9).
- 697 [20] 2021. URL: [https://twiki.cern.ch/twiki/bin/view/AtlasProtected/BTagCalibrationRecommendationsRelease21#Tools\\_for\\_Flavor\\_Tagging\\_Calibra](https://twiki.cern.ch/twiki/bin/view/AtlasProtected/BTagCalibrationRecommendationsRelease21#Tools_for_Flavor_Tagging_Calibra).
- 700 [21] ATLAS Collaboration. ‘Measurement of the fiducial and differential cross-section of a top  
 701 quark pair in association with a Z boson at 13 TeV with the ATLAS detector’. In: ATL-  
 702 COM-PHYS-2019-334 (Apr. 2019). URL: <https://cds.cern.ch/record/2672207>.

- 703 [22] T. Chen and C. Guestrin. ‘XGBoost: A Scalable Tree Boosting System’. In: *Proceedings*  
704 *of the 22nd ACM SIGKDD International Conference on Knowledge Discovery and Data*  
705 *Mining*. KDD ’16. San Francisco, California, USA: ACM, 2016, pp. 785–794. ISBN: 978-  
706 1-4503-4232-2. doi: [10.1145/2939672.2939785](https://doi.acm.org/10.1145/2939672.2939785). URL: <http://doi.acm.org/10.1145/2939672.2939785>.
- 707  
708 [23] ‘Luminosity determination in pp collisions at  $\sqrt{s} = 13$  TeV using the ATLAS detector at  
709 the LHC’. In: (June 2019).
- 710 [24] ATLAS Collaboration. ‘The new LUCID-2 detector for luminosity measurement and  
711 monitoring in ATLAS’. In: *JINST* 13.07 (2018), P07017. doi: [10.1088/1748-0221/13/07/P07017](https://doi.org/10.1088/1748-0221/13/07/P07017).
- 712  
713 [25] ATLAS Collaboration. ‘Jet energy resolution in proton-proton collisions at  $\sqrt{s} = 7$  TeV  
714 recorded in 2010 with the ATLAS detector’. In: *The European Physical Journal C* 73.3  
715 (Mar. 2013), p. 2306. ISSN: 1434-6052. doi: [10.1140/epjc/s10052-013-2306-0](https://doi.org/10.1140/epjc/s10052-013-2306-0).  
716 URL: <https://doi.org/10.1140/epjc/s10052-013-2306-0>.
- 717 [26] ATLAS Collaboration. ‘Performance of b -jet identification in the ATLAS experiment’.  
718 In: *Journal of Instrumentation* 11.04 (2016), P04008. URL: <http://stacks.iop.org/1748-0221/11/i=04/a=P04008>.
- 719  
720 [27] ATLAS Collaboration. ‘Observation of the associated production of a top quark and a  
721 Z boson in pp collisions at  $\sqrt{s}= 13$  TeV with the ATLAS detector’. In: *Journal of High*  
722 *Energy Physics* 2020.7 (July 2020). ISSN: 1029-8479. doi: [10.1007/jhep07\(2020\)124](https://doi.org/10.1007/jhep07(2020)124).  
723 URL: [http://dx.doi.org/10.1007/JHEP07\(2020\)124](http://dx.doi.org/10.1007/JHEP07(2020)124).

724 **A Appendices**

725 **A.1 Non-prompt lepton MVA**

726 A lepton MVA has been developed to better reject non-prompt leptons than standard cut  
 727 based selections based upon impact parameter, isolation and PID. The name of this MVA is  
 728 `PromptLeptonIso`. The full set of studies and detailed explanation can be found in [15].

729 The decays of W and Z bosons are commonly selected by the identification of one or two electrons  
 730 or muons. The negligible lifetimes of these bosons mean that the leptons produced in the decay  
 731 originate from the interaction vertex and are thus labelled “prompt”. Analyses using these  
 732 light leptons impose strict reconstruction quality, isolation and impact parameter requirements  
 733 to remove “fake” leptons. A significant source of the fake light leptons are non-prompt leptons  
 734 produced in decays of hadrons that contain bottom (b) or charm (c) quarks. Such hadrons  
 735 typically have microscopically significant lifetimes that can be detected experimentally.

736 These non-prompt leptons can also pass the tight selection criteria. In analyses that involve top (t)  
 737 quarks, which decay almost exclusively into a W boson and a b quark, non-prompt leptons from  
 738 the semileptonic decay of bottom and charm hadrons can be a significant source of background  
 739 events. This is particularly the case in the selection of same-sign dilepton and multilepton final  
 740 states.

741 The main idea is to identify non-prompt light leptons using lifetime information associated with a  
 742 track jet that matches the selected light lepton. This lifetime information is computed using tracks  
 743 contained within the jet. Typically, lepton lifetime is determined using the impact parameter of the  
 744 track reconstructed by the inner tracking detector which is matched to the reconstructed lepton.  
 745 Using additional reconstructed charged particle tracks increases the precision of identifying the  
 746 displaced decay vertex of bottom or charm hadrons that produced a non-prompt light lepton.  
 747 The MVA also includes information related to the isolation of the lepton to reject non-prompt  
 748 leptons.

749 `PromptLeptonIso` is a gradient boosted BDT. The training of the BDT is performed on leptons  
 750 selected from the POWHEG+PYTHIA6 non-allhad t̄t MC sample. Eight variables are used to train  
 751 the BDT in order to discriminate between prompt and non-prompt leptons. The track jets that  
 752 are matched to the non-prompt leptons correspond to jets initiated by b or c quarks, and may  
 753 contain a displaced vertex. Consequently, three of the selected variables are used to identify  
 754 b-tag jets by standard ATLAS flavour tagging algorithms. Two variables use the relationship  
 755 between the track jet and lepton: the ratio of the lepton p<sub>T</sub> with respect to the track jet p<sub>T</sub> and  
 756 ΔR between the lepton and the track jet axis. Finally three additional variables test whether the  
 757 reconstructed lepton is isolated: the number of tracks collected by the track jet and the lepton  
 758 track and calorimeter isolation variables. Table 25 describes the variables used to train the BDT  
 759 algorithm. The choice of input variables has been extensively discussed with Egamma, Muon,  
 760 Tracking, and Flavour Tagging CP groups.

761 The output distribution of the BDT is shown in Figure A.1.

Variable	Description
$N_{\text{track}}$ in track jet	Number of tracks collected by the track jet
$\text{IP2 log}(P_b/P_{\text{light}})$	Log-likelihood ratio between the b and light jet hypotheses with the IP2D algorithm
$\text{IP3 log}(P_b/P_{\text{light}})$	Log-likelihood ratio between the b and light jet hypotheses with the IP3D algorithm
$N_{\text{TrkAtVtx}}$ SV + JF	Number of tracks used in the secondary vertex found by the SV1 algorithm
$p_T^{\text{lepton}}/p_T^{\text{track jet}}$	in addition to the number of tracks from secondary vertices found by the JetFitter algorithm with at least two tracks
$\Delta R(\text{lepton}, \text{track jet})$	The ratio of the lepton $p_T$ and the track jet $p_T$
$p_T^{\text{VarCone30}}/p_T$	$\Delta R$ between the lepton and the track jet axis
$E_T^{\text{TopoCone30}}/p_T$	Lepton track isolation, with track collecting radius of $\Delta R < 0.3$

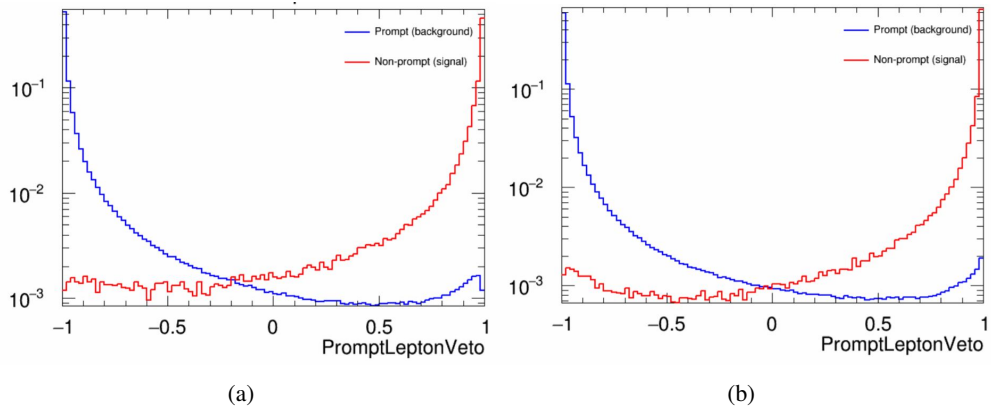
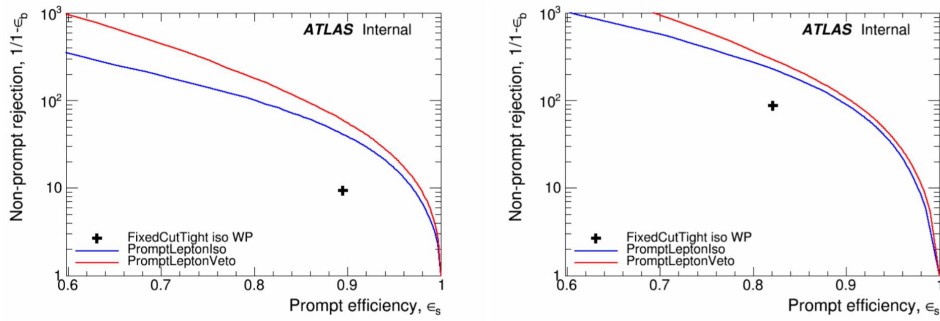
Table 25: A table of the variables used in the training of `PromptLeptonIso`.

Figure 39: Distribution of the PLV BDT discriminant for (a) electrons and (b) muons

762 The ROC curve for the BDT response, compared to the standard `FixedCutTight` WP, is shown  
 763 in figure A.1, which shows a clear improvement when using this alternate training.

Figure 40: ROC curves for the PLV as well as the performance of the standard `FixedCutTight` WP for (left) electrons and (right) muons

764 A cutoff value of -0.7 for electrons and -0.5 for muons are chosen as the WPs for this MVA, based  
 765 on an optimisation of  $S/\sqrt{B}$  performed in the preselection regions of the  $t\bar{t}H$  – ML analysis,  
 766 which have a signature similar to that of this analysis.

767 The efficiency of the tight PromptLeptonIso working point is measured using the tag and probe  
 768 method with  $Z \rightarrow \ell^+\ell^-$  events. Such calibration are performed by analysers from this analysis  
 769 in communication with the Egamma and Muon combined performance groups. The scale factor  
 770 are approximately 0.92 for  $10 < p_T < 15$  GeV, and averaging at 0.98 to 0.99 for higher  $p_T$   
 771 leptons. An extra systematic is applied to muons within  $\Delta R < 0.6$  of a calorimeter jet, since  
 772 there is a strong dependence on the scale factor due to the presence of these jets. For electrons,  
 773 the dominant systematics is coming from pile-up dependence. Overall the systematics are a  
 774 maximum of 3% at low  $p_T$  and decreasing at a function of  $p_T$ .

## 775 **A.2 Non-prompt CR Modelling**

776 In order to further validate the modeling in each of the non-prompt CRs, additional kinematic  
 777 plots are made in the Z+jets CR and  $t\bar{t}$  CR in each of the continuous b-tag regions, after the  
 778 correction factors detailed in Section 5.3 have been applied.

779 In the case of the Z+jets CR, the  $p_T$  spectrum of the lepton originating from the W candidate is  
 780 shown, as this is the distribution used to extract the scale factor applied to Z+jets. These plots  
 781 are shown in Figures 41 and 42.

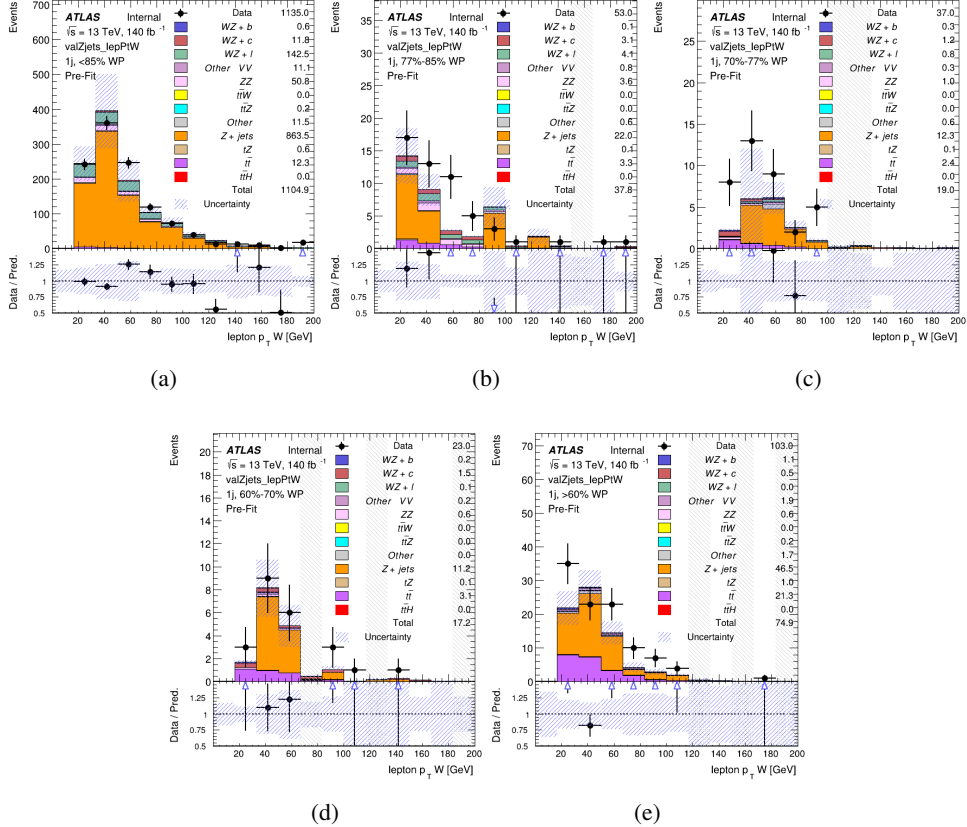


Figure 41: Comparisons between the data and MC distributions of the  $p_T$  of the lepton originating from the W-candidate in the Z+jets CR for each of the 1-jet b-tag working point regions

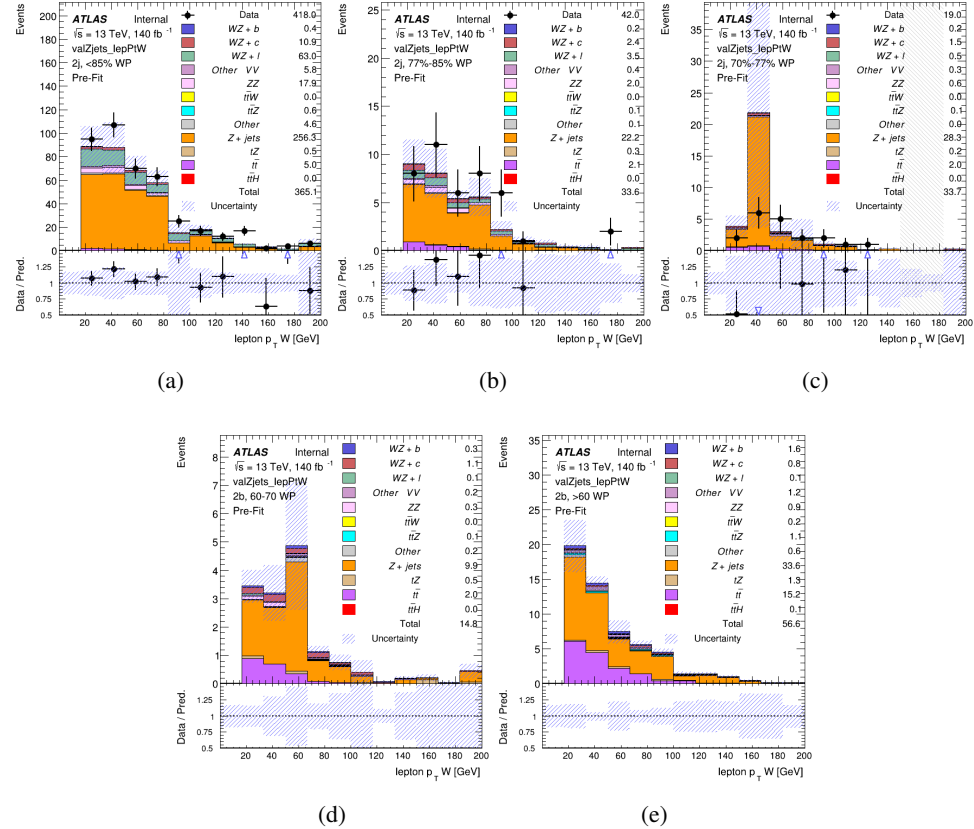


Figure 42: Comparisons between the data and MC distributions of the  $p_T$  of the lepton originating from the W-candidate in the Z+jets CR for each of the 2-jet b-tag working point regions

782 The same is shown for the  $t\bar{t}$  CR, but the  $p_T$  of the OS lepton is used instead as a representation  
 783 of the modeling, as the lepton from the W is not well defined for  $t\bar{t}$  events. These plots are shown  
 784 in Figures 43 and 44.

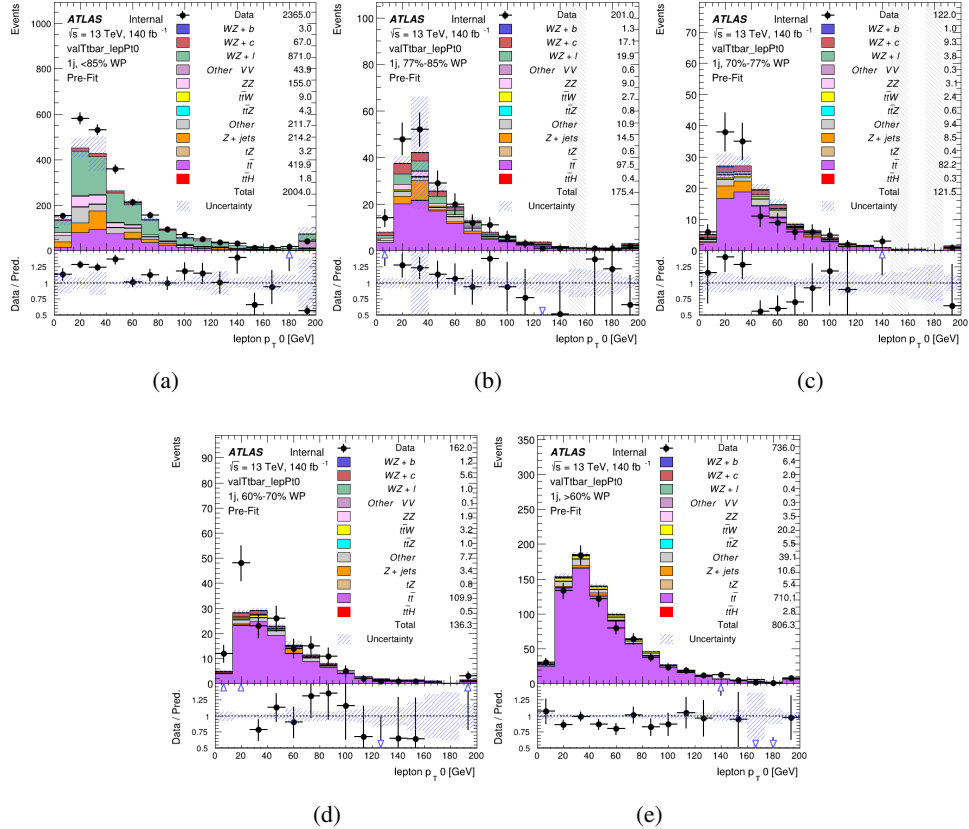


Figure 43: Comparisons between the data and MC distributions of the  $p_T$  of the OS lepton in the  $t\bar{t}$  CR for each of the 1-jet b-tag working point regions

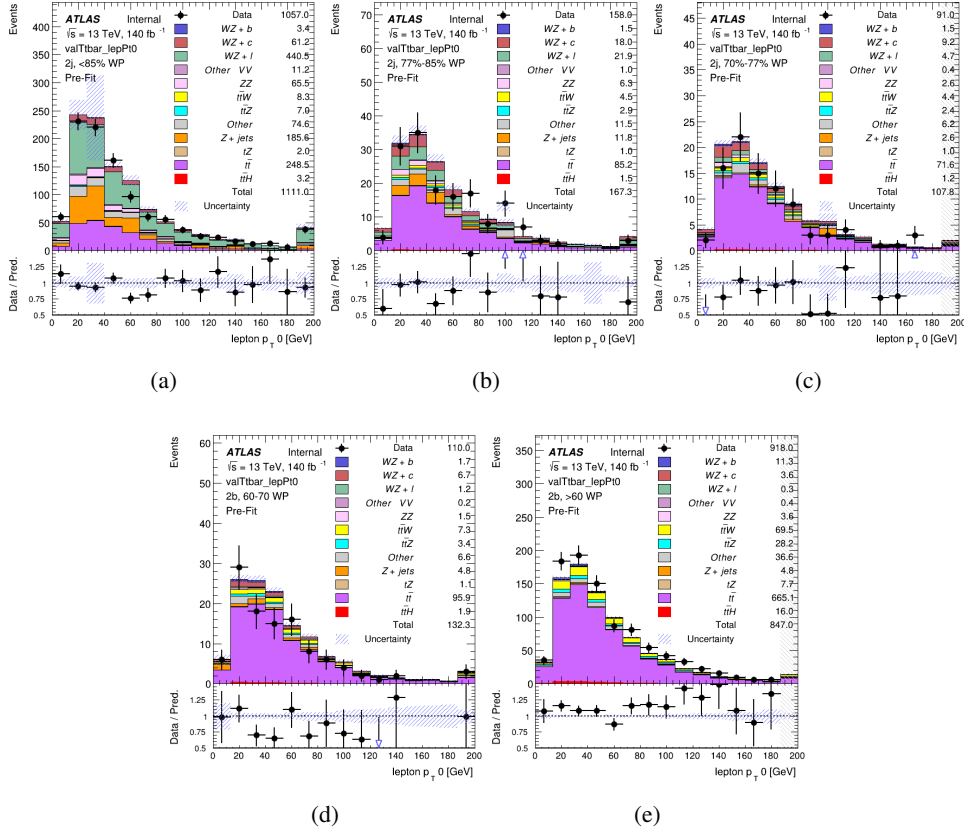


Figure 44: Comparisons between the data and MC distributions of the  $p_T$  of the OS lepton in the  $t\bar{t}$  CR for each of the 2-jet b-tag working point regions

### 785 A.3 DSID list

Data:

```
data15_13TeV.AllYear.physics_Main.PhysCont.DAOD_HIGG8D1.grp15_v01_p4134
data16_13TeV.AllYear.physics_Main.PhysCont.DAOD_HIGG8D1.grp16_v01_p4134
data17_13TeV.AllYear.physics_Main.PhysCont.DAOD_HIGG8D1.grp17_v01_p4134
data18_13TeV.AllYear.physics_Main.PhysCont.DAOD_HIGG8D1.grp18_v01_p4134
```

mc16a:

```
mc16_13TeV.361603.PowhegPy8EG_CT10nloME_AZNLOCTEQ6L1_ZZllll_mll4.deriv.DAOD_HIGG8D1.e4475_s3126_r9364_r9315_p4133
mc16_13TeV.361602.PowhegPy8EG_CT10nloME_AZNLOCTEQ6L1_WZlvvv_mll4.deriv.DAOD_HIGG8D1.e4054_s3126_r9364_r9315_p4133
mc16_13TeV.361604.PowhegPy8EG_CT10nloME_AZNLOCTEQ6L1_ZZvvll_mll4.deriv.DAOD_HIGG8D1.e4475_s3126_r9364_r9315_p4133
mc16_13TeV.361600.PowhegPy8EG_CT10nloME_AZNLOCTEQ6L1_WWlvvv.deriv.DAOD_HIGG8D1.e4616_s3126_r9364_r9315_p4133
mc16_13TeV.361605.PowhegPy8EG_CT10nloME_AZNLOCTEQ6L1_ZZvvvv_mll4.deriv.DAOD_HIGG8D1.e4054_s3126_s3136_r9364_r9315_p4133
mc16_13TeV.361601.PowhegPy8EG_CT10nloME_AZNLOCTEQ6L1_WZlvvll_mll4.deriv.DAOD_HIGG8D1.e4475_s3126_r9364_r9315_p4133
mc16_13TeV.364286.Sherpa_222_NNPDF30NNLO_llvvjj_ss_EW4.deriv.DAOD_HIGG8D1.e6055_e5984_s3126_r9364_r9315_p3983 mc16_13TeV.364285.Sherpa_222_NNPDF30NNLO_llvvjj_ss_EW4.deriv.DAOD_HIGG8D1.e7421_e5984_s3126_r9364_r9315_p4133
mc16_13TeV.364740.MGPy8EG_NNPDF30NLO_A14NNPDF23LO_llvlij_EW6_OFPlus.deriv.DAOD_HIGG8D1.e7421_e5984_s3126_r9364_r9315_p4133
mc16_13TeV.364742.MGPy8EG_NNPDF30NLO_A14NNPDF23LO_llvlij_EW6_SFPlus.deriv.DAOD_HIGG8D1.e7421_e5984_s3126_r9364_r9315_p4133
mc16_13TeV.364253.Sherpa_222_NNPDF30NNLO_llvv.deriv.DAOD_HIGG8D1.e5916_s3126_r9364_r9315_p4133
mc16_13TeV.364250.Sherpa_222_NNPDF30NNLO_llll.deriv.DAOD_HIGG8D1.e5894_s3126_r9364_r9315_p4133
mc16_13TeV.364254.Sherpa_222_NNPDF30NNLO_llvv.deriv.DAOD_HIGG8D1.e5916_s3126_r9364_r9315_p4133
```

mc16\_13TeV.364255.Sherpa\_222\_NNPDF30NNLO\_lvyy.deriv.DAOD\_HIGG8D1.e5916\_s3126\_r9364\_r9315\_p4133  
 mc16\_13TeV.410155.aMcAtNloPythia8EvtGen\_MEN30NLO\_A14N23LO\_ttW.deriv.DAOD\_HIGG8D1.e5070\_s3126\_r9364\_r9315\_p4133  
 mc16\_13TeV.410156.aMcAtNloPythia8EvtGen\_MEN30NLO\_A14N23LO\_ttZnuu.deriv.DAOD\_HIGG8D1.e5070\_s3126\_r9364\_r9315\_p4133  
 mc16\_13TeV.410157.aMcAtNloPythia8EvtGen\_MEN30NLO\_A14N23LO\_ttZqq.deriv.DAOD\_HIGG8D1.e5070\_s3126\_r9364\_r9315\_p4133  
 mc16\_13TeV.410218.aMcAtNloPythia8EvtGen\_MEN30NLO\_A14N23LO\_ttee.deriv.DAOD\_HIGG8D1.e5070\_s3126\_r9364\_r9315\_p4133  
 mc16\_13TeV.410219.aMcAtNloPythia8EvtGen\_MEN30NLO\_A14N23LO\_ttmumu.deriv.DAOD\_HIGG8D1.e5070\_s3126\_r9364\_r9315\_p4133  
 mc16\_13TeV.410220.aMcAtNloPythia8EvtGen\_MEN30NLO\_A14N23LO\_ttautau.deriv.DAOD\_HIGG8D1.e5070\_s3126\_r9364\_r9315\_p4133  
 mc16\_13TeV.412063.aMcAtNloPythia8EvtGen\_tllq\_NNPDF30\_nf4\_A4.deriv.DAOD\_TOPQ1.e7054\_e5984\_s3126\_r9364\_r9315\_p4174  
 mc16\_13TeV.410276.aMcAtNloPythia8EvtGen\_MEN30NLO\_A14N23LO\_ttee\_mll\_1\_5.deriv.DAOD\_HIGG8D1.e6087\_e5984\_s3126\_r9364\_r9315\_p4133  
 mc16\_13TeV.410277.aMcAtNloPythia8EvtGen\_MEN30NLO\_A14N23LO\_ttmumu\_mll\_1\_5.deriv.DAOD\_HIGG8D1.e6087\_e5984\_s3126\_r9364\_r9315\_p4133  
 mc16\_13TeV.410278.aMcAtNloPythia8EvtGen\_MEN30NLO\_A14N23LO\_ttautau\_mll\_1\_5.deriv.DAOD\_HIGG8D1.e6087\_e5984\_s3126\_r9364\_r9315\_p4133  
 mc16\_13TeV.410397.MadGraphPythia8EvtGen\_ttbar\_wbee\_MEN30LO\_A14N23LO.deriv.DAOD\_HIGG8D1.e6086\_e5984\_s3126\_r9364\_r9315\_p4133  
 mc16\_13TeV.410398.MadGraphPythia8EvtGen\_ttbar\_wbmumu\_MEN30LO\_A14N23LO.deriv.DAOD\_HIGG8D1.e6086\_e5984\_s3126\_r9364\_r9315\_p4133  
 mc16\_13TeV.410399.MadGraphPythia8EvtGen\_ttbar\_wbtautau\_MEN30LO\_A14N23LO.deriv.DAOD\_HIGG8D1.e6086\_e5984\_s3126\_r9364\_r9315\_p4133  
 mc16\_13TeV.410658.PhPy8EG\_A14\_tchan\_BW50\_lept\_top.deriv.DAOD\_HIGG8D1.e6671\_e5984\_s3126\_r9364\_r9315\_p4133  
 mc16\_13TeV.410659.PhPy8EG\_A14\_tchan\_BW50\_lept\_antitop.deriv.DAOD\_HIGG8D1.e6671\_e5984\_s3126\_r9364\_r9315\_p4133  
 mc16\_13TeV.410644.PowhegPythia8EvtGen\_A14\_singletop\_schan\_lept\_top.deriv.DAOD\_HIGG8D1.e6527\_e5984\_s3126\_r9364\_r9315\_p4133  
 mc16\_13TeV.410645.PowhegPythia8EvtGen\_A14\_singletop\_schan\_lept\_antitop.deriv.DAOD\_HIGG8D1.e6527\_e5984\_s3126\_r9364\_r9315\_p4133  
 mc16\_13TeV.304014.MadGraphPythia8EvtGen\_A14NNPDF23\_3top\_SM.deriv.DAOD\_HIGG8D1.e4324\_s3126\_r9364\_r9315\_p4133  
 mc16\_13TeV.410080.MadGraphPythia8EvtGen\_A14NNPDF23\_4topSM.deriv.DAOD\_HIGG8D1.e4111\_s3126\_r9364\_r9315\_p4133  
 mc16\_13TeV.410081.MadGraphPythia8EvtGen\_A14NNPDF23\_ttbarWW.deriv.DAOD\_HIGG8D1.e4111\_s3126\_r9364\_r9315\_p4133  
 mc16\_13TeV.364100.Sherpa\_221\_NNPDF30NNLO\_Zmumu\_MAXHTPTV0\_70\_CVetoBVeto.deriv.DAOD\_HIGG8D1.e5271\_s3126\_r9364\_r9315\_p4133  
 mc16\_13TeV.364101.Sherpa\_221\_NNPDF30NNLO\_Zmumu\_MAXHTPTV0\_70\_CFilterBVeto.deriv.DAOD\_HIGG8D1.e5271\_s3126\_r9364\_r9315\_p4133  
 mc16\_13TeV.364102.Sherpa\_221\_NNPDF30NNLO\_Zmumu\_MAXHTPTV0\_70\_BFilter.deriv.DAOD\_HIGG8D1.e5271\_s3126\_r9364\_r9315\_p4133  
 mc16\_13TeV.364103.Sherpa\_221\_NNPDF30NNLO\_Zmumu\_MAXHTPTV70\_140\_CVetoBVeto.deriv.DAOD\_HIGG8D1.e5271\_s3126\_r9364\_r9315\_p4133  
 mc16\_13TeV.364104.Sherpa\_221\_NNPDF30NNLO\_Zmumu\_MAXHTPTV70\_140\_CFilterBVeto.deriv.DAOD\_HIGG8D1.e5271\_s3126\_r9364\_r9315\_p4133  
 mc16\_13TeV.364106.Sherpa\_221\_NNPDF30NNLO\_Zmumu\_MAXHTPTV140\_280\_CVetoBVeto.deriv.DAOD\_HIGG8D1.e5271\_s3126\_r9364\_r9315\_p4133  
 mc16\_13TeV.364107.Sherpa\_221\_NNPDF30NNLO\_Zmumu\_MAXHTPTV140\_280\_CFilterBVeto.deriv.DAOD\_HIGG8D1.e5271\_s3126\_r9364\_r9315\_p4133  
 mc16\_13TeV.364108.Sherpa\_221\_NNPDF30NNLO\_Zmumu\_MAXHTPTV140\_280\_BFilter.deriv.DAOD\_HIGG8D1.e5271\_s3126\_r9364\_r9315\_p4133  
 mc16\_13TeV.364109.Sherpa\_221\_NNPDF30NNLO\_Zmumu\_MAXHTPTV280\_500\_CVetoBVeto.deriv.DAOD\_HIGG8D1.e5271\_s3126\_r9364\_r9315\_p4133  
 mc16\_13TeV.364110.Sherpa\_221\_NNPDF30NNLO\_Zmumu\_MAXHTPTV280\_500\_CFilterBVeto.deriv.DAOD\_HIGG8D1.e5271\_s3126\_r9364\_r9315\_p4133  
 mc16\_13TeV.364111.Sherpa\_221\_NNPDF30NNLO\_Zmumu\_MAXHTPTV280\_500\_BFilter.deriv.DAOD\_HIGG8D1.e5271\_e5984\_s3126\_r9364\_r9315\_p4133  
 mc16\_13TeV.364111.Sherpa\_221\_NNPDF30NNLO\_Zmumu\_MAXHTPTV280\_500\_BFilter.deriv.DAOD\_HIGG8D1.e5271\_s3126\_r9364\_r9315\_p4133  
 mc16\_13TeV.364112.Sherpa\_221\_NNPDF30NNLO\_Zmumu\_MAXHTPTV500\_1000.deriv.DAOD\_HIGG8D1.e5271\_s3126\_r9364\_r9315\_p4133  
 mc16\_13TeV.364113.Sherpa\_221\_NNPDF30NNLO\_Zmumu\_MAXHTPTV1000\_E\_CMS.deriv.DAOD\_HIGG8D1.e5271\_s3126\_r9364\_r9315\_p4133  
 mc16\_13TeV.364114.Sherpa\_221\_NNPDF30NNLO\_Zee\_MAXHTPTV0\_70\_CVetoBVeto.deriv.DAOD\_HIGG8D1.e5299\_s3126\_r9364\_r9315\_p4133  
 mc16\_13TeV.364115.Sherpa\_221\_NNPDF30NNLO\_Zee\_MAXHTPTV0\_70\_CFilterBVeto.deriv.DAOD\_HIGG8D1.e5299\_s3126\_r9364\_r9315\_p4133  
 mc16\_13TeV.364116.Sherpa\_221\_NNPDF30NNLO\_Zee\_MAXHTPTV0\_70\_BFilter.deriv.DAOD\_HIGG8D1.e5299\_s3126\_r9364\_r9315\_p4133  
 mc16\_13TeV.364117.Sherpa\_221\_NNPDF30NNLO\_Zee\_MAXHTPTV70\_140\_CVetoBVeto.deriv.DAOD\_HIGG8D1.e5299\_s3126\_r9364\_r9315\_p4133  
 mc16\_13TeV.364118.Sherpa\_221\_NNPDF30NNLO\_Zee\_MAXHTPTV70\_140\_CFilterBVeto.deriv.DAOD\_HIGG8D1.e5299\_s3126\_r9364\_r9315\_p4133  
 mc16\_13TeV.364119.Sherpa\_221\_NNPDF30NNLO\_Zee\_MAXHTPTV70\_140\_BFilter.deriv.DAOD\_HIGG8D1.e5299\_s3126\_r9364\_r9315\_p4133  
 mc16\_13TeV.364120.Sherpa\_221\_NNPDF30NNLO\_Zee\_MAXHTPTV140\_280\_CVetoBVeto.deriv.DAOD\_HIGG8D1.e5299\_s3126\_r9364\_r9315\_p4133  
 mc16\_13TeV.364121.Sherpa\_221\_NNPDF30NNLO\_Zee\_MAXHTPTV140\_280\_CFilterBVeto.deriv.DAOD\_HIGG8D1.e5299\_s3126\_r9364\_r9315\_p4133  
 mc16\_13TeV.364122.Sherpa\_221\_NNPDF30NNLO\_Zee\_MAXHTPTV140\_280\_BFilter.deriv.DAOD\_HIGG8D1.e5299\_s3126\_r9364\_r9315\_p4133  
 mc16\_13TeV.364123.Sherpa\_221\_NNPDF30NNLO\_Zee\_MAXHTPTV280\_500\_CVetoBVeto.deriv.DAOD\_HIGG8D1.e5299\_s3126\_r9364\_r9315\_p4133  
 mc16\_13TeV.364124.Sherpa\_221\_NNPDF30NNLO\_Zee\_MAXHTPTV280\_500\_CFilterBVeto.deriv.DAOD\_HIGG8D1.e5299\_s3126\_r9364\_r9315\_p4133  
 mc16\_13TeV.364125.Sherpa\_221\_NNPDF30NNLO\_Zee\_MAXHTPTV280\_500\_BFilter.deriv.DAOD\_HIGG8D1.e5299\_s3126\_r9364\_r9315\_p4133  
 mc16\_13TeV.364126.Sherpa\_221\_NNPDF30NNLO\_Zee\_MAXHTPTV280\_500\_BFilter.deriv.DAOD\_HIGG8D1.e5299\_s3126\_r9364\_r9315\_p4133  
 mc16\_13TeV.364127.Sherpa\_221\_NNPDF30NNLO\_Zee\_MAXHTPTV1000\_E\_CMS.deriv.DAOD\_HIGG8D1.e5299\_s3126\_r9364\_r9315\_p4133  
 mc16\_13TeV.364128.Sherpa\_221\_NNPDF30NNLO\_Ztautau\_MAXHTPTV0\_70\_CVetoBVeto.deriv.DAOD\_HIGG8D1.e5307\_s3126\_r9364\_r9315\_p4133  
 mc16\_13TeV.364129.Sherpa\_221\_NNPDF30NNLO\_Ztautau\_MAXHTPTV0\_70\_CFilterBVeto.deriv.DAOD\_HIGG8D1.e5307\_s3126\_r9364\_r9315\_p4133  
 mc16\_13TeV.364130.Sherpa\_221\_NNPDF30NNLO\_Ztautau\_MAXHTPTV0\_70\_BFilter.deriv.DAOD\_HIGG8D1.e5307\_s3126\_r9364\_r9315\_p4133  
 mc16\_13TeV.364131.Sherpa\_221\_NNPDF30NNLO\_Ztautau\_MAXHTPTV70\_140\_CVetoBVeto.deriv.DAOD\_HIGG8D1.e5307\_s3126\_r9364\_r9315\_p4133  
 mc16\_13TeV.364132.Sherpa\_221\_NNPDF30NNLO\_Ztautau\_MAXHTPTV70\_140\_CFilterBVeto.deriv.DAOD\_HIGG8D1.e5307\_s3126\_r9364\_r9315\_p4133  
 mc16\_13TeV.364133.Sherpa\_221\_NNPDF30NNLO\_Ztautau\_MAXHTPTV70\_140\_BFilter.deriv.DAOD\_HIGG8D1.e5307\_s3126\_r9364\_r9315\_p4133  
 mc16\_13TeV.364134.Sherpa\_221\_NNPDF30NNLO\_Ztautau\_MAXHTPTV140\_280\_CVetoBVeto.deriv.DAOD\_HIGG8D1.e5307\_s3126\_r9364\_r9315\_p4133  
 mc16\_13TeV.364135.Sherpa\_221\_NNPDF30NNLO\_Ztautau\_MAXHTPTV140\_280\_CFilterBVeto.deriv.DAOD\_HIGG8D1.e5307\_s3126\_r9364\_r9315\_p4133  
 mc16\_13TeV.364136.Sherpa\_221\_NNPDF30NNLO\_Ztautau\_MAXHTPTV140\_280\_BFilter.deriv.DAOD\_HIGG8D1.e5307\_s3126\_r9364\_r9315\_p4133  
 mc16\_13TeV.364137.Sherpa\_221\_NNPDF30NNLO\_Ztautau\_MAXHTPTV280\_500\_CVetoBVeto.deriv.DAOD\_HIGG8D1.e5307\_e5984\_s3126\_r9364\_r9315\_p4133  
 mc16\_13TeV.364138.Sherpa\_221\_NNPDF30NNLO\_Ztautau\_MAXHTPTV280\_500\_CFilterBVeto.deriv.DAOD\_HIGG8D1.e5313\_s3126\_r9364\_r9315\_p4133



mc16\_13TeV.364189.Sherpa\_221\_NNPDF30NNLO\_Wtaunu\_MAXHTPTV70\_140\_BFilter.deriv.DAOD\_HIGG8D1.e5340\_s3126\_r9364\_r9315\_p4133  
 mc16\_13TeV.364190.Sherpa\_221\_NNPDF30NNLO\_Wtaunu\_MAXHTPTV140\_280\_CVetoBVeto.deriv.DAOD\_HIGG8D1.e5340\_e5984\_s3126\_r9364\_r9315\_p4133  
 mc16\_13TeV.364190.Sherpa\_221\_NNPDF30NNLO\_Wtaunu\_MAXHTPTV140\_280\_CVetoBVeto.deriv.DAOD\_HIGG8D1.e5340\_s3126\_r9364\_r9315\_p4133  
 mc16\_13TeV.364191.Sherpa\_221\_NNPDF30NNLO\_Wtaunu\_MAXHTPTV140\_280\_CFilterBVeto.deriv.DAOD\_HIGG8D1.e5340\_s3126\_r9364\_r9315\_p4133  
 mc16\_13TeV.364191.Sherpa\_221\_NNPDF30NNLO\_Wtaunu\_MAXHTPTV140\_280\_CFilterBVeto.deriv.DAOD\_HIGG8D1.e5340\_e5984\_s3126\_s3136\_r9364\_r9315\_p4133  
 mc16\_13TeV.364192.Sherpa\_221\_NNPDF30NNLO\_Wtaunu\_MAXHTPTV140\_280\_BFilter.deriv.DAOD\_HIGG8D1.e5340\_s3126\_r9364\_r9315\_p4133  
 mc16\_13TeV.364193.Sherpa\_221\_NNPDF30NNLO\_Wtaunu\_MAXHTPTV280\_500\_CVetoBVeto.deriv.DAOD\_HIGG8D1.e5340\_s3126\_r9364\_r9315\_p4133  
 mc16\_13TeV.364193.Sherpa\_221\_NNPDF30NNLO\_Wtaunu\_MAXHTPTV280\_500\_CVetoBVeto.deriv.DAOD\_HIGG8D1.e5340\_e5984\_s3126\_s3136\_r9364\_r9315\_p4133  
 mc16\_13TeV.364194.Sherpa\_221\_NNPDF30NNLO\_Wtaunu\_MAXHTPTV280\_500\_CFilterBVeto.deriv.DAOD\_HIGG8D1.e5340\_s3126\_r9364\_r9315\_p4133  
 mc16\_13TeV.364194.Sherpa\_221\_NNPDF30NNLO\_Wtaunu\_MAXHTPTV280\_500\_CFilterBVeto.deriv.DAOD\_HIGG8D1.e5340\_e5984\_s3126\_s3136\_r9364\_r9315\_p4133  
 mc16\_13TeV.364195.Sherpa\_221\_NNPDF30NNLO\_Wtaunu\_MAXHTPTV280\_500\_BFilter.deriv.DAOD\_HIGG8D1.e5340\_s3126\_r9364\_r9315\_p4133  
 mc16\_13TeV.364196.Sherpa\_221\_NNPDF30NNLO\_Wtaunu\_MAXHTPTV500\_1000.deriv.DAOD\_HIGG8D1.e5340\_s3126\_r9364\_r9315\_p4133  
 mc16\_13TeV.364197.Sherpa\_221\_NNPDF30NNLO\_Wtaunu\_MAXHTPTV1000\_E\_CMS.deriv.DAOD\_HIGG8D1.e5340\_s3126\_r9364\_r9315\_p4133  
 mc16\_13TeV.364500.Sherpa\_222\_NNPDF30NNLO\_eegamma\_pty\_7\_15.deriv.DAOD\_HIGG8D1.e5928\_e5984\_s3126\_r9364\_r9315\_p4133  
 mc16\_13TeV.364501.Sherpa\_222\_NNPDF30NNLO\_eegamma\_pty\_15\_35.deriv.DAOD\_HIGG8D1.e5928\_e5984\_s3126\_r9364\_r9315\_p4133  
 mc16\_13TeV.364502.Sherpa\_222\_NNPDF30NNLO\_eegamma\_pty\_35\_70.deriv.DAOD\_HIGG8D1.e5928\_e5984\_s3126\_r9364\_r9315\_p4133  
 mc16\_13TeV.364503.Sherpa\_222\_NNPDF30NNLO\_eegamma\_pty\_70\_140.deriv.DAOD\_HIGG8D1.e5928\_e5984\_s3126\_r9364\_r9315\_p4133  
 mc16\_13TeV.364504.Sherpa\_222\_NNPDF30NNLO\_eegamma\_pty\_140\_E\_CMS.deriv.DAOD\_HIGG8D1.e5928\_e5984\_s3126\_r9364\_r9315\_p4133  
 mc16\_13TeV.364505.Sherpa\_222\_NNPDF30NNLO\_mumugamma\_pty\_7\_15.deriv.DAOD\_HIGG8D1.e5928\_e5984\_s3126\_r9364\_r9315\_p4133  
 mc16\_13TeV.364506.Sherpa\_222\_NNPDF30NNLO\_mumugamma\_pty\_15\_35.deriv.DAOD\_HIGG8D1.e5988\_e5984\_s3126\_r9364\_r9315\_p4133  
 mc16\_13TeV.364507.Sherpa\_222\_NNPDF30NNLO\_mumugamma\_pty\_35\_70.deriv.DAOD\_HIGG8D1.e5928\_e5984\_s3126\_r9364\_r9315\_p4133  
 mc16\_13TeV.364508.Sherpa\_222\_NNPDF30NNLO\_mumugamma\_pty\_70\_140.deriv.DAOD\_HIGG8D1.e5928\_e5984\_s3126\_r9364\_r9315\_p4133  
 mc16\_13TeV.364509.Sherpa\_222\_NNPDF30NNLO\_mumugamma\_pty\_140\_E\_CMS.deriv.DAOD\_HIGG8D1.e5928\_e5984\_s3126\_r9364\_r9315\_p4133  
 mc16\_13TeV.364510.Sherpa\_222\_NNPDF30NNLO\_tautaugamma\_pty\_7\_15.deriv.DAOD\_HIGG8D1.e5928\_s3126\_r9364\_r9315\_p4133  
 mc16\_13TeV.364511.Sherpa\_222\_NNPDF30NNLO\_tautaugamma\_pty\_15\_35.deriv.DAOD\_HIGG8D1.e5928\_s3126\_r9364\_r9315\_p4133  
 mc16\_13TeV.364512.Sherpa\_222\_NNPDF30NNLO\_tautaugamma\_pty\_35\_70.deriv.DAOD\_HIGG8D1.e5928\_s3126\_r9364\_r9315\_p4133  
 mc16\_13TeV.364513.Sherpa\_222\_NNPDF30NNLO\_tautaugamma\_pty\_70\_140.deriv.DAOD\_HIGG8D1.e5982\_s3126\_r9364\_r9315\_p4133  
 mc16\_13TeV.364514.Sherpa\_222\_NNPDF30NNLO\_tautaugamma\_pty\_140\_E\_CMS.deriv.DAOD\_HIGG8D1.e5928\_s3126\_r9364\_r9315\_p4133  
 mc16\_13TeV.364521.Sherpa\_222\_NNPDF30NNLO\_enugamma\_pty\_7\_15.deriv.DAOD\_HIGG8D1.e5928\_s3126\_r9364\_r9315\_p4133  
 mc16\_13TeV.364522.Sherpa\_222\_NNPDF30NNLO\_enugamma\_pty\_15\_35.deriv.DAOD\_HIGG8D1.e5928\_s3126\_r9364\_r9315\_p4133  
 mc16\_13TeV.364523.Sherpa\_222\_NNPDF30NNLO\_enugamma\_pty\_35\_70.deriv.DAOD\_HIGG8D1.e5928\_s3126\_r9364\_r9315\_p4133  
 mc16\_13TeV.364524.Sherpa\_222\_NNPDF30NNLO\_enugamma\_pty\_70\_140.deriv.DAOD\_HIGG8D1.e5928\_s3126\_r9364\_r9315\_p4133  
 mc16\_13TeV.364525.Sherpa\_222\_NNPDF30NNLO\_enugamma\_pty\_140\_E\_CMS.deriv.DAOD\_HIGG8D1.e5928\_s3126\_r9364\_r9315\_p4133  
 mc16\_13TeV.364525.Sherpa\_222\_NNPDF30NNLO\_enugamma\_pty\_140\_E\_CMS.deriv.DAOD\_HIGG8D1.e5928\_e5984\_s3126\_r9364\_r9315\_p4133  
 mc16\_13TeV.364526.Sherpa\_222\_NNPDF30NNLO\_munugamma\_pty\_7\_15.deriv.DAOD\_HIGG8D1.e5928\_s3126\_r9364\_r9315\_p4133  
 mc16\_13TeV.364527.Sherpa\_222\_NNPDF30NNLO\_munugamma\_pty\_15\_35.deriv.DAOD\_HIGG8D1.e5928\_s3126\_r9364\_r9315\_p4133  
 mc16\_13TeV.364528.Sherpa\_222\_NNPDF30NNLO\_munugamma\_pty\_35\_70.deriv.DAOD\_HIGG8D1.e5928\_s3126\_r9364\_r9315\_p4133  
 mc16\_13TeV.364529.Sherpa\_222\_NNPDF30NNLO\_munugamma\_pty\_70\_140.deriv.DAOD\_HIGG8D1.e5928\_s3126\_r9364\_r9315\_p4133  
 mc16\_13TeV.364530.Sherpa\_222\_NNPDF30NNLO\_munugamma\_pty\_140\_E\_CMS.deriv.DAOD\_HIGG8D1.e5928\_s3126\_r9364\_r9315\_p4133  
 mc16\_13TeV.364530.Sherpa\_222\_NNPDF30NNLO\_munugamma\_pty\_140\_E\_CMS.deriv.DAOD\_HIGG8D1.e5928\_e5984\_s3126\_r9364\_r9315\_p4133  
 mc16\_13TeV.364531.Sherpa\_222\_NNPDF30NNLO\_taunugamma\_pty\_7\_15.deriv.DAOD\_HIGG8D1.e5928\_s3126\_r9364\_r9315\_p4133  
 mc16\_13TeV.364532.Sherpa\_222\_NNPDF30NNLO\_taunugamma\_pty\_15\_35.deriv.DAOD\_HIGG8D1.e5928\_s3126\_r9364\_r9315\_p4133  
 mc16\_13TeV.364533.Sherpa\_222\_NNPDF30NNLO\_taunugamma\_pty\_35\_70.deriv.DAOD\_HIGG8D1.e5928\_s3126\_r9364\_r9315\_p4133  
 mc16\_13TeV.364534.Sherpa\_222\_NNPDF30NNLO\_taunugamma\_pty\_70\_140.deriv.DAOD\_HIGG8D1.e5928\_s3126\_r9364\_r9315\_p4133  
 mc16\_13TeV.364535.Sherpa\_222\_NNPDF30NNLO\_taunugamma\_pty\_140\_E\_CMS.deriv.DAOD\_HIGG8D1.e5928\_s3126\_r9364\_r9315\_p4133  
 mc16\_13TeV.364535.Sherpa\_222\_NNPDF30NNLO\_taunugamma\_pty\_140\_E\_CMS.deriv.DAOD\_HIGG8D1.e5928\_e5984\_s3126\_r9364\_r9315\_p4133  
 mc16\_13TeV.410560.MadGraphPythia8EvtGen\_A14\_Z\_4fl\_tchan\_noAllHad.deriv.DAOD\_HIGG8D1.e5803\_s3126\_r9364\_r9315\_p4133  
 mc16\_13TeV.410013.PowhegPythiaEvtGen\_P2012\_Wt\_inclusive\_top.deriv.DAOD\_HIGG8D1.e3753\_s3126\_r9364\_r9315\_p4133  
 mc16\_13TeV.410014.PowhegPythiaEvtGen\_P2012\_Wt\_inclusive\_antitop.deriv.DAOD\_HIGG8D1.e3753\_s3126\_r9364\_r9315\_p4133  
 mc16\_13TeV.410408.aMcAtNloPythia8EvtGen\_tWZ\_Tzoll\_minDR1.deriv.DAOD\_HIGG8D1.e6423\_e5984\_s3126\_r9364\_r9315\_p4133  
 mc16\_13TeV.364242.Sherpa\_222\_NNPDF30NNLO\_WWW\_31v\_EW6.deriv.DAOD\_HIGG8D1.e5887\_s3126\_r9364\_r9315\_p4133  
 mc16\_13TeV.364243.Sherpa\_222\_NNPDF30NNLO\_WWW\_412v\_EW6.deriv.DAOD\_HIGG8D1.e5887\_s3126\_r9364\_r9315\_p4133  
 mc16\_13TeV.364244.Sherpa\_222\_NNPDF30NNLO\_WWW\_214v\_EW6.deriv.DAOD\_HIGG8D1.e5887\_s3126\_r9364\_r9315\_p4133  
 mc16\_13TeV.364245.Sherpa\_222\_NNPDF30NNLO\_WZZ\_51v\_EW6.deriv.DAOD\_HIGG8D1.e5887\_s3126\_r9364\_r9315\_p4133  
 mc16\_13TeV.364246.Sherpa\_222\_NNPDF30NNLO\_WZZ\_313v\_EW6.deriv.DAOD\_HIGG8D1.e5887\_s3126\_r9364\_r9315\_p4133  
 mc16\_13TeV.364247.Sherpa\_222\_NNPDF30NNLO\_ZZZ\_610v\_EW6.deriv.DAOD\_HIGG8D1.e5887\_s3126\_r9364\_r9315\_p4133  
 mc16\_13TeV.364248.Sherpa\_222\_NNPDF30NNLO\_ZZZ\_412v\_EW6.deriv.DAOD\_HIGG8D1.e5887\_s3126\_r9364\_r9315\_p4133  
 mc16\_13TeV.364249.Sherpa\_222\_NNPDF30NNLO\_ZZZ\_214v\_EW6.deriv.DAOD\_HIGG8D1.e5887\_s3126\_r9364\_r9315\_p4133  
 mc16\_13TeV.342284.Pythia8EvtGen\_A14NNPDF23LO\_WH125\_inc.deriv.DAOD\_HIGG8D1.e4246\_s3126\_r9364\_r9315\_p4133  
 mc16\_13TeV.342285.Pythia8EvtGen\_A14NNPDF23LO\_ZH125\_inc.deriv.DAOD\_HIGG8D1.e4246\_s3126\_r9364\_r9315\_p4133  
 mc16\_13TeV.341998.aMcAtNloHppEG\_UEEE5\_CTEQ6L1\_CT10ME\_tWH125\_gamgam\_yt\_plus1.deriv.DAOD\_HIGG8D1.e4394\_e5984\_s3126\_r9364\_r9315\_p4133  
 mc16\_13TeV.410389.MadGraphPythia8EvtGen\_A14NNPDF23\_ttgamma\_nonallhadronic.deriv.DAOD\_HIGG8D1.e6155\_e5984\_s3126\_r9364\_r9315\_p4133

mc16\_13TeV.410470.PhPy8EG\_A14\_ttbar\_hdamp258p75\_nonallhad.deriv.DAOD\_HIGG8D1.e6337\_e5984\_s3126\_r9364\_r9315\_p4133  
 mc16\_13TeV.410472.PhPy8EG\_A14\_ttbar\_hdamp258p75\_dil.deriv.DAOD\_HIGG8D1.e6348\_e5984\_s3126\_r9364\_r9315\_p4133  
 mc16\_13TeV.346343.PhPy8EG\_A14NNPDF23\_NNPDF30ME\_ttH125\_allhad.deriv.DAOD\_HIGG8D1.e7148\_e5984\_s3126\_r9364\_r9315\_p4133  
 mc16\_13TeV.346344.PhPy8EG\_A14NNPDF23\_NNPDF30ME\_ttH125\_semilep.deriv.DAOD\_HIGG8D1.e7148\_e5984\_s3126\_r9364\_r9315\_p4133  
 mc16\_13TeV.346345.PhPy8EG\_A14NNPDF23\_NNPDF30ME\_ttH125\_dilep.deriv.DAOD\_HIGG8D1.e7148\_e5984\_s3126\_r9364\_r9315\_p4133  
  
 mc16d:  
 mc16\_13TeV.364253.Sherpa\_222\_NNPDF30NNLO\_lllv.deriv.DAOD\_HIGG8D1.e5916\_e5984\_s3126\_r10201\_r10210\_p4133  
 mc16\_13TeV.364250.Sherpa\_222\_NNPDF30NNLO\_llll.deriv.DAOD\_HIGG8D1.e5984\_e5984\_s3126\_r10201\_r10210\_p4133  
 mc16\_13TeV.364254.Sherpa\_222\_NNPDF30NNLO\_llvv.deriv.DAOD\_HIGG8D1.e5916\_e5984\_s3126\_r10201\_r10210\_p4133  
 mc16\_13TeV.364255.Sherpa\_222\_NNPDF30NNLO\_lvvv.deriv.DAOD\_HIGG8D1.e5916\_e5984\_s3126\_r10201\_r10210\_p4133  
 mc16\_13TeV.410155.aMcAtNloPythia8EvtGen\_MEN30NLO\_A14N23LO\_ttW.deriv.DAOD\_HIGG8D1.e5070\_e5984\_s3126\_r10201\_r10210\_p4133  
 mc16\_13TeV.410156.aMcAtNloPythia8EvtGen\_MEN30NLO\_A14N23LO\_ttZnunu.deriv.DAOD\_HIGG8D1.e5070\_e5984\_s3126\_r10201\_r10210\_p4133  
 mc16\_13TeV.410157.aMcAtNloPythia8EvtGen\_MEN30NLO\_A14N23LO\_ttZqq.deriv.DAOD\_HIGG8D1.e5070\_e5984\_s3126\_r10201\_r10210\_p4133  
 mc16\_13TeV.410218.aMcAtNloPythia8EvtGen\_MEN30NLO\_A14N23LO\_ttee.deriv.DAOD\_HIGG8D1.e5070\_e5984\_s3126\_r10201\_r10210\_p4133  
 mc16\_13TeV.410219.aMcAtNloPythia8EvtGen\_MEN30NLO\_A14N23LO\_ttmumu.deriv.DAOD\_HIGG8D1.e5070\_e5984\_s3126\_r10201\_r10210\_p4133  
 mc16\_13TeV.410220.aMcAtNloPythia8EvtGen\_MEN30NLO\_A14N23LO\_ttautau.deriv.DAOD\_HIGG8D1.e5070\_e5984\_s3126\_r10201\_r10210\_p4133  
 mc16\_13TeV.410276.aMcAtNloPythia8EvtGen\_MEN30NLO\_A14N23LO\_ttautau\_mll\_1\_5.deriv.DAOD\_HIGG8D1.e6087\_e5984\_s3126\_r10201\_r10210\_p4133  
 mc16\_13TeV.410277.aMcAtNloPythia8EvtGen\_MEN30NLO\_A14N23LO\_ttautau\_mll\_1\_5.deriv.DAOD\_HIGG8D1.e6087\_e5984\_s3126\_r10201\_r10210\_p4133  
 mc16\_13TeV.410278.aMcAtNloPythia8EvtGen\_MEN30NLO\_A14N23LO\_ttautau\_mll\_1\_5.deriv.DAOD\_HIGG8D1.e6087\_e5984\_s3126\_r10201\_r10210\_p4133  
 mc16\_13TeV.410397.MadGraphPythia8EvtGen\_ttbar\_wbee\_MEN30LO\_A14N23LO.deriv.DAOD\_HIGG8D1.e6086\_e5984\_s3126\_r10201\_r10210\_p4133  
 mc16\_13TeV.410398.MadGraphPythia8EvtGen\_ttbar\_wbmumu\_MEN30LO\_A14N23LO.deriv.DAOD\_HIGG8D1.e6086\_e5984\_s3126\_r10201\_r10210\_p4133  
 mc16\_13TeV.410399.MadGraphPythia8EvtGen\_ttbar\_wbtautau\_MEN30LO\_A14N23LO.deriv.DAOD\_HIGG8D1.e6086\_e5984\_s3126\_r10201\_r10210\_p4133  
 mc16\_13TeV.410658.PhPy8EG\_A14\_tchan\_BW50\_lept\_top.deriv.DAOD\_HIGG8D1.e6671\_e5984\_s3126\_r10201\_r10210\_p4133  
 mc16\_13TeV.410659.PhPy8EG\_A14\_tchan\_BW50\_lept\_antitop.deriv.DAOD\_HIGG8D1.e6671\_e5984\_s3126\_r10201\_r10210\_p4133  
 mc16\_13TeV.410644.PowhegPythia8EvtGen\_A14\_singleton\_schan\_lept\_top.deriv.DAOD\_HIGG8D1.e6527\_e5984\_s3126\_r10201\_r10210\_p4133  
 mc16\_13TeV.410645.PowhegPythia8EvtGen\_A14\_singleton\_schan\_lept\_antitop.deriv.DAOD\_HIGG8D1.e6527\_s3126\_r10201\_r10210\_p4133  
 mc16\_13TeV.412063.aMcAtNloPythia8EvtGen\_tllq\_NNPDF30\_nf4\_A14.deriv.DAOD\_TOPQ1.e7054\_e5984\_s3126\_r10201\_r10210\_p4174  
 mc16\_13TeV.304014.MadGraphPythia8EvtGen\_A14NNPDF23\_3top\_SM.deriv.DAOD\_HIGG8D1.e4324\_e5984\_s3126\_r10201\_r10210\_p4133  
 mc16\_13TeV.410080.MadGraphPythia8EvtGen\_A14NNPDF23\_4topSM.deriv.DAOD\_HIGG8D1.e4111\_e5984\_s3126\_r10201\_r10210\_p4133  
 mc16\_13TeV.410081.MadGraphPythia8EvtGen\_A14NNPDF23\_ttbarWW.deriv.DAOD\_HIGG8D1.e4111\_e5984\_s3126\_r10201\_r10210\_p4133  
 mc16\_13TeV.364100.Sherpa\_221\_NNPDF30NNLO\_Zmumu\_MAXHTPTV0\_70\_CVetoBVeto.deriv.DAOD\_HIGG8D1.e5271\_s3126\_r10201\_r10210\_p4133  
 mc16\_13TeV.364101.Sherpa\_221\_NNPDF30NNLO\_Zmumu\_MAXHTPTV0\_70\_CFilterBVeto.deriv.DAOD\_HIGG8D1.e5271\_s3126\_r10201\_r10210\_p4133  
 mc16\_13TeV.364101.Sherpa\_221\_NNPDF30NNLO\_Zmumu\_MAXHTPTV0\_70\_CFilterBVeto.deriv.DAOD\_HIGG8D1.e5271\_s3126\_r10201\_r10210\_p4133  
 mc16\_13TeV.364102.Sherpa\_221\_NNPDF30NNLO\_Zmumu\_MAXHTPTV0\_70\_BFilter.deriv.DAOD\_HIGG8D1.e5271\_s3126\_r10201\_r10210\_p4133  
 mc16\_13TeV.364103.Sherpa\_221\_NNPDF30NNLO\_Zmumu\_MAXHTPTV70\_140\_CVetoBVeto.deriv.DAOD\_HIGG8D1.e5271\_s3126\_r10201\_r10210\_p4133  
 mc16\_13TeV.364104.Sherpa\_221\_NNPDF30NNLO\_Zmumu\_MAXHTPTV70\_140\_CFilterBVeto.deriv.DAOD\_HIGG8D1.e5271\_s3126\_r10201\_r10210\_p4133  
 mc16\_13TeV.364106.Sherpa\_221\_NNPDF30NNLO\_Zmumu\_MAXHTPTV140\_280\_CVetoBVeto.deriv.DAOD\_HIGG8D1.e5271\_s3126\_r10201\_r10210\_p4133  
 mc16\_13TeV.364107.Sherpa\_221\_NNPDF30NNLO\_Zmumu\_MAXHTPTV140\_280\_CFilterBVeto.deriv.DAOD\_HIGG8D1.e5271\_s3126\_r10201\_r10210\_p4133  
 mc16\_13TeV.364108.Sherpa\_221\_NNPDF30NNLO\_Zmumu\_MAXHTPTV140\_280\_BFilter.deriv.DAOD\_HIGG8D1.e5271\_s3126\_r10201\_r10210\_p4133  
 mc16\_13TeV.364108.Sherpa\_221\_NNPDF30NNLO\_Zmumu\_MAXHTPTV140\_280\_BFilter.deriv.DAOD\_HIGG8D1.e5271\_s3126\_r10201\_r10210\_p4133  
 mc16\_13TeV.364109.Sherpa\_221\_NNPDF30NNLO\_Zmumu\_MAXHTPTV280\_500\_CVetoBVeto.deriv.DAOD\_HIGG8D1.e5271\_s3126\_r10201\_r10210\_p4133  
 mc16\_13TeV.364109.Sherpa\_221\_NNPDF30NNLO\_Zmumu\_MAXHTPTV280\_500\_CVetoBVeto.deriv.DAOD\_HIGG8D1.e5271\_s3126\_r10201\_r10210\_p4133  
 mc16\_13TeV.364110.Sherpa\_221\_NNPDF30NNLO\_Zmumu\_MAXHTPTV280\_500\_CFilterBVeto.deriv.DAOD\_HIGG8D1.e5271\_s3126\_r10201\_r10210\_p4133  
 mc16\_13TeV.364111.Sherpa\_221\_NNPDF30NNLO\_Zmumu\_MAXHTPTV280\_500\_BFilter.deriv.DAOD\_HIGG8D1.e5271\_s3126\_r10201\_r10210\_p4133  
 mc16\_13TeV.364112.Sherpa\_221\_NNPDF30NNLO\_Zmumu\_MAXHTPTV280\_500\_BFilter.deriv.DAOD\_HIGG8D1.e5271\_s3126\_r10201\_r10210\_p4133  
 mc16\_13TeV.364112.Sherpa\_221\_NNPDF30NNLO\_Zmumu\_MAXHTPTV500\_1000.deriv.DAOD\_HIGG8D1.e5271\_s3126\_r10201\_r10210\_p4133  
 mc16\_13TeV.364113.Sherpa\_221\_NNPDF30NNLO\_Zmumu\_MAXHTPTV1000\_E\_CMS.deriv.DAOD\_HIGG8D1.e5271\_s3126\_r10201\_r10210\_p4133  
 mc16\_13TeV.364114.Sherpa\_221\_NNPDF30NNLO\_Zee\_MAXHTPTV0\_70\_CVetoBVeto.deriv.DAOD\_HIGG8D1.e5299\_s3126\_r10201\_r10210\_p4133  
 mc16\_13TeV.364115.Sherpa\_221\_NNPDF30NNLO\_Zee\_MAXHTPTV0\_70\_CFilterBVeto.deriv.DAOD\_HIGG8D1.e5299\_e5984\_s3126\_r10201\_r10210\_p4133  
 mc16\_13TeV.364116.Sherpa\_221\_NNPDF30NNLO\_Zee\_MAXHTPTV0\_70\_BFilter.deriv.DAOD\_HIGG8D1.e5299\_e5984\_s3126\_r10201\_r10210\_p4133  
 mc16\_13TeV.364117.Sherpa\_221\_NNPDF30NNLO\_Zee\_MAXHTPTV70\_140\_CVetoBVeto.deriv.DAOD\_HIGG8D1.e5299\_e5984\_s3126\_r10201\_r10210\_p4133  
 mc16\_13TeV.364118.Sherpa\_221\_NNPDF30NNLO\_Zee\_MAXHTPTV70\_140\_CFilterBVeto.deriv.DAOD\_HIGG8D1.e5299\_e5984\_s3126\_r10201\_r10210\_p4133  
 mc16\_13TeV.364119.Sherpa\_221\_NNPDF30NNLO\_Zee\_MAXHTPTV70\_140\_BFilter.deriv.DAOD\_HIGG8D1.e5299\_e5984\_s3126\_r10201\_r10210\_p4133  
 mc16\_13TeV.364120.Sherpa\_221\_NNPDF30NNLO\_Zee\_MAXHTPTV140\_280\_CVetoBVeto.deriv.DAOD\_HIGG8D1.e5299\_e5984\_s3126\_r10201\_r10210\_p4133  
 mc16\_13TeV.364121.Sherpa\_221\_NNPDF30NNLO\_Zee\_MAXHTPTV140\_280\_CFilterBVeto.deriv.DAOD\_HIGG8D1.e5299\_e5984\_s3126\_r10201\_r10210\_p4133  
 mc16\_13TeV.364122.Sherpa\_221\_NNPDF30NNLO\_Zee\_MAXHTPTV140\_280\_BFilter.deriv.DAOD\_HIGG8D1.e5299\_e5984\_s3126\_r10201\_r10210\_p4133  
 mc16\_13TeV.364123.Sherpa\_221\_NNPDF30NNLO\_Zee\_MAXHTPTV280\_500\_CVetoBVeto.deriv.DAOD\_HIGG8D1.e5299\_e5984\_s3126\_r10201\_r10210\_p4133  
 mc16\_13TeV.364124.Sherpa\_221\_NNPDF30NNLO\_Zee\_MAXHTPTV280\_500\_CFilterBVeto.deriv.DAOD\_HIGG8D1.e5299\_e5984\_s3126\_r10201\_r10210\_p4133  
 mc16\_13TeV.364125.Sherpa\_221\_NNPDF30NNLO\_Zee\_MAXHTPTV280\_500\_BFilter.deriv.DAOD\_HIGG8D1.e5299\_e5984\_s3126\_r10201\_r10210\_p4133  
 mc16\_13TeV.364126.Sherpa\_221\_NNPDF30NNLO\_Zee\_MAXHTPTV500\_1000.deriv.DAOD\_HIGG8D1.e5299\_e5984\_s3126\_r10201\_r10210\_p4133





mc16\_13TeV.364506.Sherpa\_222\_NNPDF30NNLO\_mumugamma\_pty\_15\_35.deriv.DAOD\_HIGG8D1.e5928\_e5984\_s3126\_r10201\_r10210\_p4133  
mc16\_13TeV.364507.Sherpa\_222\_NNPDF30NNLO\_mumugamma\_pty\_35\_70.deriv.DAOD\_HIGG8D1.e5928\_e5984\_s3126\_r10201\_r10210\_p4133  
mc16\_13TeV.364508.Sherpa\_222\_NNPDF30NNLO\_mumugamma\_pty\_70\_140.deriv.DAOD\_HIGG8D1.e5928\_e5984\_s3126\_r10201\_r10210\_p4133  
mc16\_13TeV.364509.Sherpa\_222\_NNPDF30NNLO\_mumugamma\_pty\_140\_E\_CMS.deriv.DAOD\_HIGG8D1.e5928\_e5984\_s3126\_r10201\_r10210\_p4133  
mc16\_13TeV.364510.Sherpa\_222\_NNPDF30NNLO\_tautaugamma\_pty\_7\_15.deriv.DAOD\_HIGG8D1.e5928\_e5984\_s3126\_r10201\_r10210\_p4133  
mc16\_13TeV.364511.Sherpa\_222\_NNPDF30NNLO\_tautaugamma\_pty\_15\_35.deriv.DAOD\_HIGG8D1.e5928\_e5984\_s3126\_r10201\_r10210\_p4133  
mc16\_13TeV.364512.Sherpa\_222\_NNPDF30NNLO\_tautaugamma\_pty\_35\_70.deriv.DAOD\_HIGG8D1.e5928\_e5984\_s3126\_r10201\_r10210\_p4133  
mc16\_13TeV.364513.Sherpa\_222\_NNPDF30NNLO\_tautaugamma\_pty\_70\_140.deriv.DAOD\_HIGG8D1.e5928\_e5984\_s3126\_r10201\_r10210\_p4133  
mc16\_13TeV.364513.Sherpa\_222\_NNPDF30NNLO\_tautaugamma\_pty\_70\_140.deriv.DAOD\_HIGG8D1.e5928\_e5984\_s3126\_r10201\_r10210\_p4133  
mc16\_13TeV.364514.Sherpa\_222\_NNPDF30NNLO\_tautaugamma\_pty\_140\_E\_CMS.deriv.DAOD\_HIGG8D1.e5928\_e5984\_s3126\_r10201\_r10210\_p4133  
mc16\_13TeV.364521.Sherpa\_222\_NNPDF30NNLO\_enugamma\_pty\_7\_15.deriv.DAOD\_HIGG8D1.e5928\_e5984\_s3126\_r10201\_r10210\_p4133  
mc16\_13TeV.364522.Sherpa\_222\_NNPDF30NNLO\_enugamma\_pty\_15\_35.deriv.DAOD\_HIGG8D1.e5928\_e5984\_s3126\_r10201\_r10210\_p4133  
mc16\_13TeV.364523.Sherpa\_222\_NNPDF30NNLO\_enugamma\_pty\_35\_70.deriv.DAOD\_HIGG8D1.e5928\_e5984\_s3126\_r10201\_r10210\_p4133  
mc16\_13TeV.364524.Sherpa\_222\_NNPDF30NNLO\_enugamma\_pty\_70\_140.deriv.DAOD\_HIGG8D1.e5928\_e5984\_s3126\_r10201\_r10210\_p4133  
mc16\_13TeV.364525.Sherpa\_222\_NNPDF30NNLO\_enugamma\_pty\_140\_E\_CMS.deriv.DAOD\_HIGG8D1.e5928\_e5984\_s3126\_r10201\_r10210\_p4133  
mc16\_13TeV.364526.Sherpa\_222\_NNPDF30NNLO\_munugamma\_pty\_7\_15.deriv.DAOD\_HIGG8D1.e5928\_e5984\_s3126\_r10201\_r10210\_p4133  
mc16\_13TeV.364527.Sherpa\_222\_NNPDF30NNLO\_munugamma\_pty\_15\_35.deriv.DAOD\_HIGG8D1.e5928\_e5984\_s3126\_r10201\_r10210\_p4133  
mc16\_13TeV.364528.Sherpa\_222\_NNPDF30NNLO\_munugamma\_pty\_35\_70.deriv.DAOD\_HIGG8D1.e5928\_e5984\_s3126\_r10201\_r10210\_p4133  
mc16\_13TeV.364529.Sherpa\_222\_NNPDF30NNLO\_munugamma\_pty\_70\_140.deriv.DAOD\_HIGG8D1.e5928\_e5984\_s3126\_r10201\_r10210\_p4133  
mc16\_13TeV.364530.Sherpa\_222\_NNPDF30NNLO\_munugamma\_pty\_140\_E\_CMS.deriv.DAOD\_HIGG8D1.e5928\_e5984\_s3126\_r10201\_r10210\_p4133  
mc16\_13TeV.364531.Sherpa\_222\_NNPDF30NNLO\_taunugamma\_pty\_7\_15.deriv.DAOD\_HIGG8D1.e5928\_e5984\_s3126\_r10201\_r10210\_p4133  
mc16\_13TeV.364532.Sherpa\_222\_NNPDF30NNLO\_taunugamma\_pty\_15\_35.deriv.DAOD\_HIGG8D1.e5928\_e5984\_s3126\_r10201\_r10210\_p4133  
mc16\_13TeV.364533.Sherpa\_222\_NNPDF30NNLO\_taunugamma\_pty\_35\_70.deriv.DAOD\_HIGG8D1.e5928\_e5984\_s3126\_r10201\_r10210\_p4133  
mc16\_13TeV.364534.Sherpa\_222\_NNPDF30NNLO\_taunugamma\_pty\_70\_140.deriv.DAOD\_HIGG8D1.e5928\_e5984\_s3126\_r10201\_r10210\_p4133  
mc16\_13TeV.364535.Sherpa\_222\_NNPDF30NNLO\_taunugamma\_pty\_140\_E\_CMS.deriv.DAOD\_HIGG8D1.e5928\_e5984\_s3126\_r10201\_r10210\_p4133  
mc16\_13TeV.410056.MadGraphPythiaEvtGen\_A14\_iZ\_4fl\_tchan\_noAllHad.deriv.DAOD\_HIGG8D1.e5803\_e5984\_s3126\_r10201\_r10210\_p4133  
mc16\_13TeV.410013.PowhegPythiaEvtGen\_P2012\_Wt\_inclusive\_top.deriv.DAOD\_HIGG8D1.e3753\_s3126\_r10201\_r10210\_p4133  
mc16\_13TeV.410014.PowhegPythiaEvtGen\_P2012\_Wt\_inclusive\_antitop.deriv.DAOD\_HIGG8D1.e3753\_s3126\_r10201\_r10210\_p4133  
mc16\_13TeV.410408.aMcAtNloPythia8EvtGen\_tWZ\_Ztoll\_minDR1.deriv.DAOD\_HIGG8D1.e6423\_e5984\_s3126\_r10201\_r10210\_p4133  
mc16\_13TeV.364242.Sherpa\_222\_NNPDF30NNLO\_WWW\_313v\_EW6.deriv.DAOD\_HIGG8D1.e5887\_e5984\_s3126\_r10201\_r10210\_p4133  
mc16\_13TeV.364243.Sherpa\_222\_NNPDF30NNLO\_WWZ\_412v\_EW6.deriv.DAOD\_HIGG8D1.e5887\_e5984\_s3126\_r10201\_r10210\_p4133  
mc16\_13TeV.364244.Sherpa\_222\_NNPDF30NNLO\_WWZ\_214v\_EW6.deriv.DAOD\_HIGG8D1.e5887\_e5984\_s3126\_r10201\_r10210\_p4133  
mc16\_13TeV.364245.Sherpa\_222\_NNPDF30NNLO\_WZZ\_511v\_EW6.deriv.DAOD\_HIGG8D1.e5887\_e5984\_s3126\_r10201\_r10210\_p4133  
mc16\_13TeV.364246.Sherpa\_222\_NNPDF30NNLO\_WZZ\_313v\_EW6.deriv.DAOD\_HIGG8D1.e5887\_e5984\_s3126\_r10201\_r10210\_p4133  
mc16\_13TeV.364247.Sherpa\_222\_NNPDF30NNLO\_ZZZ\_610v\_EW6.deriv.DAOD\_HIGG8D1.e5887\_e5984\_s3126\_r10201\_r10210\_p4133  
mc16\_13TeV.364248.Sherpa\_222\_NNPDF30NNLO\_ZZZ\_412v\_EW6.deriv.DAOD\_HIGG8D1.e5887\_e5984\_s3126\_r10201\_r10210\_p4133  
mc16\_13TeV.364249.Sherpa\_222\_NNPDF30NNLO\_ZZZ\_214v\_EW6.deriv.DAOD\_HIGG8D1.e5887\_e5984\_s3126\_r10201\_r10210\_p4133  
mc16\_13TeV.342284.Pythia8EvtGen\_A14NNPDF23LO\_WH125\_inc.deriv.DAOD\_HIGG8D1.e4246\_e5984\_s3126\_r10201\_r10210\_p4133  
mc16\_13TeV.342285.Pythia8EvtGen\_A14NNPDF23LO\_ZH125\_inc.deriv.DAOD\_HIGG8D1.e4246\_e5984\_s3126\_r10201\_r10210\_p4133  
mc16\_13TeV.341998.aMcAtNloHppEG\_UEEE5\_CTEQ6L1\_CT10ME\_tWH125\_gamgam\_yt\_plus1.deriv.DAOD\_HIGG8D1.e4394\_e5984\_s3126\_r10201\_r10210\_p4133  
mc16\_13TeV.410470.PhPy8EG\_A14\_ttbar\_hdamp258p75\_nonallhad.deriv.DAOD\_HIGG8D1.e6337\_e5984\_s3126\_r10201\_r10210\_p4133  
mc16\_13TeV.410472.PhPy8EG\_A14\_ttbar\_hdamp258p75\_dil.deriv.DAOD\_HIGG8D1.e6348\_e5984\_s3126\_r10201\_r10210\_p4133  
mc16\_13TeV.346343.PhPy8EG\_A14NNPDF23\_NNPDF30ME\_ttH125\_allhad.deriv.DAOD\_HIGG8D1.e7148\_e5984\_s3126\_r10201\_r10210\_p4133  
mc16\_13TeV.346344.PhPy8EG\_A14NNPDF23\_NNPDF30ME\_ttH125\_semilep.deriv.DAOD\_HIGG8D1.e7148\_e5984\_a875\_r10201\_r10210\_p4133  
mc16\_13TeV.346345.PhPy8EG\_A14NNPDF23\_NNPDF30ME\_ttH125\_dilep.deriv.DAOD\_HIGG8D1.e7148\_e5984\_a875\_r10201\_r10210\_p4133

mc16e:

mc16\_13TeV.361605.PowhegPy8EG\_CT10nloME\_AZNLOCTEQ6L1\_ZZvvvv\_mll4.deriv.DAOD\_HIGG8D1.e4054\_e5984\_s3126\_r10724\_r10726\_p4133  
mc16\_13TeV.361602.PowhegPy8EG\_CT10nloME\_AZNLOCTEQ6L1\_WZlvvv\_mll4.deriv.DAOD\_HIGG8D1.e4054\_e5984\_s3126\_r10724\_r10726\_p4133  
mc16\_13TeV.361601.PowhegPy8EG\_CT10nloME\_AZNLOCTEQ6L1\_WZlavl\_mll4.deriv.DAOD\_HIGG8D1.e4475\_e5984\_s3126\_r10724\_r10726\_p4133  
mc16\_13TeV.361600.PowhegPy8EG\_CT10nloME\_AZNLOCTEQ6L1\_WWlvlv.deriv.DAOD\_HIGG8D1.e4616\_e5984\_s3126\_r10724\_r10726\_p4133  
mc16\_13TeV.361603.PowhegPy8EG\_CT10nloME\_AZNLOCTEQ6L1\_ZZllll\_mll4.deriv.DAOD\_HIGG8D1.e4475\_e5984\_s3126\_r10724\_r10726\_p4133  
mc16\_13TeV.361604.PowhegPy8EG\_CT10nloME\_AZNLOCTEQ6L1\_ZZvvll\_mll4.deriv.DAOD\_HIGG8D1.e4475\_e5984\_s3126\_r10724\_r10726\_p4133  
mc16\_13TeV.364288.Sherpa\_222\_NNPDF30NNLO\_llll\_lowMllPtComplement.deriv.DAOD\_HIGG8D1.e6096\_s3126\_r10724\_p3983 mc16\_13TeV.364287.Sherpa\_222\_NNPDF30NNLO\_llll\_lowMllPtComplement.deriv.DAOD\_HIGG8D1.e6096\_s3126\_r10724\_p3983  
mc16\_13TeV.364285.Sherpa\_222\_NNPDF30NNLO\_llvjj\_EW6.deriv.DAOD\_HIGG8D1.e6055\_s3126\_r10724\_p3983  
mc16\_13TeV.364284.Sherpa\_222\_NNPDF30NNLO\_llvjj\_EW6.deriv.DAOD\_HIGG8D1.e6055\_s3126\_r10724\_p3983  
mc16\_13TeV.364283.Sherpa\_222\_NNPDF30NNLO\_lllijj\_EW6.deriv.DAOD\_HIGG8D1.e6055\_s3126\_r10724\_p3983  
mc16\_13TeV.364739.MGPy8EG\_NNPDF30NLO\_A14NNPDF23LO\_lvjlljjEW6\_OFMinus.deriv.DAOD\_HIGG8D1.e7421\_e5984\_s3126\_r10724\_r10726\_p4133  
mc16\_13TeV.364742.MGPy8EG\_NNPDF30NLO\_A14NNPDF23LO\_lvjlljjEW6\_SFPlus.deriv.DAOD\_HIGG8D1.e7421\_e5984\_s3126\_r10724\_r10726\_p4133  
mc16\_13TeV.364740.MGPy8EG\_NNPDF30NLO\_A14NNPDF23LO\_lvjlljjEW6\_OFPlus.deriv.DAOD\_HIGG8D1.e7421\_e5984\_s3126\_r10724\_r10726\_p4133  
mc16\_13TeV.364741.MGPy8EG\_NNPDF30NLO\_A14NNPDF23LO\_lvjlljjEW6\_SFMinus.deriv.DAOD\_HIGG8D1.e7421\_e5984\_s3126\_r10724\_r10726\_p4133  
mc16\_13TeV.364253.Sherpa\_222\_NNPDF30NNLO\_llv.deriv.DAOD\_HIGG8D1.e5916\_e5984\_s3126\_r10724\_r10726\_p4133

mc16\_13TeV.364250.Sherpa\_222\_NNPDF30NNLO\_llll.deriv.DAOD\_HIGG8D1.e5894\_e5984\_s3126\_r10724\_r10726\_p4133  
 mc16\_13TeV.364254.Sherpa\_222\_NNPDF30NNLO\_llvv.deriv.DAOD\_HIGG8D1.e5916\_e5984\_s3126\_r10724\_r10726\_p4133  
 mc16\_13TeV.364255.Sherpa\_222\_NNPDF30NNLO\_lvvv.deriv.DAOD\_HIGG8D1.e5916\_e5984\_s3126\_r10724\_r10726\_p4133  
 mc16\_13TeV.410155.aMcAtNloPythia8EvtGen\_MEN30NLO\_A14N23LO\_ttW.deriv.DAOD\_HIGG8D1.e5070\_e5984\_s3126\_r10724\_r10726\_p4133  
 mc16\_13TeV.410156.aMcAtNloPythia8EvtGen\_MEN30NLO\_A14N23LO\_ttZnunu.deriv.DAOD\_HIGG8D1.e5070\_e5984\_s3126\_r10724\_r10726\_p4133  
 mc16\_13TeV.410157.aMcAtNloPythia8EvtGen\_MEN30NLO\_A14N23LO\_ttZqq.deriv.DAOD\_HIGG8D1.e5070\_e5984\_s3126\_r10724\_r10726\_p4133  
 mc16\_13TeV.410218.aMcAtNloPythia8EvtGen\_MEN30NLO\_A14N23LO\_ttee.deriv.DAOD\_HIGG8D1.e5070\_e5984\_s3126\_r10724\_r10726\_p4133  
 mc16\_13TeV.410219.aMcAtNloPythia8EvtGen\_MEN30NLO\_A14N23LO\_ttmumu.deriv.DAOD\_HIGG8D1.e5070\_e5984\_s3126\_r10724\_r10726\_p4133  
 mc16\_13TeV.410220.aMcAtNloPythia8EvtGen\_MEN30NLO\_A14N23LO\_ttautau.deriv.DAOD\_HIGG8D1.e5070\_e5984\_s3126\_r10724\_r10726\_p4133  
 mc16\_13TeV.410276.aMcAtNloPythia8EvtGen\_MEN30NLO\_A14N23LO\_ttee\_mll\_1\_5.deriv.DAOD\_HIGG8D1.e6087\_e5984\_s3126\_r10724\_r10726\_p4133  
 mc16\_13TeV.410277.aMcAtNloPythia8EvtGen\_MEN30NLO\_A14N23LO\_ttmumu\_mll\_1\_5.deriv.DAOD\_HIGG8D1.e6087\_e5984\_s3126\_r10724\_r10726\_p4133  
 mc16\_13TeV.410278.aMcAtNloPythia8EvtGen\_MEN30NLO\_A14N23LO\_ttautau\_mll\_1\_5.deriv.DAOD\_HIGG8D1.e6087\_e5984\_s3126\_r10724\_r10726\_p4133  
 mc16\_13TeV.410397.MadGraphPythia8EvtGen\_ttbar\_wbee\_MEN30NLO\_A14N23LO.deriv.DAOD\_HIGG8D1.e6086\_e5984\_s3126\_r10724\_r10726\_p4133  
 mc16\_13TeV.410398.MadGraphPythia8EvtGen\_ttbar\_wbmumu\_MEN30NLO\_A14N23LO.deriv.DAOD\_HIGG8D1.e6086\_e5984\_s3126\_r10724\_r10726\_p4133  
 mc16\_13TeV.410399.MadGraphPythia8EvtGen\_ttbar\_wbtautau\_MEN30NLO\_A14N23LO.deriv.DAOD\_HIGG8D1.e6086\_e5984\_s3126\_r10724\_r10726\_p4133  
 mc16\_13TeV.410658.PhPy8EG\_A14\_tchan\_BW50\_lept\_top.deriv.DAOD\_HIGG8D1.e6671\_e5984\_s3126\_s3136\_r10724\_r10726\_p4133  
 mc16\_13TeV.410659.PhPy8EG\_A14\_tchan\_BW50\_lept\_antitop.deriv.DAOD\_HIGG8D1.e6671\_e5984\_s3126\_s3136\_r10724\_r10726\_p4133  
 mc16\_13TeV.410644.PowhegPythia8EvtGen\_A14\_singletop\_schan\_lept\_top.deriv.DAOD\_HIGG8D1.e6527\_e5984\_s3126\_r10724\_r10726\_p4133  
 mc16\_13TeV.410645.PowhegPythia8EvtGen\_A14\_singletop\_schan\_lept\_antitop.deriv.DAOD\_HIGG8D1.e6527\_e5984\_s3126\_r10724\_r10726\_p4133  
 mc16\_13TeV.412063.aMcAtNloPythia8EvtGen\_tllq\_NNPDF30\_nf4\_A14.deriv.DAOD\_TOPQ1.e7054\_e5984\_s3126\_r10724\_r10726\_p4174  
 mc16\_13TeV.304014.MadGraphPythia8EvtGen\_A14NNPDF23\_3top\_SM.deriv.DAOD\_HIGG8D1.e4324\_e5984\_s3126\_r10724\_r10726\_p4133  
 mc16\_13TeV.410080.MadGraphPythia8EvtGen\_A14NNPDF23\_4topSM.deriv.DAOD\_HIGG8D1.e4111\_e5984\_s3126\_r10724\_r10726\_p4133  
 mc16\_13TeV.410081.MadGraphPythia8EvtGen\_A14NNPDF23\_ttbarWW.deriv.DAOD\_HIGG8D1.e4111\_e5984\_s3126\_r10724\_r10726\_p4133  
 mc16\_13TeV.364100.Sherpa\_221\_NNPDF30NNLO\_Zmumu\_MAXHPTV0\_70\_CVetoBVeto.deriv.DAOD\_HIGG8D1.e5271\_e5984\_s3126\_s3136\_r10724\_r10726\_p4133  
 mc16\_13TeV.364100.Sherpa\_221\_NNPDF30NNLO\_Zmumu\_MAXHPTV0\_70\_CVetoBVeto.deriv.DAOD\_HIGG8D1.e5271\_e5984\_s3126\_r10724\_r10726\_p4133  
 mc16\_13TeV.364101.Sherpa\_221\_NNPDF30NNLO\_Zmumu\_MAXHPTV0\_70\_CFilterBVeto.deriv.DAOD\_HIGG8D1.e5271\_e5984\_s3126\_r10724\_r10726\_p4133  
 mc16\_13TeV.364102.Sherpa\_221\_NNPDF30NNLO\_Zmumu\_MAXHPTV0\_70\_BFilter.deriv.DAOD\_HIGG8D1.e5271\_e5984\_s3126\_s3136\_r10724\_r10726\_p4133  
 mc16\_13TeV.364102.Sherpa\_221\_NNPDF30NNLO\_Zmumu\_MAXHPTV0\_70\_BFilter.deriv.DAOD\_HIGG8D1.e5271\_e5984\_s3126\_r10724\_r10726\_p4133  
 mc16\_13TeV.364103.Sherpa\_221\_NNPDF30NNLO\_Zmumu\_MAXHPTV70\_140\_CVetoBVeto.deriv.DAOD\_HIGG8D1.e5271\_e5984\_s3126\_r10724\_r10726\_p4133  
 mc16\_13TeV.364103.Sherpa\_221\_NNPDF30NNLO\_Zmumu\_MAXHPTV70\_140\_CVetoBVeto.deriv.DAOD\_HIGG8D1.e5271\_e5984\_s3126\_s3136\_r10724\_r10726\_p4133  
 mc16\_13TeV.364104.Sherpa\_221\_NNPDF30NNLO\_Zmumu\_MAXHPTV70\_140\_CFilterBVeto.deriv.DAOD\_HIGG8D1.e5271\_e5984\_s3126\_r10724\_r10726\_p4133  
 mc16\_13TeV.364104.Sherpa\_221\_NNPDF30NNLO\_Zmumu\_MAXHPTV70\_140\_CFilterBVeto.deriv.DAOD\_HIGG8D1.e5271\_e5984\_s3126\_s3136\_r10724\_r10726\_p4133  
 mc16\_13TeV.364106.Sherpa\_221\_NNPDF30NNLO\_Zmumu\_MAXHPTV140\_280\_CVetoBVeto.deriv.DAOD\_HIGG8D1.e5271\_e5984\_s3126\_s3136\_r10724\_r10726\_p4133  
 mc16\_13TeV.364106.Sherpa\_221\_NNPDF30NNLO\_Zmumu\_MAXHPTV140\_280\_CVetoBVeto.deriv.DAOD\_HIGG8D1.e5271\_e5984\_s3126\_r10724\_r10726\_p4133  
 mc16\_13TeV.364107.Sherpa\_221\_NNPDF30NNLO\_Zmumu\_MAXHPTV140\_280\_CFilterBVeto.deriv.DAOD\_HIGG8D1.e5271\_e5984\_s3126\_r10724\_r10726\_p4133  
 mc16\_13TeV.364107.Sherpa\_221\_NNPDF30NNLO\_Zmumu\_MAXHPTV140\_280\_CFilterBVeto.deriv.DAOD\_HIGG8D1.e5271\_e5984\_s3126\_s3136\_r10724\_r10726\_p4133  
 mc16\_13TeV.364108.Sherpa\_221\_NNPDF30NNLO\_Zmumu\_MAXHPTV140\_280\_BFilter.deriv.DAOD\_HIGG8D1.e5271\_e5984\_s3126\_r10724\_r10726\_p4133  
 mc16\_13TeV.364109.Sherpa\_221\_NNPDF30NNLO\_Zmumu\_MAXHPTV280\_500\_CVetoBVeto.deriv.DAOD\_HIGG8D1.e5271\_e5984\_s3126\_r10724\_r10726\_p4133  
 mc16\_13TeV.364110.Sherpa\_221\_NNPDF30NNLO\_Zmumu\_MAXHPTV280\_500\_CFilterBVeto.deriv.DAOD\_HIGG8D1.e5271\_e5984\_s3126\_r10724\_r10726\_p4133  
 mc16\_13TeV.364110.Sherpa\_221\_NNPDF30NNLO\_Zmumu\_MAXHPTV280\_500\_CFilterBVeto.deriv.DAOD\_HIGG8D1.e5271\_e5984\_s3126\_s3136\_r10724\_r10726\_p4133  
 mc16\_13TeV.364111.Sherpa\_221\_NNPDF30NNLO\_Zmumu\_MAXHPTV280\_500\_BFilter.deriv.DAOD\_HIGG8D1.e5271\_e5984\_s3126\_s3136\_r10724\_r10726\_p4133  
 mc16\_13TeV.364111.Sherpa\_221\_NNPDF30NNLO\_Zmumu\_MAXHPTV280\_500\_BFilter.deriv.DAOD\_HIGG8D1.e5271\_e5984\_s3126\_r10724\_r10726\_p4133  
 mc16\_13TeV.364112.Sherpa\_221\_NNPDF30NNLO\_Zmumu\_MAXHPTV500\_1000.deriv.DAOD\_HIGG8D1.e5271\_e5984\_s3126\_r10724\_r10726\_p4133  
 mc16\_13TeV.364113.Sherpa\_221\_NNPDF30NNLO\_Zmumu\_MAXHPTV1000\_E\_CMS.deriv.DAOD\_HIGG8D1.e5271\_e5984\_s3126\_r10724\_r10726\_p4133  
 mc16\_13TeV.364113.Sherpa\_221\_NNPDF30NNLO\_Zmumu\_MAXHPTV1000\_E\_CMS.deriv.DAOD\_HIGG8D1.e5271\_e5984\_s3126\_s3136\_r10724\_r10726\_p4133  
 mc16\_13TeV.364114.Sherpa\_221\_NNPDF30NNLO\_Zee\_MAXHPTV0\_70\_CVetoBVeto.deriv.DAOD\_HIGG8D1.e5299\_e5984\_s3126\_s3136\_r10724\_r10726\_p4133  
 mc16\_13TeV.364114.Sherpa\_221\_NNPDF30NNLO\_Zee\_MAXHPTV0\_70\_CVetoBVeto.deriv.DAOD\_HIGG8D1.e5299\_e5984\_s3126\_r10724\_r10726\_p4133  
 mc16\_13TeV.364115.Sherpa\_221\_NNPDF30NNLO\_Zee\_MAXHPTV0\_70\_CFilterBVeto.deriv.DAOD\_HIGG8D1.e5299\_e5984\_s3126\_s3136\_r10724\_r10726\_p4133  
 mc16\_13TeV.364115.Sherpa\_221\_NNPDF30NNLO\_Zee\_MAXHPTV0\_70\_CFilterBVeto.deriv.DAOD\_HIGG8D1.e5299\_e5984\_s3126\_r10724\_r10726\_p4133  
 mc16\_13TeV.364116.Sherpa\_221\_NNPDF30NNLO\_Zee\_MAXHPTV0\_70\_BFilter.deriv.DAOD\_HIGG8D1.e5299\_e5984\_s3126\_r10724\_r10726\_p4133  
 mc16\_13TeV.364117.Sherpa\_221\_NNPDF30NNLO\_Zee\_MAXHPTV70\_140\_CVetoBVeto.deriv.DAOD\_HIGG8D1.e5299\_e5984\_s3126\_s3136\_r10724\_r10726\_p4133  
 mc16\_13TeV.364117.Sherpa\_221\_NNPDF30NNLO\_Zee\_MAXHPTV70\_140\_CVetoBVeto.deriv.DAOD\_HIGG8D1.e5299\_e5984\_s3126\_r10724\_r10726\_p4133  
 mc16\_13TeV.364118.Sherpa\_221\_NNPDF30NNLO\_Zee\_MAXHPTV70\_140\_CFilterBVeto.deriv.DAOD\_HIGG8D1.e5299\_e5984\_s3126\_s3136\_r10724\_r10726\_p4133  
 mc16\_13TeV.364118.Sherpa\_221\_NNPDF30NNLO\_Zee\_MAXHPTV70\_140\_CFilterBVeto.deriv.DAOD\_HIGG8D1.e5299\_e5984\_s3126\_r10724\_r10726\_p4133  
 mc16\_13TeV.364119.Sherpa\_221\_NNPDF30NNLO\_Zee\_MAXHPTV70\_140\_BFilter.deriv.DAOD\_HIGG8D1.e5299\_e5984\_s3126\_r10724\_r10726\_p4133  
 mc16\_13TeV.364120.Sherpa\_221\_NNPDF30NNLO\_Zee\_MAXHPTV140\_280\_CVetoBVeto.deriv.DAOD\_HIGG8D1.e5299\_e5984\_s3126\_r10724\_r10726\_p4133  
 mc16\_13TeV.364121.Sherpa\_221\_NNPDF30NNLO\_Zee\_MAXHPTV140\_280\_CFilterBVeto.deriv.DAOD\_HIGG8D1.e5299\_e5984\_s3126\_r10724\_r10726\_p4133  
 mc16\_13TeV.364122.Sherpa\_221\_NNPDF30NNLO\_Zee\_MAXHPTV140\_280\_BFilter.deriv.DAOD\_HIGG8D1.e5299\_e5984\_s3126\_s3136\_r10724\_r10726\_p4133  
 mc16\_13TeV.364122.Sherpa\_221\_NNPDF30NNLO\_Zee\_MAXHPTV140\_280\_BFilter.deriv.DAOD\_HIGG8D1.e5299\_e5984\_s3126\_r10724\_r10726\_p4133  
 mc16\_13TeV.364123.Sherpa\_221\_NNPDF30NNLO\_Zee\_MAXHPTV280\_500\_CVetoBVeto.deriv.DAOD\_HIGG8D1.e5299\_e5984\_s3126\_r10724\_r10726\_p4133  
 mc16\_13TeV.364124.Sherpa\_221\_NNPDF30NNLO\_Zee\_MAXHPTV280\_500\_CFilterBVeto.deriv.DAOD\_HIGG8D1.e5299\_e5984\_s3126\_r10724\_r10726\_p4133  
 mc16\_13TeV.364125.Sherpa\_221\_NNPDF30NNLO\_Zee\_MAXHPTV280\_500\_BFilter.deriv.DAOD\_HIGG8D1.e5299\_e5984\_s3126\_s3136\_r10724\_r10726\_p4133





mc16\_13TeV.364513.Sherpa\_222\_NNPDF30NNLO\_tautaugamma\_pty\_70\_140.deriv.DAOD\_HIGG8D1.e5982\_e5984\_s3126\_r10724\_r10726\_p4133  
 mc16\_13TeV.364514.Sherpa\_222\_NNPDF30NNLO\_tautaugamma\_pty\_140\_E\_CMS.deriv.DAOD\_HIGG8D1.e5928\_e5984\_s3126\_r10724\_r10726\_p4133  
 mc16\_13TeV.364522.Sherpa\_222\_NNPDF30NNLO\_enugamma\_pty\_15\_35.deriv.DAOD\_HIGG8D1.e5928\_e5984\_s3126\_r10724\_r10726\_p4133  
 mc16\_13TeV.364523.Sherpa\_222\_NNPDF30NNLO\_enugamma\_pty\_35\_70.deriv.DAOD\_HIGG8D1.e5928\_e5984\_s3126\_r10724\_r10726\_p4133  
 mc16\_13TeV.364524.Sherpa\_222\_NNPDF30NNLO\_enugamma\_pty\_70\_140.deriv.DAOD\_HIGG8D1.e5928\_e5984\_s3126\_r10724\_r10726\_p4133  
 mc16\_13TeV.364525.Sherpa\_222\_NNPDF30NNLO\_enugamma\_pty\_140\_E\_CMS.deriv.DAOD\_HIGG8D1.e5928\_e5984\_s3126\_r10724\_r10726\_p4133  
 mc16\_13TeV.364527.Sherpa\_222\_NNPDF30NNLO\_munugamma\_pty\_15\_35.deriv.DAOD\_HIGG8D1.e5928\_e5984\_s3126\_r10724\_r10726\_p4133  
 mc16\_13TeV.364528.Sherpa\_222\_NNPDF30NNLO\_munugamma\_pty\_35\_70.deriv.DAOD\_HIGG8D1.e5928\_e5984\_s3126\_r10724\_r10726\_p4133  
 mc16\_13TeV.364529.Sherpa\_222\_NNPDF30NNLO\_munugamma\_pty\_70\_140.deriv.DAOD\_HIGG8D1.e5928\_e5984\_s3126\_r10724\_r10726\_p4133  
 mc16\_13TeV.364530.Sherpa\_222\_NNPDF30NNLO\_munugamma\_pty\_140\_E\_CMS.deriv.DAOD\_HIGG8D1.e5928\_e5984\_s3126\_r10724\_r10726\_p4133  
 mc16\_13TeV.364532.Sherpa\_222\_NNPDF30NNLO\_taunugamma\_pty\_15\_35.deriv.DAOD\_HIGG8D1.e5928\_e5984\_s3126\_r10724\_r10726\_p4133  
 mc16\_13TeV.364533.Sherpa\_222\_NNPDF30NNLO\_taunugamma\_pty\_35\_70.deriv.DAOD\_HIGG8D1.e5928\_e5984\_s3126\_r10724\_r10726\_p4133  
 mc16\_13TeV.364534.Sherpa\_222\_NNPDF30NNLO\_taunugamma\_pty\_70\_140.deriv.DAOD\_HIGG8D1.e5928\_e5984\_s3126\_r10724\_r10726\_p4133  
 mc16\_13TeV.364535.Sherpa\_222\_NNPDF30NNLO\_taunugamma\_pty\_140\_E\_CMS.deriv.DAOD\_HIGG8D1.e5928\_e5984\_s3126\_r10724\_r10726\_p4133  
 mc16\_13TeV.410560.MadGraphPythia8EvtGen\_A14\_tZ\_4fl\_tchan\_noAllHad.deriv.DAOD\_HIGG8D1.e5803\_e5984\_s3126\_r10724\_r10726\_p4133  
 mc16\_13TeV.410408.aMcAtNloPythia8EvtGen\_tWZ\_Ztoll\_minDR1.deriv.DAOD\_HIGG8D1.e6423\_e5984\_s3126\_r10724\_r10726\_p4133  
 mc16\_13TeV.364242.Sherpa\_222\_NNPDF30NNLO\_WWW\_3l3v\_EW6.deriv.DAOD\_HIGG8D1.e5887\_e5984\_s3126\_r10724\_r10726\_p4133  
 mc16\_13TeV.364243.Sherpa\_222\_NNPDF30NNLO\_WWZ\_4l2v\_EW6.deriv.DAOD\_HIGG8D1.e5887\_e5984\_s3126\_r10724\_r10726\_p4133  
 mc16\_13TeV.364244.Sherpa\_222\_NNPDF30NNLO\_WWZ\_2l4v\_EW6.deriv.DAOD\_HIGG8D1.e5887\_e5984\_s3126\_r10724\_r10726\_p4133  
 mc16\_13TeV.364245.Sherpa\_222\_NNPDF30NNLO\_WZZ\_5l1v\_EW6.deriv.DAOD\_HIGG8D1.e5887\_e5984\_s3126\_r10724\_r10726\_p4133  
 mc16\_13TeV.364246.Sherpa\_222\_NNPDF30NNLO\_WZZ\_3l3v\_EW6.deriv.DAOD\_HIGG8D1.e5887\_e5984\_s3126\_r10724\_r10726\_p4133  
 mc16\_13TeV.364247.Sherpa\_222\_NNPDF30NNLO\_ZZZ\_6l0v\_EW6.deriv.DAOD\_HIGG8D1.e5887\_e5984\_s3126\_r10724\_r10726\_p4133  
 mc16\_13TeV.364248.Sherpa\_222\_NNPDF30NNLO\_ZZZ\_4l2v\_EW6.deriv.DAOD\_HIGG8D1.e5887\_e5984\_s3126\_r10724\_r10726\_p4133  
 mc16\_13TeV.364249.Sherpa\_222\_NNPDF30NNLO\_ZZZ\_2l4v\_EW6.deriv.DAOD\_HIGG8D1.e5887\_e5984\_s3126\_r10724\_r10726\_p4133  
 mc16\_13TeV.342284.Pythia8EvtGen\_A14NNPDF23LO\_WH125\_inc.deriv.DAOD\_HIGG8D1.e4246\_e5984\_s3126\_r10724\_r10726\_p4133  
 mc16\_13TeV.342285.Pythia8EvtGen\_A14NNPDF23LO\_ZH125\_inc.deriv.DAOD\_HIGG8D1.e4246\_e5984\_s3126\_r10724\_r10726\_p4133  
 mc16\_13TeV.341998.aMcAtNloHppEG\_UEEE5\_CTEQ6L1\_CT10ME\_tWH125\_gamgam\_yt\_plus1.deriv.DAOD\_HIGG8D1.e4394\_e5984\_s3126\_r10724\_r10726\_p4133  
 mc16\_13TeV.410389.MadGraphPythia8EvtGen\_A14NNPDF23\_ttgamma\_nonallhadronic.deriv.DAOD\_HIGG8D1.e6155\_e5984\_s3126\_r10724\_r10726\_p4133  
 mc16\_13TeV.410470.PhPy8EG\_A14\_ttbar\_hdamp258p75\_nonallhad.deriv.DAOD\_HIGG8D1.e6337\_e5984\_s3126\_r10724\_r10726\_p4133  
 mc16\_13TeV.410472.PhPy8EG\_A14\_ttbar\_hdamp258p75\_dil.deriv.DAOD\_HIGG8D1.e6348\_e5984\_s3126\_r10724\_r10726\_p4133  
 mc16\_13TeV.346343.PhPy8EG\_A14NNPDF23\_NNPDF30ME\_ttH125\_allhad.deriv.DAOD\_HIGG8D1.e7148\_e5984\_s3126\_r10724\_r10726\_p4133  
 mc16\_13TeV.346343.PhPy8EG\_A14NNPDF23\_NNPDF30ME\_ttH125\_allhad.deriv.DAOD\_HIGG8D1.e7148\_e5984\_a875\_r10724\_r10726\_p4133  
 mc16\_13TeV.346344.PhPy8EG\_A14NNPDF23\_NNPDF30ME\_ttH125\_semilep.deriv.DAOD\_HIGG8D1.e7148\_e5984\_a875\_r10724\_r10726\_p4133  
 mc16\_13TeV.346344.PhPy8EG\_A14NNPDF23\_NNPDF30ME\_ttH125\_semilep.deriv.DAOD\_HIGG8D1.e7148\_e5984\_s3126\_r10724\_r10726\_p4133  
 mc16\_13TeV.346345.PhPy8EG\_A14NNPDF23\_NNPDF30ME\_ttH125\_dilep.deriv.DAOD\_HIGG8D1.e7148\_e5984\_a875\_r10724\_r10726\_p4133  
 mc16\_13TeV.346345.PhPy8EG\_A14NNPDF23\_NNPDF30ME\_ttH125\_dilep.deriv.DAOD\_HIGG8D1.e7148\_e5984\_s3126\_r10724\_r10726\_p4133